

Kirkwood gaps and diffusion along mean motion resonances in the restricted planar three-body problem

Jacques Féjoz*, Marcel Guàrdia†, Vadim Kaloshin‡ and Pablo Roldán§

February 18, 2022

Abstract

We study the dynamics of the restricted planar three-body problem near mean motion resonances, i.e. a resonance involving the Keplerian periods of the two lighter bodies revolving around the most massive one. This problem is often used to model Sun–Jupiter–asteroid systems. For the primaries (Sun and Jupiter), we pick a realistic mass ratio $\mu = 10^{-3}$ and a small eccentricity $e_0 > 0$. The main result is a construction of a variety of *non local* diffusing orbits which show a drastic change of the osculating (instant) eccentricity of the asteroid, while the osculating semi major axis is kept almost constant. The proof relies on the careful analysis of the circular problem, which has a hyperbolic structure, but for which diffusion is prevented by KAM tori. In the proof we verify certain non-degeneracy conditions numerically.

Based on the work of Treschev, it is natural to conjecture that the time of diffusion for this problem is $\sim \frac{-\ln(\mu e_0)}{\mu^{3/2} e_0}$. We expect our instability mechanism to apply to realistic values of e_0 and we give heuristic arguments in its favor. If so, the applicability of Nekhoroshev theory to the three-body problem as well as the long time stability become questionable.

It is well known that, in the Asteroid Belt, located between the orbits of Mars and Jupiter, the distribution of asteroids has the so-called *Kirkwood gaps* exactly at mean motion resonances of low order. Our mechanism gives a possible explanation of their existence. To relate the existence of Kirkwood gaps with Arnol’d diffusion, we also state a conjecture on its existence for a typical ε -perturbation of the product of the pendulum and the rotator. Namely, we predict that a positive conditional measure of initial conditions concentrated in the main resonance exhibits Arnol’d diffusion on time scales $\frac{-\ln \varepsilon}{\varepsilon^2}$.

Contents

1	Introduction and main results	2
1.1	The problem of the stability of gravitating bodies	2
1.2	An example of relevance in astronomy	4
1.3	Main results	6
1.4	Refinements and comments	8
1.5	Mechanism of instability	9
1.6	Sketch of the proof	10
1.7	Nature of numerics	12
1.8	Main theorem for the 1 : 7 resonance	13
2	The circular problem	15
2.1	Normally hyperbolic invariant cylinders	15
2.2	The inner map	17
2.3	The outer map	17

*Université Paris-Dauphine and Observatoire de Paris (fejoz@imcce.fr)

†University of Maryland at College Park (marcel.guardia@upc.edu)

‡University of Maryland at College Park (kaloshin@math.umd.edu)

§Universitat Politècnica de Catalunya (pablo.roldan@upc.edu)

3	The elliptic problem	21
3.1	The specific form of the inner and outer maps	21
3.2	The e_0 -expansion of the elliptic Hamiltonian	23
3.3	Perturbative analysis of the flow	25
3.4	Perturbative analysis of the invariant cylinder and its inner map	26
3.5	The outer map	28
4	Existence of diffusing orbits	30
4.1	Existence of a transition chain of whiskered tori	30
4.2	Shadowing	34
A	Numerical study of the normally hyperbolic invariant cylinder of the circular problem.	35
A.1	Computation of the periodic orbits	35
A.2	Computation of invariant manifolds	39
A.3	Computation of transversal homoclinic points and splitting angle	41
A.4	Accuracy of computations	44
B	Numerical study of the inner and outer dynamics	45
B.1	From Cartesian to Delaunay and computation of $\partial_G \Delta H_{\text{circ}}$	46
B.2	Inner and outer dynamics of the circular problem	48
B.3	Inner and outer dynamics of the elliptic problem	51
B.4	Comparison of the inner and outer dynamics of the elliptic problem	52
C	The Main Result for the 3 : 1 resonance: instabilities in the Kirkwood gaps	53
C.1	The circular problem	54
C.2	The elliptic problem	56
C.3	Numerical study of the 3 : 1 resonance	60
D	Conjectures on the speed of diffusion	63
D.1	Speed of diffusion for a priori unstable systems and Positive measure	65
D.2	Structure of the restricted planar elliptic three-body problem	66
D.3	The Mather accelerating problem and its speed of diffusion	67
D.4	Modified positive measure conjecture	67

1 Introduction and main results

1.1 The problem of the stability of gravitating bodies

The stability of the Solar System is a longstanding problem. Over the centuries, mathematicians and astronomers have spent an inordinate amount of energy proving stronger and stronger stability theorems for dynamical systems closely related to the Solar System, generally within the frame of the Newtonian N -body problem:

$$\ddot{q}_i = \sum_{j \neq i} m_j \frac{q_j - q_i}{\|q_j - q_i\|^3}, \quad q_i \in \mathbf{R}^2, \quad i = 0, 1, \dots, N-1, \quad (1)$$

and its planetary subproblem, where the mass m_0 (modelling the Sun) is much larger than the other masses m_i .

A famous theorem of Lagrange entails that the observed variations in the motion of Jupiter and Saturn come from resonant terms of large amplitude and long period, but with zero average (see [Las06] and references therein, or [AKN88, Example 6.16]). Yet it is a mistake, which Laplace made, to infer the topological stability of the planetary system, since the theorem deals only with an approximation of the first order with respect to the masses, eccentricities and inclinations of the planets [Lap89, p. 296]. Another key result is Arnol'd's theorem, which proves the existence of a set of positive Lebesgue measure

filled by invariant tori in planetary systems, provided that the masses of the planets are small [Arn63, Féj04]. However, in the phase space the gaps left by the invariant tori leave room for instability.

It was a big surprise when the numerical computations of Sussman, Wisdom and Laskar showed that over the life span of the Sun, or even over a few million years, collisions and ejections of inner planets are probable (due to the exponential divergence of solutions, only a probabilistic result seems within the reach of numerical experiments); see for example [SW92, Las94], or [Las10] for a recent account. Our Solar System, as well as newly discovered extra-solar systems, are now widely believed to be unstable, and the general conjecture about the N -body problem is quite the opposite of what it used to be:

Conjecture 1.1 (Global instability of the N -body problem). *In restriction to any energy level of the N -body problem, the non-wandering set is nowhere dense. (One can reparameterize orbits to have a complete flow, despite collisions.)*

According to Herman [Her98], this is the oldest open problem in dynamical systems (see also [Kol57]). This conjecture would imply that bounded orbits form a *nowhere dense set* and that no topological stability whatsoever holds, in a very strong sense. It is largely confirmed by numerical experiments. In our Solar System, Laskar for instance has shown that collisions between Mars and Venus could occur within a few billion years. The coexistence of a nowhere dense set of positive measure of bounded quasi-periodic motions with an open and dense set of initial conditions with unbounded orbits is a remarkable conjecture.

Currently the above conjecture is largely out of reach. A more modest but still very challenging goal, also stated in [Her98], is a local version of the conjecture:

Conjecture 1.2 (Instability of the planetary problem). *If the masses of the planets are small enough, the wandering set accumulates on the set of circular, coplanar, Keplerian motions.*

There have been some prior attempts to prove such a conjecture. For instance, Moeckel discovered an instability mechanism in a special configuration of the 5-body problem [Moe96]. His proof of diffusion was limited by the so-called big gaps problem between hyperbolic invariant tori; this problem was later solved in this setting by Zheng [Zhe10]. A somewhat opposite strategy was developed by Bolotin and McKay, using the Poincaré orbits of the second species to show the existence of symbolic dynamics in the three-body problem, hence of chaotic orbits, but considering far from integrable, non-planetary conditions; see for example [Bol06]. Also, Delshams, Gidea and Roldán have shown an instability mechanism in the spatial restricted three-body problem, but only locally around the equilibrium point L_1 (see [DGR11]).

In this paper we prove the existence of large instabilities in a realistic planetary system and describe the associated instability mechanism. We thus provide a step towards the proof of Conjecture 1.2.

In his famous paper [Arn64], Arnol'd says: “In contradistinction with stability, instability¹ is itself stable. I believe that the mechanism of “transition chain” which guarantees that instability in our example is also applicable to the general case (for example, to the problem of three bodies)”. In this paper we exhibit a regime of realistic motions of a three body problem where “transition chains” **do** occur and lead to Arnol'd’s mechanism of instability. Such instabilities occur near mean motion resonances, defined below. To the best of our knowledge, this is the first regime of motions of the problem of three bodies naturally modelling a region in the Solar system, where nonlocal transition chains are established². Previous results showing transition chains of tori in the problem of three bodies naturally modelling a region in the Solar system are confined to small neighborhoods of the Lagrangian Equilibrium points [CZ11, DGR11], and therefore, are local in the Configuration and Phase space.

The instability mechanism shown in this paper is related to a generalized version of Mather’s acceleration problem [Mat96, BT99, DdLS00, GT08, Kal03, Pif06]. Some parts of the proof rely on numerical computations, but our strategy allows us to keep these computations simple and convincing.

¹In the translation the word “nonstability” is used, which seems to refer to instability.

²“Nonlocal” means that motions on the boundary tori in this chain differ significantly, uniformly with respect to the small parameter. In our case, the eccentricity of orbits of the massless planet (asteroid) varies by $\mathcal{O}(1)$, uniformly with respect to small values of the eccentricity of the primaries, while the semi major axis stays nearly constant. See Section 1.3 for more details.

We consider the planetary problem (1) with one planet mass (say, m_1) larger than the others: $m_0 \gg m_1 \gg m_2, \dots, m_{N-1}$. The equations of motion of the lighter objects ($i = 2, \dots, N-1$) can advantageously be written as

$$\ddot{q}_i = m_0 \frac{q_0 - q_i}{\|q_0 - q_i\|^3} + m_1 \frac{q_1 - q_i}{\|q_1 - q_i\|^3} + \sum_{j \neq i, j > 1} m_j \frac{q_j - q_i}{\|q_j - q_i\|^3}. \quad (2)$$

Letting the masses m_j tend to 0 for $j = 2, \dots, N-1$, we obtain a collection of $(N-2)$ independent *restricted problems*:

$$\ddot{q}_i = m_0 \frac{q_0 - q_i}{\|q_0 - q_i\|^3} + m_1 \frac{q_1 - q_i}{\|q_1 - q_i\|^3}, \quad (3)$$

where the massless bodies are influenced by, without themselves influencing, the *primaries* of masses m_0 and m_1 .

For $N = 3$, this model is often used to approximate the dynamics of Sun-Jupiter-asteroid or other Sun-planet-object problems, and it is the simplest one conjectured to have a wide range of instabilities.

1.2 An example of relevance in astronomy

1.2.1 The asteroid belt

One place in the Solar system where the dynamics is well approximated by the restricted three-body problem is the asteroid belt. The asteroid belt is located between the orbits of Mars and Jupiter and consists of 1.7 million objects ranging from asteroids of 950 kilometers to dust particles. Since the mass of Jupiter is approximately 2960 masses of Mars, away from close encounters with Mars, one can neglect the influence of Mars on the asteroids and focus on the influence of Jupiter. We also omit interactions with the second biggest planet in the Solar System, namely Saturn, which actually is not so small. Indeed, its mass is about a third of the mass of Jupiter and its semi major axis is about 1.83 times the semi major axis of Jupiter. This implies that the strength of interaction with Saturn is around 10% of the strength of interaction with Jupiter. However, instabilities discussed in this paper are fairly robust and we believe that they are not destroyed by the interaction with Saturn (or other celestial bodies), which to some degree averages out.

With these assumptions one can model the motion of the objects in the asteroid belt by the restricted problem. Denote by $\mu = m_1/(m_0 + m_1)$ the mass ratio, where m_0 is the mass of the Sun and m_1 is the mass of Jupiter. For $\mu = 0$ (namely, neglecting the influence of Jupiter), bounded orbits of the asteroid are ellipses. Up to orientation, the ellipses are characterized by their semi major axis a and eccentricity e .

The aforementioned theorem of Lagrange asserts that, for small $\mu > 0$, the semi major axis $a(t)$ of an asteroid satisfies $|a(t) - a(0)| \lesssim \mu$ for all $|t| \lesssim 1/\mu$. For very small μ the time of stability was greatly improved by Niederman [Nie96] using Nekhoroshev theory; see the discussion in the next section. Nevertheless, if one looks at the asteroid distribution in terms of their semi major axis, one encounters several gaps, the so-called *Kirkwood gaps*. It is believed that the existence of these gaps is due to instability mechanisms.

1.2.2 Kirkwood gaps and Wisdom's ejection mechanism

Mean motion resonances occur when the ratio between the period of Jupiter and the period of the asteroid is rational. In particular, the Kirkwood gaps correspond to the ratios 3 : 1, 5 : 2 and 7 : 3.

In this section we present a heuristic explanation of the reason why these gaps exist.

It is conjectured and confirmed by numerical data [Wis82] that the eccentricities of asteroids appropriately placed in the Kirkwood gaps change by a magnitude of order one. Notice that in the real data, the eccentricities of most asteroids in the asteroid belt are between 0 and 0.25; see for example <http://en.wikipedia.org/wiki/File:Mainbeltevs.png>.

As the eccentricity of the asteroid grows while its semi major axis is nearly constant, its perihelion gets closer and closer to the origin, namely at the distance $a(t)[1 - e(t)]$, where $a(t)$ and $e(t)$ are the semi major axis and eccentricity of the asteroid respectively (see Figure 2, where the inner circle is the orbit

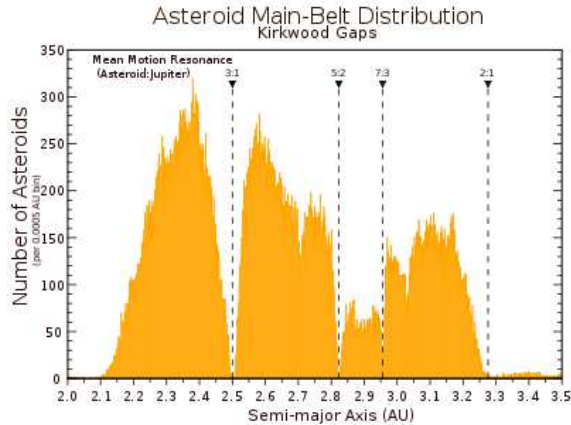


Figure 1: Kirkwood gaps

of Mars). In particular, a close encounter with Mars becomes increasingly probable. Eventually Mars and the asteroid come close to each other, and the asteroid most probably gets ejected from the asteroid belt.

A surprising fact is that *the change of eccentricity of the asteroid is only possible due to the ellipticity of the motion of Jupiter*, due to the following count of dimensions. For circular motions of Jupiter the problem reduces to two degrees of freedom (see Section 1.8) and plausibly there are invariant 2-dimensional tori separating the three dimensional energy surfaces; see for example [GDF⁺89, F  j02b, CC07]. If the eccentricity of Jupiter is not zero, the system has two and a half degrees of freedom and then KAM tori do not prevent drastic changes in the eccentricity.

Heuristically, the conclusion is that, if the eccentricity of the asteroid changes by a magnitude of order one in the Sun-Jupiter-asteroid restricted problem, then the asteroid might come into zones where the restricted problem does not describe the dynamics appropriately, due to the influence of Mars.

The main result of this paper is that for certain mean motion resonances there are unstable motions which lead to significant changes in the eccentricity. We only present results for two particular resonances (1 : 7 and 3 : 1), because the proof relies on numerical computations. The resonance 3 : 1 corresponds to one of most noticeable Kirkwood gaps. We are confident that our mechanism of instability applies to other resonances, and thus to the other Kirkwood gaps, as long as the orbits of the unperturbed problem stay away from collisions. Thus, the instability mechanism showed in this paper gives insight into the existence of the Kirkwood gaps.

Another instability mechanism, using the adiabatic invariant theory, can be seen in [NS04] where a heuristic explanation is given. Let $\varepsilon_J = \mu_J^{1/2}/e_J$, where μ_J is mass ratio and e_J is eccentricity of Jupiter. They study the case when ε_J is relatively small: 0.025, 0.05, 0.1, 0.2. In reality it is close to 0.6. In contrast, we study the case of large ε_J .

1.2.3 Capture in resonance of other objects

Many known light objects in the Solar System display a mean motion resonance of low order with Jupiter or some other planet. Some of them are: Trojan satellites, which librate around one of the two Lagrangian points of a planet, hence in 1 : 1 resonance with the planet; Uranus, which is close to the 1 : 7 resonance with Jupiter, thus giving an example of an “outer” restricted problem that is close in phase space to the solutions we are studying; or the Kuiper Belt beyond Neptune, whose objects, behaving in the exact opposite manner to those of the asteroid belt, seem to *concentrate* close to mean motion resonances (in particular, the Keplerian ellipse of the dwarf planet Pluto notoriously meets the ellipse of Neptune). The current existence of these resonant objects, and thus their relative stability, seemingly contradicts the above mechanism. This calls at least for a short explanation, although there are many effects at work.

The main point is that an elliptic stability zone lies in the eye of a resonance, where some kind of long term stability prevails. Besides, the geometry of the system often prevents the ejection mechanism described in Section 1.2.2, because there is no such body as Mars to propel the asteroid through a close encounter. In many cases, the mean motion resonance itself precludes collisions with the main planet, for example the Trojan asteroids with respect to Jupiter, or Pluto with respect to Neptune; for a discussion of this effect in the asteroid belt, see [Rob05].

The complete picture certainly includes secular resonances, close encounters between asteroids, as well as more complicated kinds of resonance involving more bodies (for example the second Kirkwood gap, where a four-body problem resonance seems to play a crucial role). We refer to [Mor02, Rob05] for further astronomical details.

1.3 Main results

Let us consider the three-body problem and assume that the massless body moves in the same plane as the two primaries. We normalize the total mass to one, and we call the three bodies the Sun (mass $1 - \mu$), Jupiter (mass μ with $0 < \mu \ll 1$) and the asteroid (zero mass). If the energy of the primaries is negative, their orbits describe two ellipses with the same eccentricity, say $e_0 \geq 0$. For convenience, we denote by $q_0(t)$ the normalized position of the primaries (or “fictitious body”), so that the Sun and Jupiter have respective positions $-\mu q_0(t)$ and $(1 - \mu)q_0(t)$. The Hamiltonian of the asteroid is

$$K(q, p, t) = \frac{\|p\|^2}{2} - \frac{1 - \mu}{\|q + \mu q_0(t)\|} - \frac{\mu}{\|q - (1 - \mu)q_0(t)\|} \quad (4)$$

where $q, p \in \mathbb{R}^2$. Without loss of generality one can assume that $q_0(t)$ has semi major axis equal to 1 and period 2π . For $e_0 \geq 0$ this system has two and a half degrees of freedom.

When $e_0 = 0$, the primaries describe uniform circular motions around their center of mass. (This system is called the restricted planar circular three-body problem). Thus, in a frame rotating with the primaries, the system becomes autonomous and hence has only 2 degrees of freedom. Its energy in the rotating frame is a first integral, called *the Jacobi integral*³. It is defined by

$$J = \frac{\|p\|^2}{2} - \frac{1 - \mu}{\|q + \mu q_0(t)\|} - \frac{\mu}{\|q - (1 - \mu)q_0(t)\|} - (q_1 p_2 - q_2 p_1). \quad (5)$$

The aforementioned KAM theory applies to both the circular and the elliptic problem [Arn63, SM95] and asserts that if the mass of Jupiter is small enough, there is a set of initial conditions of positive Lebesgue measure leading to quasiperiodic motions, in the neighborhood of circular motions of the asteroid.

If Jupiter has a circular motion, since the system has only 2 degrees of freedom, KAM invariant tori are 2-dimensional and separate the 3-dimensional energy surfaces. But in the elliptic problem, 3-dimensional KAM tori do not prevent orbits from wandering on a 5-dimensional phase space. In this paper we prove the existence of a wide enough set of wandering orbits in the elliptic planar restricted three-body problem.

Let us write the Hamiltonian (4) as

$$K(q, p, t) = K_0(q, p) + K_1(q, p, t, \mu),$$

with

$$K_0(q, p) = \frac{\|p\|^2}{2} - \frac{1}{\|q\|},$$

$$K_1(q, p, t, \mu) = \frac{1}{\|q\|} - \frac{1 - \mu}{\|q + \mu q_0(t)\|} - \frac{\mu}{\|q - (1 - \mu)q_0(t)\|}.$$

The Keplerian part K_0 allows us to associate elliptical elements to every point (q, p) of the phase space of negative energy K_0 . We are interested in the drift of the eccentricity e under the flow of K . (The reader will easily distinguish this notation from other meanings of e).

³Celestial mechanics’s works often prefer to use the *Jacobi constant* C , given by $J = \frac{(1-\mu)\mu - C}{2}$.

We will see later that $K_1 = \mathcal{O}(\mu)$ uniformly, away from collisions. Notice that there is a competition between the integrability of K_0 and the non-integrability of K_1 , which allows for wandering. In this work we consider a realistic value of the mass ratio, $\mu = 10^{-3}$.

Notation 1.3. *In what follows, we abbreviate the restricted planar circular three-body problem to the circular problem, and the restricted planar elliptic three-body problem to the elliptic problem.*

Here is the main result of this paper.

Main Result (resonance 1 : 7). *Consider the elliptic problem with mass ratio $\mu = 10^{-3}$ and eccentricity of Jupiter $e_0 > 0$. Assume it is in general position⁴. Then, for e_0 small enough, there exists a time $T > 0$ and a trajectory whose eccentricity $e(t)$ satisfies that*

$$e(0) < 0.48 \quad \text{and} \quad e(T) > 0.67$$

while

$$|a(t) - 7^{2/3}| \leq 0.027 \quad \text{for } t \in [0, T].$$

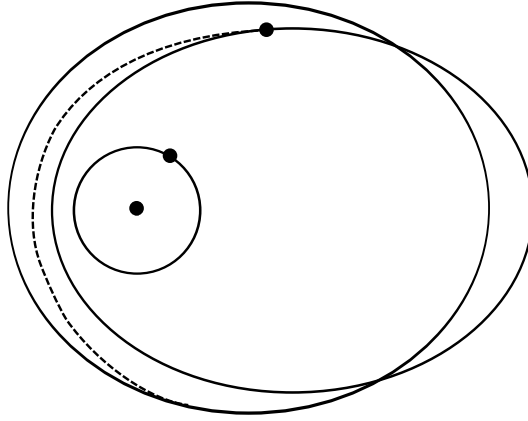


Figure 2: Transition from the instant ellipse of eccentricity $e = 0.48$ to the instant ellipse of eccentricity $e = 0.67$. The dashed line represents the transition; however, the actual diffusing orbit is very complicated and the diffusion is very slow.

We will make this result more precise in Section 1.8, Theorem 1, after providing some appropriate definitions. We stress that the instabilities discussed in the Main Result are non-local neither in the action space nor in the configuration space. This is the first result showing nonlocal instabilities in the planetary three body problem.

In [GK10b, GK10a, GK11] it is shown that in the circular problem with realistic mass ratio $\mu = 10^{-3}$ there exists an unbounded Birkhoff region of instability for eccentricities larger than 0.66 and Jacobi integral $J = 1.8$. This allows them to prove a variety of unstable motions, including oscillatory motions and all types of final motions of Chazy.

The analogous result for the 3 : 1 resonance is as follows.

Main Result (resonance 3 : 1). *Consider the elliptic problem with mass ratio $\mu = 10^{-3}$ and eccentricity of Jupiter $e_0 > 0$. Assume it is in general position. Then, for e_0 small enough, there exists a time $T > 0$ and a trajectory whose eccentricity $e(t)$ satisfies that*

$$e(0) < 0.59 \quad \text{and} \quad e(T) > 0.91$$

⁴Later we state three Ansätze that formalize the non-degeneracy conditions we need.

while

$$\left|a(t) - 3^{-2/3}\right| \leq 0.149 \quad \text{for } t \in [0, T].$$

Thus we claim the existence of orbits of the asteroid whose change in eccentricity is above 0.3. In Appendix D, we state two conjectures about the stochastic behavior of orbits near a resonance: one is for Arnol'd's example and another one is for our elliptic problem. These conjectures are based on numerical experiments; see for example [Chi79, SUZ88, Wis82]. We also provide some heuristic arguments using the dynamical structures explored in this paper. Loosely speaking, we claim that near a resonance there is polynomial instability for a positive measure set of initial conditions on the time scale $\frac{-\ln(\mu e_0)}{\mu^{3/2}e_0}$.

Most of the paper is devoted to the resonance 1 : 7. But the proof seems robust with respect to the precise resonance considered. In appendix C, we show how to modify the proof of the main result to deal with the resonance 3 : 1, whose importance in explaining the Kirkwood gaps is emphasized in the introduction.

We believe that our mechanism applies to a substantially larger interval of eccentricities, but proving this requires more sophisticated numerics; see Remark A.4.

1.4 Refinements and comments

1.4.1 Smallness of the eccentricity of Jupiter

When Jupiter describes a circular motion, the Jacobi integral is an integral of motion and then KAM theory prevents global instabilities. We consider the eccentricity e_0 as a small parameter so that we can compare the dynamics of the elliptic problem with the dynamics of the circular one.

The difference between the elliptic and circular Hamiltonians is $\mathcal{O}(\mu e_0)$. The analysis of the difference, performed in Section 3.2, shows that this difference can be reduced to $\mathcal{O}(\mu e_0^5)$ (or even smaller) using averaging. This makes us believe that e_0 does not need to be infinitesimally small for our mechanism to work. Even the realistic value $e_0 \approx 0.048$ is not out of question. However, having a realistic e_0 becomes mostly a matter of *numerical experiment, not of mathematical proof*—the limit and the interest of perturbation theory is to describe dynamical behavior in terms of asymptotic models. See Appendix D.2 for more details.

1.4.2 On infinitesimally small masses μ

In the Main Result, we do not know what happens asymptotically if we let $\mu \rightarrow 0$, since our estimates worsen. Indeed, one of the crucial steps of the proof is to study the transversality of certain invariant manifolds (see Section 1.6) and this transversality becomes exponentially small with respect to μ as $\mu \rightarrow 0$. On the other hand, the Main Result holds for realistic values of μ , which is out of reach of many qualitative results of perturbation theory where parameters are conveniently assumed to be as small as needed. See Appendix D for more details.

1.4.3 Speed of diffusion

In Appendix D we discuss the relation of our problem with a priori unstable systems and Mather's accelerating problem. We conjecture that, for the orbits constructed in this paper, the diffusion time T can be chosen to be

$$T \sim -\frac{\ln(\mu e_0)}{\mu^{3/2}e_0}. \quad (6)$$

Time estimates in the a priori unstable setting can be found in [BB02, BBB03, Tre04, GdlL06].

De la Llave [dlL04], Gelfreich-Turaev [GT08], and Piftankin [Pif06], using Treschev's techniques of separatrix maps (see for instance [PT07]), proved linear diffusion for Mather's acceleration problem. Using these techniques, a smart choice of diffusing orbits might lead to even faster diffusion in our problem, in times of the order $T \sim -\ln(\mu^{3/2}e_0)^{-1}$; see Appendix D for more details⁵.

⁵This does not seem crucial, since the real value e_0 is not smaller than μ .

An analytic proof of this conjecture might require restrictive conditions between μ and e_0 . However, for realistic values of μ and e_0 or smaller, that is $0 < \mu \leq 10^{-3}$ and $0 < e_0 < 0.048$, we expect that the speed of our mechanism of diffusion also obeys the above heuristic formula.

On the other hand, the above formula probably does not hold in the neighborhood of circular motions of the massless body, which might be much more stable than more eccentric motions. This could explain the fact that Uranus, whose eccentricity of 0.04 is significantly smaller than most asteroids from the asteroid belt, and which is roughly in 1 : 7-resonance with Jupiter (its period is 7.11 times larger than that of Jupiter) has not been expelled yet; see also Section 1.2.3. However, a deeper analysis would require to compare the distances of the various celestial bodies to the mean motion resonance, as well as the splitting of their invariant manifolds.

1.4.4 On Nekhoroshev's stability

Consider an analytic nearly integrable system of the form $H_\varepsilon(\theta, I) = H_0(I) + \varepsilon H_1(\theta, I)$ with $\theta \in \mathbb{T}^n$ and I in the unit ball B^n . Suppose H_0 is *convex* (or even suppose the weaker condition that H_0 is *steep*).⁶ Then a famous result of Nekhoroshev states that for some $c > 0$ independent of ε we have

$$|I(t) - I(0)| \lesssim \varepsilon^{1/2n} \quad \text{for} \quad |t| \lesssim \exp(c\varepsilon^{-1/2n}).$$

See for instance [Nie96] for the history and precise references and [Xue10] for the estimate on the involved constant c .

Niedermaier [Nie96] applied Nekhoroshev theory to the planetary N -body problem. He showed that the *semi major axis* obeys the above estimate for exponentially long time, $\exp(c\varepsilon^{-1/2n})$, with ε being the smallness of the planetary masses. However, the constant c along with other constants involved in the proof are not optimal. Specifically, ε needs to be as small as $3 \cdot 10^{-24}$ to have stability time comparable to the age of the Solar system. Moreover, the stability of semi major axis does not imply the stability of the eccentricity, which we conjecture has substantial deviations in polynomially long time.

Notice that our results along the predictions of Treschev's (see Appendix D) state the possibility of polynomial instability for eccentricities for the elliptic problem.

With $\varepsilon \sim \mu$, there was a hope to apply this result to the long time stability of e.g. the Sun-Jupiter-Saturn system; see [GG85]). However, (6) indicates absence of even $\mathcal{O}(\varepsilon^{-2})$ -stability. Indeed, the unperturbed Hamiltonian of the three body problem is neither convex, nor steep. This turns out to be not just a technical problem but a true obstruction to exponentially long time stability, since Nekhoroshev's theory does not apply to this kind of systems. See Appendix D for more details.

1.5 Mechanism of instability

The Main Result gives an example of large instability for this mechanical system. It can be interpreted as an example of Arnol'd diffusion; see [Arn64]. Nevertheless, Arnol'd diffusion usually refers to nearly integrable systems, whereas Hamiltonian (4) cannot be considered so close to integrable since $\mu = 10^{-3}$. The mechanism of diffusion used in this paper is similar to the so-called Mather's accelerating problem ([Mat96, BT99, DdlS00, GT08, Kal03, Pif06]). This analogy is explained in Section 2.3.

Arguably, the main source of instabilities are *resonances*. One of the most natural kind of resonances in the three-body problem is *mean motion orbital resonances*⁷. Along such a resonance, Jupiter and the asteroid will regularly be in the same relative position. Over a long time interval, Jupiter's perturbative effect could thus pile up and (despite its small amplitude due to the small mass of Jupiter) could modify the eccentricity of the asteroid, instead of averaging out.

According to Kepler's third Law, this resonance takes place when $a^{3/2}$ is close to a rational, where a is the semi major axis of the instant ellipse of the asteroid. In our case we consider $a^{3/2}$ *close to 7* in Section 1.8 and $a^{3/2}$ *close to 1/3* in appendix C. Nevertheless, we expect that the same mechanism takes place for a large number of mean motion orbital resonances.

⁶Recall that H_0 is called *steep* if for any affine subspace L of \mathbb{R}^n the restriction $H_0|_L$ has only isolated critical points.

⁷The mean motions are the frequencies of the Keplerian revolution of Jupiter and the asteroid around the Sun: in our case the asteroid makes one full revolution while Jupiter makes seven revolutions.

The semi major axis a and the eccentricity e describe completely an instant ellipse of the asteroid (up to orientation). Thus, geometrically the Main Results say that the asteroid evolves from a Keplerian ellipse of eccentricity $e = 0.48$ to one of eccentricity $e = 0.67$ (for the resonance $1 : 7$) and from $e = 0.59$ to $e = 0.91$ (for the resonance $3 : 1$), while keeping its semi major axis almost constant; see Figure 2. In Figure 3 we consider the plane (a, e) , which describes the ellipse of the asteroid. The diffusing orbits given by the Main Results correspond to nearly horizontal lines.

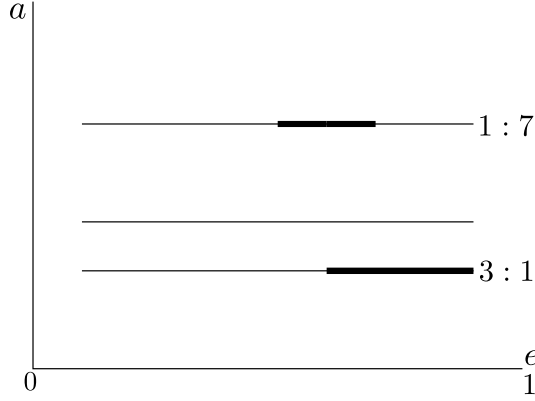


Figure 3: The diffusion path that we study in the (a, e) plane. The horizontal lines represent the resonances along which we drift. The thick segments are the diffusion paths whose existence we prove in this paper.

A qualitative description of such a diffusing orbit is given at the end of section 4.

1.6 Sketch of the proof

Our overall strategy is to:

- (A) Carefully study the structure of the restricted three-body problem along a chosen resonance.
- (B) Show that, generically within the class of problems sharing the same structure, global instabilities exist. One could say that this step is similar, in spirit, to “abstract” proofs of existence of instabilities for generic perturbations of a priori chaotic systems such as in Mather’s accelerating problem.
- (C) Check numerically that the generic conditions (which we call *Ansätze*) are satisfied in our case.

Step (B) is the core of the paper and we now give more details about it.

For the elliptic problem, the diffusing orbit that we are looking for lies in a neighborhood of a (3-dimensional) normally hyperbolic invariant cylinder Λ and its local invariant manifolds, which exist near our mean motion resonance. The vertical component of the cylinder can be parameterized by the eccentricity of the asteroid and the horizontal components by its mean longitude and time.

If the stable and unstable invariant manifolds of Λ intersect transversally, the elliptic problem induces two different dynamics on the cylinder (see Sections 3.4 and 3.5): *the inner and the outer dynamics*. The inner dynamics is simply the restriction of the Newtonian flow to Λ . The outer dynamics is obtained by a limiting process: it is observed asymptotically by starting very close to the cylinder and its unstable manifold, traveling all the way to a homoclinic intersection, and coming back close to the cylinder along its stable manifold; see Definition 2.3.

Since the system has different homoclinic orbits to the cylinder, one can define different outer dynamics. In our diffusing mechanism we use two different outer maps. The reason is that each of the outer maps fails to be defined in the whole cylinder, and so we need to combine the two of them to achieve diffusion; see Section 2.

The proof consists in the following five steps:

1. Construct a smooth family of hyperbolic periodic orbits for the circular problem with varying Jacobi integral (Ansatz 1).
2. Prove the existence of the normally hyperbolic invariant cylinder Λ , whose vertical size is lower bounded uniformly with respect to small values of e_0 (Corollary 2.1 and Theorem 2).
3. Establish the transversality of the stable and unstable invariant manifolds of this cylinder (Ansatz 1 and Theorem 2), a key feature to define a limiting “outer dynamics”, in addition to the inner dynamics, over Λ (section 2.3).
4. Compare the inner and outer dynamics on Λ and, in particular, check that they do not share any common invariant circles (Theorem 3 and 4). Then one can drift along Λ by alternating the inner and outer maps in a carefully chosen order [Moe02].
5. Construct diffusing orbits by shadowing such a polyorbit (Lemma 4.4).

This program faces difficulties at each step, as explained next.

1.6.1 Existence of a family of hyperbolic periodic orbits of the circular problem

This part is mainly numerical. Using averaging and the symmetry of the problem we guess a location of periodic orbits of a certain properly chosen Poincaré map of the circular problem. Then for an interval of Jacobi integral $[J_-, J_+]$ and each $J \in [J_-, J_+]$ we compute them numerically and verify that they are hyperbolic. For infinitesimally small μ hyperbolicity follows from averaging.

1.6.2 Existence of a normally hyperbolic invariant cylinder Λ

The first difficulty comes from the proper degeneracy of the Newtonian potential: at the limit $\mu = 0$ (no Jupiter), the asteroid has a one-frequency, Keplerian motion, whereas symplectic geometry allows for a three-frequency motion (as with any potential other than the Newtonian potential $1/r$ and the elastic potential r^2). Due to this degeneracy, switching to $\mu > 0$ (even with $e_0 = 0$) is a singular perturbation.

1.6.3 Transversality of the stable and unstable invariant manifolds

Establishing the transversality of the invariant manifolds of Λ , is a delicate problem, even for $e_0 = 0$. Asymptotically when $\mu \rightarrow 0$, the difference (splitting angle) between the invariant manifolds becomes exponentially small with respect to μ , that is of order $\exp(-c/\sqrt{\mu})$ for some constant $c > 0$. Despite inordinate efforts of specialists, all known techniques fail to estimate this splitting, because the relevant Poincaré-Melnikov integral is not algebraic. Note that this step is significantly simpler when one studies generic systems.

At the expense of creating other difficulties, setting $\mu = 10^{-3}$ avoids this splitting problem, since for this value of the parameter we see that the splitting of separatrices is not extremely small and can be detected by means of a computer. Besides, 10^{-3} is a realistic value of the mass ratio for the Sun-Jupiter model. Since the splitting of the separatrices varies smoothly with respect to the eccentricity e_0 of the primaries, it suffices to estimate the splitting for $e_0 = 0$, that is in the circular problem. *This is a key point for the numerical computation*, which thus remains relatively simple. On the other hand, in the next two steps it is crucial to have $e_0 > 0$, otherwise the KAM tori separates the Jacobi integral energy levels.

Moreover, recall that the cylinder Λ has two branches of both stable and unstable invariant manifolds (both originated by a family of periodic orbits of the circular problem, see Figures 17, 18 for 1 : 7 and Figures 26, 28 for 3 : 1). In certain regions, the intersection between one of the branches of the stable and unstable invariant manifolds is tangential, which prevents us from defining the outer map. Nevertheless, then we check that the other two branches intersect transversally and we define a different outer map. Thus, we combine the two outer maps depending on which branches of the invariant manifolds intersect transversally.

1.6.4 Asymptotic formulas for the outer and inner maps

Using classical perturbation theory and the specific properties of the underlying system, we reduce the inner and (the two different) outer dynamics to three 2-dimensional symplectic smooth maps of the form

$$\mathcal{F}_{e_0}^{\text{in}} : \begin{pmatrix} I \\ t \end{pmatrix} \mapsto \begin{pmatrix} I + e_0 (A^+(I, \mu)e^{it} + A^-(I, \mu)e^{-it}) + \mathcal{O}(\mu e_0^2) \\ t + \mu \mathcal{T}_0(I, \mu) + \mathcal{O}(\mu e_0) \end{pmatrix} \quad (7)$$

and

$$\mathcal{F}_{e_0}^{\text{out},*} : \begin{pmatrix} I \\ t \end{pmatrix} \mapsto \begin{pmatrix} I + e_0 (B^{*,+}(I, \mu)e^{it} + B^{*,,-}(I, \mu)e^{-it}) + \mathcal{O}(\mu e_0^2) \\ t + \mu \omega^*(I, \mu) + \mathcal{O}(\mu e_0) \end{pmatrix}, \quad * = \text{f, b}, \quad (8)$$

where (I, t) are conjugate variables which parameterize a connected component of the 3-dimensional normally hyperbolic invariant cylinder Λ intersected with a transversal Poincaré section, and $A^\pm, \mathcal{T}_0, B^{*,\pm}, \omega^*$ are smooth functions. The superindexes f and b stand for the forward and backward heteroclinic orbits that are used to define the outer maps. The choice of this notation will be clear in Section 2. Note that these maps are real and thus A^- and $B^{*,,-}$ are complex conjugate to A^+ and $B^{*,+}$ respectively.

1.6.5 Non-degeneracy implies the existence of diffusing orbits

As shown in Section 4, the existence of diffusing orbits is established provided that the smooth functions

$$\mathcal{K}^{*,+}(I, \mu) = B^{*,+}(I, \mu) - \frac{e^{i\mu\omega^*(I, \mu)} - 1}{e^{i\mu\mathcal{T}_0(I, \mu)} - 1} A^+(I, \mu) \quad * = \text{f, b} \quad (9)$$

do not vanish on the set $I \in [I_-, I_+]$ where the corresponding outer map is defined. Since A^+ and A^- are complex conjugate, as well as $B^{*,+}$ and $B^{*,,-}$, we do not need to consider the complex conjugate $\mathcal{K}^{*,,-}(I, \mu)$. We check numerically that $\mathcal{K}^{*,+}(I, \mu) \neq 0$ in their domain of definition. The conditions $\mathcal{K}^{*,+}(I, \mu) \neq 0$ imply the absence of common invariant curves for the inner and outer maps. This reduces the proof of the Main Result to shadowing, which therefore leads to the existence of diffusing orbits.

It turns out that, in this problem, *no large gaps* appear. This fact is not surprising since the elliptic problem has three time scales.

Finally, notice that the complex functions $\mathcal{K}^{*,+}(I, \mu)$ can be regarded as a 2-dimensional real-valued function depending smoothly on (I, μ) . If the dependence on μ is non-trivial, a complex valued function $\mathcal{K}^{*,+}(I, \mu)$ does not vanish at any point of its domain of definition except for a finite number of values μ .

1.7 Nature of numerics

In this section we outline which parts of the mechanism are based on numerics.

- On each 3-dimensional energy surface the circular problem has a well-defined Poincaré map $F_J : \Sigma_J \rightarrow \Sigma_J$ of a 2-dimensional cylinder Σ_J for a range of energies J . For each J in some interval $[J_-, J_+]$ we establish the existence of a saddle periodic orbit p_J such that $F_J^7(p_J) = p_J$.
- We show that for all $J \in [J_-, J_+]$ there are two intersections of $W^s(p_J)$ and $W^u(p_J)$. Each intersection is transversal for almost all values of J , but it becomes tangent at an exceptional (discrete) set of values of J . Nevertheless, we check that at least one of the two intersections is transversal for each $J \in [J_-, J_+]$; see Figure 15.
- Each transversal intersection q_J gives rise to a homoclinic orbit, denoted γ_J . For each $J \in [J_-, J_+]$ we compute several Melnikov integrals of certain quantities related to ΔH_{ell} along γ_J and p_J . Out of these integrals we compute the leading terms of the dynamics of the elliptic problem and verify a necessary condition for diffusion.

The precise hypotheses which are based on numerics are Ansätze 1, 2 (Section 2) and 3 (Section 4).

As seen in the appendices A-B, the numerical values that we deal with are several orders of magnitude larger than the estimated error of our computations, and therefore these computations are reliable. Moreover, all the computations that we perform are standard and low-dimensional.

1.8 Main theorem for the 1 : 7 resonance

The model of the Sun, Jupiter and a massless asteroid in Cartesian coordinates is given by the Hamiltonian (4). First, let us consider the case $\mu = 0$, that is, we consider Jupiter with zero mass. In this case, Jupiter and the asteroid do not influence each other and thus the system reduces to two uncoupled 2-body problems (Sun-Jupiter and Sun-asteroid) which are integrable.

Let us introduce the so-called Delaunay variables, denoted by (ℓ, L, \hat{g}, G) , which are angle-action coordinates of the Sun-asteroid system. The variable ℓ is the mean anomaly, L is the square root of the semi major axis, \hat{g} is the argument of the perihelion and G is the angular momentum. Delaunay variables are obtained from Cartesian variables via the following symplectic transformation (see [AKN88] for more details and background, or [Féj13, Appendix] for a straightforward definition). First define polar coordinates for the position:

$$q = (r \cos \phi, r \sin \phi).$$

Then, the actions of the Delaunay coordinates are defined by

$$-\frac{1}{2L^2} = \frac{\|p\|^2}{2} - \frac{1}{\|q\|} \quad \text{and} \quad G = -J - \frac{1}{2L^2} \quad (10)$$

(recall that $\mu = 0$ for these definitions). Using these actions, the eccentricity of the asteroid is expressed as

$$e = \sqrt{1 - \frac{G^2}{L^2}}. \quad (11)$$

To define the angles ℓ and \hat{g} , let v be the true anomaly, so that

$$\phi = v + \hat{g}. \quad (12)$$

Then, from v one can obtain the eccentric anomaly u using

$$\tan \frac{v}{2} = \sqrt{\frac{1+e}{1-e}} \tan \frac{u}{2}. \quad (13)$$

From the eccentric anomaly, the mean anomaly is given by Kepler's equation

$$u - e \sin u = \ell. \quad (14)$$

We apply the Delaunay change of coordinates given above to the elliptic problem; see Appendix B.1. In Delaunay coordinates, the Hamiltonian (4) can be split into the Keplerian part $-1/(2L^2)$, the circular part of the perturbing function $\mu \Delta H_{\text{circ}}$, and the remainder which vanishes when $e_0 = 0$:

$$\hat{H}(L, \ell, G, \hat{g} - t, t) = -\frac{1}{2L^2} + \mu \Delta H_{\text{circ}}(L, \ell, G, \hat{g} - t, \mu) + \mu e_0 \Delta H_{\text{ell}}(L, \ell, G, \hat{g} - t, t, \mu, e_0). \quad (15)$$

For $e_0 = 0$, the circular problem only depends on $\hat{g} - t$. To simplify the comparison with the circular problem, we consider rotating Delaunay coordinates, in which ΔH_{circ} is autonomous. Define the new angle $g = \hat{g} - t$ (the argument of the pericenter, measured in the rotating frame) and a new variable I conjugate to time t . Then we have

$$H(L, \ell, G, g, I, t) = -\frac{1}{2L^2} - G + \mu \Delta H_{\text{circ}}(L, \ell, G, g, \mu) + \mu e_0 \Delta H_{\text{ell}}(L, \ell, G, g, t, \mu, e_0) + I. \quad (16)$$

In these new variables, the difference in the number of degrees of freedom of the elliptic and circular problems becomes more apparent. When $e_0 = 0$ the system is autonomous and then I is constant, which corresponds to the conservation of the Jacobi integral (5). Therefore, the circular problem reduces to 2 degrees of freedom. Moreover, it will later be crucial to view the circular problem as an approximation of the elliptic one, in order to reduce the (possibly impracticable) numerical computations needed by a direct approach to the corresponding lower dimensional, and thus simpler, computations of the circular problem.

Recall that, in this section, we consider the 1 : 7 mean motion orbital resonance between Jupiter and the asteroid, that is, the period of the asteroid is approximately seven times the period of Jupiter. In rotating Delaunay variables, this corresponds to

$$\dot{\ell} \sim \frac{1}{7} \quad \text{and} \quad \dot{g} \sim -1. \quad (17)$$

A nearby resonance is $\dot{\ell} \sim \frac{1}{7}$ and $\dot{t} \sim 1$, but we stick to the previous one.

The resonance takes place when $L \sim 7^{1/3}$. We study the dynamics in a large neighborhood of this resonance and we show that one can drift along it. Namely, we find trajectories that keep L close to $7^{1/3}$ while the G -component changes noticeably. Using (11), we see that e also changes by order one. In this setting, the Main Result can be rephrased as follows.

Theorem 1. *Assume Ansätze 1, 2 and 3. Then there exists $e_0^* > 0$ such that for every e_0 with $0 < e_0 < e_0^*$, there exist $T > 0$ and an orbit of the Hamiltonian (16) which satisfy*

$$G(0) > 1.67 \text{ and } G(T) < 1.42$$

whereas

$$|L(t) - 7^{1/3}| \leq 0.007.$$

Ansätze 1 (Section 2), 2 (Section 2) and 3 (Section 4) are hypotheses which, broadly speaking, assert that the Hamiltonian (16) is in general position in some domain of the phase space; see also Section 1.7. They are backed up by the numerics in the appendices.

By definition the Hamiltonian (16) is autonomous and thus preserved. Hence, we will restrict ourselves to a level of energy which, without loss of generality, can be taken as $H = 0$. Therefore, since $|I - G| = \mathcal{O}(\mu)$, the drift in G is equivalent to the drift in I for orbits satisfying $|L(t) - 7^{1/3}| \leq 7\mu$.

The proof of Theorem 1 is structured as follows.

In Section 2, we study the dynamics of the circular problem ($e_0 = 0$). The Hamiltonian (16) becomes

$$H_{\text{circ}}(L, \ell, G, g) = -\frac{1}{2L^2} - G + \mu \Delta H_{\text{circ}}(L, \ell, G, g, \mu). \quad (18)$$

1. Ansatz 1 says that for an interval of Jacobi energies $[J_-, J_+]$ the circular problem has a smooth family of hyperbolic periodic orbits λ_J , whose stable and unstable manifolds intersect transversally for each $J \in [J_-, J_+]$.
2. Ansatz 2 asserts that the period of these periodic orbits changes monotonically with respect to the Jacobi integral.
3. Ansatz 3 asserts that Melnikov functions associated with symmetric homoclinic orbits created by the above periodic orbits are in general position.

Ansatz 1 implies the existence of a normally hyperbolic invariant cylinder (Corollary 2.1). Later in the section (Subsections 2.2 and 2.3) we calculate the aforementioned outer and inner maps for the circular problem (see (7) and (8)).

Then in Section 3 we consider the elliptic case ($0 < e_0 \ll 1$) as a perturbation of the circular case. Theorem 2 asserts that the normally hyperbolic invariant cylinder obtained for the circular problem persists, and its stable and unstable manifolds intersect transversally for each $J \in [J_- + \delta, J_+ - \delta]$ with small $\delta > 0$. These objects give rise to the inner and outer maps for the elliptic problem. Theorem 3 provides expansions for the inner and outer maps; see formulas (45) and (48) respectively.

Finally, in Section 4, Theorem 4 completes the proof of Theorem 1. This is done by comparing the inner and the two outer maps in Lemma 4.2 and constructing a transition chain of tori. Ansatz 3 ensures that the first order of the inner and outer maps of the elliptic problem are in general position. It turns out that in this problem there are **no large gaps**, due to the specific structure of times scales and the Fourier series involved. This contrasts with the typical situation near a resonance; see for instance [DdILS06].

Notation 1.4. *From now on, we omit the dependence on the mass ratio μ (keeping in mind the question of what would happen if we let μ vary). Recall that in this work we consider a realistic value $\mu = 10^{-3}$.*

2 The circular problem

2.1 Normally hyperbolic invariant cylinders

The circular problem is given by the Hamiltonian (16) with $e_0 = 0$. Since it does not depend on t , I is an integral of motion. We study the dynamics close to the resonance $7\ell + \dot{g} \sim 0$. Since t is a cyclic variable, we consider the two degree of freedom Hamiltonian of the circular problem H_{circ} , for which conservation of energy corresponds to conservation of the Jacobi constant (5).

Note that the circular problem is reversible with respect to the involution

$$\Psi(L, \ell, G, g, I, t) = (L, -\ell, G, -g, I, -t). \quad (19)$$

This symmetry facilitates several numerical computations.

Ansatz 1. Consider the Hamiltonian (18) with $\mu = 10^{-3}$. In every energy level $J \in [J_-, J_+] = [-1.81, -1.56]$, there exists a hyperbolic periodic orbit $\lambda_J = (L_J(t), \ell_J(t), G_J(t), g_J(t))$ of period T_J with

$$|T_J - 14\pi| < 60\mu,$$

such that

$$|L_J(t) - 7^{1/3}| < 7\mu$$

for all $t \in \mathbb{R}$. The periodic orbit and its period depend smoothly on J .

Every λ_J has two branches of stable and unstable invariant manifolds $W^{s,j}(\lambda_J)$ and $W^{u,j}(\lambda_J)$ for $j = 1, 2$. For every $J \in [J_-, J_+]$ either $W^{s,1}(\lambda_J)$ and $W^{u,1}(\lambda_J)$ intersect transversally or $W^{s,2}(\lambda_J)$ and $W^{u,2}(\lambda_J)$ intersect transversally.

This ansatz is backed up by the numerics of Appendix A.

We study the elliptic problem as a perturbation of the circular one. In contrast with Ansatz 1, in the perturbative setting we do *not* reduce the dimension of the phase space to study the inner and outer dynamics of the circular problem. Namely, we consider the *Extended Circular Problem* given by the Hamiltonian (16) with $e_0 = 0$. In other words, we keep the conjugate variables (I, t) even if t is a cyclic variable. Consider the energy level $H = 0$, so that $I = -H_{\text{circ}}(\ell, L, g, G)$. Therefore, the periodic orbits obtained in Ansatz 1 become invariant 2-dimensional tori which belong to constant hyperplanes $I = I_0$ for every

$$I_0 \in [I_-, I_+] = [-J_+, -J_-] = [1.56, 1.81]. \quad (20)$$

The union of these 2-dimensional invariant tori forms a normally hyperbolic invariant 3-dimensional manifold Λ_0 , diffeomorphic to a cylinder. Applying the implicit function theorem with the energy as a parameter, we see that the cylinder Λ_0 is analytic (by Ansatz 1, the periodic orbits are hyperbolic, thus non-degenerate).

Corollary 2.1. Assume Ansatz 1. The Hamiltonian (16) with $\mu = 10^{-3}$ and $e_0 = 0$ has an analytic normally hyperbolic invariant 3-dimensional cylinder Λ_0 , which is foliated by 2-dimensional invariant tori.

The cylinder Λ_0 has two branches of stable and unstable invariant manifolds, which we call $W^{s,j}(\Lambda_0)$ and $W^{u,j}(\Lambda_0)$ for $j = 1, 2$. In the constant invariant planes $I = I_0$, for every $I_0 \in [I_-, I_+]$ either $W^{s,1}(\Lambda_0)$ and $W^{u,1}(\Lambda_0)$ intersect transversally or $W^{s,2}(\Lambda_0)$ and $W^{u,2}(\Lambda_0)$ intersect transversally.

We define a global Poincaré section and work with maps to reduce the dimension by one. Two choices are natural: $\{t = 0\}$ and $\{g = 0\}$, since both variables t and g satisfy $\dot{t} \neq 0$ and $\dot{g} \neq 0$. We choose the section $\{g = 0\}$, with associated Poincaré map

$$\mathcal{P}_0 : \{g = 0\} \longrightarrow \{g = 0\}. \quad (21)$$

Since we are studying the resonance (17), the intersection of the cylinder Λ_0 with the section $\{g = 0\}$ is formed by seven cylinders (see Figure 4), denoted $\tilde{\Lambda}_0^j$, $j = 0, \dots, 6$. Namely,

$$\Lambda_0 \cap \{g = 0\} = \tilde{\Lambda}_0 = \bigcup_{j=0}^6 \tilde{\Lambda}_0^j. \quad (22)$$

As a whole, $\tilde{\Lambda}_0$ is a normally hyperbolic invariant manifold for the Poincaré map \mathcal{P}_0 . One can also consider the Poincaré map \mathcal{P}_0^7 —the seventh iterate of \mathcal{P}_0 . For this map, each $\tilde{\Lambda}_0^j$ is a normally hyperbolic invariant manifold (of course, so is their union). We focus on the connected components $\tilde{\Lambda}_0^j$ since they have a natural system of coordinates. This system of coordinates is used later to study the inner and outer dynamics on them. We particularly work with $\tilde{\Lambda}_0^3$ and $\tilde{\Lambda}_0^4$ for, in every invariant plane $I = I_0$, they are connected by at least one heteroclinic connection (of \mathcal{P}_0^7) that is symmetric with respect to the involution (19). We call it a *forward heteroclinic orbit* if it is asymptotic to $\tilde{\Lambda}_0^3$ in the past and $\tilde{\Lambda}_0^4$ in the future, and a *backward heteroclinic orbit* if it is asymptotic to $\tilde{\Lambda}_0^4$ in the past and $\tilde{\Lambda}_0^3$ in the future.

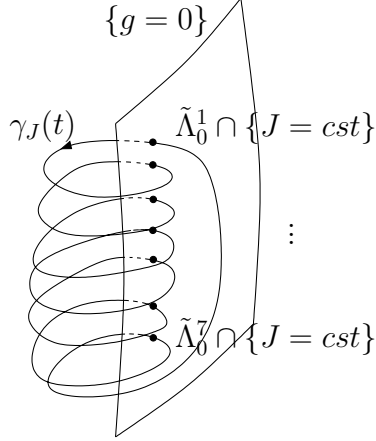


Figure 4: The periodic orbit obtained for every energy level intersects the Poincaré section $\{g = 0\}$ seven times, as shown schematically in this picture. Thus, for the Poincaré map \mathcal{P}_0 , the normally hyperbolic invariant manifold $\tilde{\Lambda}_0$ has seven connected components $\tilde{\Lambda}_0^0, \dots, \tilde{\Lambda}_0^6$.

Let \mathcal{D}^f (where f stands for forward) denote the subset of $[I_-, I_+]$ where $W^u(\tilde{\Lambda}_0^3)$ and $W^s(\tilde{\Lambda}_0^4)$ intersect transversally and let \mathcal{D}^b (where b stands for backward) denote the subset of $[I_-, I_+]$ where $W^s(\tilde{\Lambda}_0^3)$ and $W^u(\tilde{\Lambda}_0^4)$ intersect transversally. By Corollary 2.1 we have $\mathcal{D}^f \cup \mathcal{D}^b = [I_-, I_+]$.

Corollary 2.2. *Assume Ansatz 1. The Poincaré map \mathcal{P}_0^7 defined in (21), which is induced by the Hamiltonian (16) with $\mu = 10^{-3}$ and $e_0 = 0$, has seven analytic normally hyperbolic invariant manifolds $\tilde{\Lambda}_0^j$ for $j = 0, \dots, 6$. They are foliated by one-dimensional invariant curves. For each j , there exists an analytic function $\mathcal{G}_0^j : [I_-, I_+] \times \mathbb{T} \rightarrow (\mathbb{R} \times \mathbb{T})^3$,*

$$\mathcal{G}_0^j(I, t) = \left(\tilde{\mathcal{G}}_0^j(I), 0, I, t \right) = \left(\mathcal{G}_0^{j,L}(I), \mathcal{G}_0^{j,\ell}(I), \mathcal{G}_0^{j,G}(I), 0, I, t \right), \quad (23)$$

that parameterizes $\tilde{\Lambda}_0^j$:

$$\tilde{\Lambda}_0^j = \left\{ \mathcal{G}_0^j(I, t) : (I, t) \in [I_-, I_+] \times \mathbb{T} \right\}.$$

Moreover, the associated invariant manifolds $W^u(\tilde{\Lambda}_0^3)$ and $W^s(\tilde{\Lambda}_0^4)$ intersect transversally within the hypersurface $I = I_0$ provided $I_0 \in \mathcal{D}^f$. The manifolds $W^s(\tilde{\Lambda}_0^3)$ and $W^u(\tilde{\Lambda}_0^4)$ intersect transversally within the hypersurface $I = I_0$ provided $I_0 \in \mathcal{D}^b$. Within the hypersurface $I = I_0$, each of these intersections has one point on the symmetry axis of the involution (19). Let Γ_0^* , where $*$ = f, b, denote the set of transversal intersections on the symmetry axis. For both the forward and backward case, there exists an analytic function

$$\mathcal{C}_0^* : \mathcal{D}^* \times \mathbb{R} \rightarrow (\mathbb{R} \times \mathbb{T})^3, \quad (I, t) \mapsto \mathcal{C}_0^*(I, t), \quad * = f, b$$

that parameterizes Γ_0^* :

$$\Gamma_0^* = \left\{ \mathcal{C}_0^*(I, t) = (\mathcal{C}_0^{*,L}(I), \mathcal{C}_0^{*,\ell}(I), \mathcal{C}_0^{*,G}(I), 0, I, t) : (I, t) \in \mathcal{D}^* \times \mathbb{T} \right\}, \quad * = f, b.$$

The subscript 0 in the parameterizations \mathcal{G} and \mathcal{C} indicates the g -coordinate. We keep it although it is redundant in the Poincaré section because later we use these parameterizations in the full phase space.

Again, the implicit function theorem implies that $W^s(\tilde{\Lambda}_0^3)$ and $W^u(\tilde{\Lambda}_0^4)$ are analytic (taking the distance from the cylinder $\tilde{\Lambda}_0^3$ or $\tilde{\Lambda}_0^4$ as a small parameter, as in [Mey75] with the cylinder as factor variable).

Corollary 2.1 gives global coordinates (I, t) for each cylinder $\tilde{\Lambda}_0^j$. These coordinates are symplectic with respect to the canonical symplectic form

$$\Omega_0 = dI \wedge dt. \quad (24)$$

Indeed, consider the pullback of the canonical form $dL \wedge d\ell + dG \wedge dg + dI \wedge dt$ to the cylinders $\tilde{\Lambda}_0^j$. By Corollary 2.2 in the cylinders we have $g = 0$, $\ell = \mathcal{G}_0^{j,\ell}(I)$ and $L = \mathcal{G}_0^{j,L}(I)$. Then, it is easy to see that the pullback of $dL \wedge d\ell + dG \wedge dg + dI \wedge dt$ is just Ω_0 .

Next we consider the inner and the two outer maps in one of these cylinders. We choose $\tilde{\Lambda}_0^3$. As explained before, the reason is that the heteroclinic connections with the following cylinder $\tilde{\Lambda}_0^4$ intersect the symmetry axis of the involution (19) and thus they are easier to study numerically (see Figure 11). Since I is conserved by the inner and outer maps, these maps are integrable and the variables (I, t) are the action-angle variables. In these variables, it is easier to understand the influence of ellipticity.

2.2 The inner map

To study the diffusion mechanism, one could consider the normally hyperbolic invariant manifold $\tilde{\Lambda}_0 = \bigcup_{j=0}^6 \tilde{\Lambda}_0^j$. Nevertheless, since $\tilde{\Lambda}_0$ is not connected, it is more convenient to consider just one of the cylinders that form $\tilde{\Lambda}_0$, for instance $\tilde{\Lambda}_0^3$. Then the inner map $\mathcal{F}_0^{\text{in}} : \tilde{\Lambda}_0^3 \rightarrow \tilde{\Lambda}_0^3$ is defined as the analytic Poincaré map \mathcal{P}_0^7 restricted to the symplectic invariant submanifold $\tilde{\Lambda}_0^3$. We express $\mathcal{F}_0^{\text{in}}$ using the global coordinates (I, t) of $\tilde{\Lambda}_0^3$.

Since I is an integral of motion, the inner map has the form

$$\mathcal{F}_0^{\text{in}} : \begin{pmatrix} I \\ t \end{pmatrix} \mapsto \begin{pmatrix} I \\ t + \mu \mathcal{T}_0(I) \end{pmatrix}, \quad (25)$$

where the function \mathcal{T}_0 is independent of t because the inner map preserves the differential form (24), which does not depend on t , and I is a first integral. In fact, $14\pi + \mu \mathcal{T}_0(I)$ is the period of the periodic orbit obtained in Ansatz 1 on the corresponding energy surface. In Section 2.3, the function $\mathcal{T}_0(I)$ is written as an integral; see (38).

Ansatz 2. *The analytic symplectic inner map $\mathcal{F}_0^{\text{in}}$ defined in (25) is twist, that is*

$$\partial_I \mathcal{T}_0(I) \neq 0 \quad \text{for } I \in [I_-, I_+].$$

Moreover, the function $\mathcal{T}_0(I)$ satisfies

$$0 < \mu \mathcal{T}_0(I) < \pi. \quad (26)$$

This ansatz is based on the numerics of Appendix A. The ansatz is crucial in Section 4 to prove the existence of a transition chain of invariant tori.

2.3 The outer map

First we recall the construction of the outer map in a general perturbative setting. Next we apply it to the circular problem, and in section 3.1 to the elliptic problem. The outer map is sometimes called scattering map; see for instance [DdLS08].

Let \mathcal{P}_0 be a map of a compact manifold M . Let $\Lambda_0 \subset M$ be a normally hyperbolic invariant manifold of \mathcal{P}_0 , whose inner map $\mathcal{P}_0|_{\Lambda_0}$ has zero Lyapunov exponents: $\lim_{n \rightarrow +\infty} \ln \|d\mathcal{P}_0^n(z)v\|/n = 0$ for any $z \in \Lambda_0$ and $v \in T_z \Lambda_0$ (where $\|\cdot\|$ is some smooth Riemannian norm on M). Further assume that the stable and unstable invariant manifolds of Λ_0 intersect transversally.

Let \mathcal{P} be a small perturbation of \mathcal{P}_0 . Since Λ_0 is normally hyperbolic it persists under small perturbation of \mathcal{P}_0 . Let $\Lambda \subset M$ be a normally hyperbolic invariant manifold of \mathcal{P} .

Then, the outer map associated to \mathcal{P} and Λ (a particular case being $\mathcal{P} = \mathcal{P}_0$ and $\Lambda = \Lambda_0$) is defined over some domain as follows.

Definition 2.3. Assume that W_Λ^s and W_Λ^u intersect transversally along a homoclinic manifold Γ , that is

$$T_z W_\Lambda^s + T_z W_\Lambda^u = T_z M \quad \text{and} \quad T_z W_\Lambda^s \cap T_z W_\Lambda^u = T_z \Gamma \quad \text{for } z \in \Gamma.$$

Then, we say that $\mathcal{S}(x_-) = x_+$, if there exists a point $z \in \Gamma$ such that for some $C > 0$ we have

$$\text{dist}(\mathcal{P}^n(z), \mathcal{P}^n(x_\pm)) < C\lambda^{-|n|} \quad \text{for all } n \in \mathbb{Z}^\pm. \quad (27)$$

Condition (27) indeed defines a map $x_- \mapsto x_+$ locally uniquely, as justified in [DdlLS08].

Remark 2.4. Since Λ is normally hyperbolic, for every point $x \in \Lambda$ there are strong stable and unstable manifolds $W^{ss}(x)$ and $W^{su}(x)$. Then $\mathcal{S}(x_-) = x_+$ holds if and only if $W^{su}(x_-) \cap W^{ss}(x_+) \neq \emptyset$ and the intersection occurs on Γ .

When the Lyapunov exponents of the inner dynamics $\mathcal{P}|_\Lambda$ are positive, for the points x_- and x_+ to be still uniquely defined given $z \in \gamma$, λ must exceed the maximal Lyapunov exponent i.e., the convergence towards Λ must dominate the motion inside of Λ . Otherwise, one cannot distinguish if the orbit of z is (backward- or forward-) asymptotic to a point of Λ or to the stable manifold of this point.

Remark 2.5. If the Lyapunov exponents of the inner map $\mathcal{P}|_\Lambda$ are zero (and, in particular, of the unperturbed map \mathcal{P}_0), the outer map \mathcal{S} is C^∞ . If the Lyapunov exponents of the inner map are small (thus in particular for a map \mathcal{P} close enough to \mathcal{P}_0), the outer map is C^k , where k tends to infinity as the Lyapunov exponents tend to 0.

Strictly speaking, there is hardly any published regularity theorem from which these assertions follow directly. In order to prove them, one can first localize in the neighborhood of a small continuous set of hyperbolic periodic orbits of \mathcal{P}_0 , modify \mathcal{P} outside this neighborhood in order to embed the periodic orbits into a compact *invariant* normally hyperbolic cylinder, and characterize the stable and unstable manifolds of the modified system in terms of an equation of class C^k , the perturbative parameter being the distance from the invariant cylinder. Such arguments belong to the well understood theory of normally hyperbolic invariant manifolds, and we omit further details, referring to the techniques developed in [Fen72, Cha04], or [BKZ11, Appendix B] for a closer context.

We apply a variant of this definition to the dynamics of the circular problem (unperturbed case). As in the previous section, we look for an outer map that sends $\tilde{\Lambda}_0^3$ to itself. Now one has to be more careful since the transversal intersections obtained in Corollary 2.2 correspond to heteroclinic connections between $\tilde{\Lambda}_0^3$ and $\tilde{\Lambda}_0^4$ and between $\tilde{\Lambda}_0^4$ and $\tilde{\Lambda}_0^3$. Thus the outer maps induced by \mathcal{P}_0^7 do not leave $\tilde{\Lambda}_0^3$ invariant. To overcome this problem we compose these heteroclinic outer maps (denoted by \mathcal{S}^f and \mathcal{S}^b below) with the Poincaré map \mathcal{P}_0 as many times as necessary so that the composition sends $\tilde{\Lambda}_0^3$ to itself.

Therefore, the smooth outer maps $\mathcal{F}_0^{\text{out}, \pm}$ that we consider connect $\tilde{\Lambda}_0^3$ to itself and are defined as

$$\begin{aligned} \mathcal{F}_0^{\text{out}, f} &= \mathcal{P}_0^6 \circ \mathcal{S}^f : \tilde{\Lambda}_0^3 \longrightarrow \tilde{\Lambda}_0^3, \\ \mathcal{F}_0^{\text{out}, b} &= \mathcal{S}^b \circ \mathcal{P}_0 : \tilde{\Lambda}_0^3 \longrightarrow \tilde{\Lambda}_0^3, \end{aligned} \quad (28)$$

where \mathcal{S}^f is the outer map which connects $\tilde{\Lambda}_0^3$ and $\tilde{\Lambda}_0^4$ through $W^u(\tilde{\Lambda}_0^3) \cap W^s(\tilde{\Lambda}_0^4)$, and \mathcal{S}^b is the outer map which connects $\tilde{\Lambda}_0^4$ and $\tilde{\Lambda}_0^3$ through $W^u(\tilde{\Lambda}_0^4) \cap W^s(\tilde{\Lambda}_0^3)$. Note the abuse of notation since the forward and backward outer maps are only defined provided $I \in \mathcal{D}^f$ and $I \in \mathcal{D}^b$ respectively and not in the whole cylinder $\tilde{\Lambda}_0^3$.

The outer map is always exact symplectic; see [DdlLS08]. So, in the circular problem, since I is preserved, the outer maps are of the form

$$\mathcal{F}_0^{\text{out}, *}: \begin{pmatrix} I \\ t \end{pmatrix} \mapsto \begin{pmatrix} I \\ t + \mu\omega^*(I) \end{pmatrix}, \quad * = f, b. \quad (29)$$

Outer maps can be defined with either discrete or continuous time. Since the Poincaré-Melnikov theory is considerably simpler for flows than for maps, we compute $\mathcal{F}_0^{\text{out},*}$ using continuous time. Moreover, in Section 3.5 we also use flows to study the outer map of the elliptic problem as a perturbation of (29).

The outer map induced by the flow associated to Hamiltonian (16) with $e_0 = 0$ does not preserve the section $\{g = 0\}$ but the inner map does. We reparameterize the flow so that both maps preserve this section. This reparameterization corresponds to identifying the variable g with time and is given by

$$\begin{aligned} \frac{d}{ds}\ell &= \frac{\partial_L H}{-1 + \mu\partial_G \Delta H_{\text{circ}}} & \frac{d}{ds}L &= -\frac{\partial_\ell H}{-1 + \mu\partial_G \Delta H_{\text{circ}}} \\ \frac{d}{ds}g &= 1 & \frac{d}{ds}G &= -\frac{\partial_g H}{-1 + \mu\partial_G \Delta H_{\text{circ}}} \\ \frac{d}{ds}t &= \frac{1}{-1 + \mu\partial_G \Delta H_{\text{circ}}} & \frac{d}{ds}I &= 0 \end{aligned} \quad (30)$$

where H is Hamiltonian (16) with $e_0 = 0$. Notice that this reparameterization implies the change of direction of time. However, the geometric objects stay the same. In particular, the new flow also possesses the normally hyperbolic invariant cylinder obtained in Corollary 2.1 and its invariant manifolds.

We refer to this system as the *reduced circular problem*. We call it reduced because we identify g with the time s . Note that the right hand side of equation (30) does not depend on t . Let Φ_0^{circ} denote the flow associated to the (L, ℓ, G, g) components of equation (30) (which are independent of t and I). Componentwise it can be written as

$$\Phi_0^{\text{circ}}\{s, (L, \ell, G, g)\} = (\Phi_0^L\{s, (L, \ell, G, g)\}, \Phi_0^\ell\{s, (L, \ell, G, g)\}, \Phi_0^G\{s, (L, \ell, G, g)\}, g + s). \quad (31)$$

Then, the outer map is computed as follows. Let

$$\begin{aligned} \gamma_I^*(\sigma) &= \Phi_0^{\text{circ}}\{\sigma, (\mathcal{C}_0^{*,L}(I), \mathcal{C}_0^{*,\ell}(I), \mathcal{C}_0^{*,G}(I), 0)\}, \quad * = \text{f, b} \\ \lambda_I^j(\sigma) &= \Phi_0^{\text{circ}}\{\sigma, (\mathcal{G}_0^{j,L}(I), \mathcal{G}_0^{j,\ell}(I), \mathcal{G}_0^{j,G}(I), 0)\} \quad j = 3, 4 \end{aligned} \quad (32)$$

be trajectories of the circular problem. Every trajectory γ_I^* has the initial condition at the heteroclinic point of the Poincaré map \mathcal{P}_0^7 obtained in Ansatz 1 with action I , since \mathcal{C}_0^* is the parameterization of the intersection Γ_0^* given in Corollary 2.2. Every trajectory λ_I^j has the initial condition at the fixed point of the Poincaré map \mathcal{P}_0^7 , since \mathcal{G}_0^j is the parameterization of the invariant cylinder $\tilde{\Lambda}_0^j$ given in Corollary 2.2.

Lemma 2.6. *Assume Ansatz 1. The functions $\omega^{\text{f,b}}(I)$ involved in the definition of the outer maps in (29) are given by*

$$\omega^*(I) = \omega_{\text{out}}^*(I) + \omega_{\text{in}}^*(I),$$

where

$$\omega_{\text{out}}^*(I) = \omega_+^*(I) - \omega_-^*(I) \quad (33)$$

with

$$\begin{aligned} \omega_+^*(I) &= \lim_{N \rightarrow +\infty} \left(\int_0^{14N\pi} \frac{(\partial_G \Delta H_{\text{circ}}) \circ \gamma_I^*(\sigma)}{-1 + \mu(\partial_G \Delta H_{\text{circ}}) \circ \gamma_I^*(\sigma)} d\sigma + N\mathcal{T}_0(I) \right) \\ \omega_-^*(I) &= \lim_{N \rightarrow -\infty} \left(\int_0^{14N\pi} \frac{(\partial_G \Delta H_{\text{circ}}) \circ \gamma_I^*(\sigma)}{-1 + \mu(\partial_G \Delta H_{\text{circ}}) \circ \gamma_I^*(\sigma)} d\sigma + N\mathcal{T}_0(I) \right), \quad * = \text{f, b} \end{aligned} \quad (34)$$

and

$$\begin{aligned} \omega_{\text{in}}^{\text{f}}(I) &= \int_0^{-12\pi} \frac{(\partial_G \Delta H_{\text{circ}}) \circ \lambda_I^4(\sigma)}{-1 + \mu(\partial_G \Delta H_{\text{circ}}) \circ \lambda_I^4(\sigma)} d\sigma \\ \omega_{\text{in}}^{\text{b}}(I) &= \int_0^{-2\pi} \frac{(\partial_G \Delta H_{\text{circ}}) \circ \lambda_I^3(\sigma)}{-1 + \mu(\partial_G \Delta H_{\text{circ}}) \circ \lambda_I^3(\sigma)} d\sigma. \end{aligned} \quad (35)$$

(Recall that $\mathcal{T}_0(I)$ is defined by (25)).

Note that the minus sign in the limit of integration of $\omega_{\text{in}}^*(I)$ appears because the reparameterized flow (30) reverses time.

Using that the circular problem is symmetric with respect to (19) and that the heteroclinic points \mathcal{C}_0^f and \mathcal{C}_0^b belong to the symmetry axis, we find that $\omega_-^* = -\omega_+^*$, $*$ = f, b.

The geometric interpretation of $\omega^{f,b}(I)$ is that the t -shift occurs since the homoclinic orbits approach different points of the same invariant curve in the future and in the past. This shift is equivalent to the shift in t that appears in Mather's Problem [Mat96]. See, for instance, formula (2.1) in Theorem 2.1 of [DdlLS00] and the constants a and b used in formula (1.4) of [BT99].

Proof. We compute $\omega^f(I)$. The function $\omega^b(I)$ is computed analogously. Since the t -component of the reduced circular system (30) does not depend on t , its behavior is given by

$$\Phi_0^t\{s, (L, \ell, G, g, t)\} = t + \tilde{\Phi}_0\{s, (L, \ell, G, g)\}$$

where

$$\tilde{\Phi}_0\{s, (L, \ell, G, g)\} = \int_0^s \frac{1}{-1 + \mu \partial_G \Delta H_{\text{circ}}(\Phi_0^{\text{circ}}\{\sigma, (L, \ell, G, g)\})} d\sigma. \quad (36)$$

Note that, using this reduced flow, the inner map (25) is just the (-14π) -time map in the time s . Then, the original period of the periodic orbits obtained in Ansatz 1 is expressed using the reduced flow as

$$14\pi + \mu \mathcal{T}_0(I) = \int_0^{-14\pi} \frac{1}{-1 + \mu(\partial_G \Delta H_{\text{circ}}) \circ \lambda_I^3(\sigma)} d\sigma. \quad (37)$$

This allows us to define the function $\mathcal{T}_0(I)$ in (25) through integrals as

$$\mathcal{T}_0(I) = \int_0^{-14\pi} \frac{(\partial_G \Delta H_{\text{circ}}) \circ \lambda_I^3(\sigma)}{-1 + \mu(\partial_G \Delta H_{\text{circ}}) \circ \lambda_I^3(\sigma)} d\sigma. \quad (38)$$

Consider now a point $(\mathcal{C}_0^{f,L}(I), \mathcal{C}_0^{f,\ell}(I), \mathcal{C}_0^{f,G}(I), 0, I, t)$ in $W^u(\tilde{\Lambda}_0^3) \cap W^s(\tilde{\Lambda}_0^4) \cap \{g = 0\}$. Since the first four components are independent of t , this point is forward asymptotic (in the reparameterized time) to a point

$$(\mathcal{G}_0^{3,L}(I), \mathcal{G}_0^{3,\ell}(I), \mathcal{G}_0^{3,G}(I), 0, I, t + \mu \omega_+^f(I))$$

and backward asymptotic (in the reparameterized time) to a point

$$(\mathcal{G}_0^{4,L}(I), \mathcal{G}_0^{4,\ell}(I), \mathcal{G}_0^{4,G}(I), 0, I, t + \mu \omega_-^f(I)).$$

Using (36), the functions $\omega_{\pm}^f(I)$ can be defined as

$$\begin{aligned} \omega_+^f(I) &= \lim_{T \rightarrow +\infty} \int_0^T \left(\frac{1}{-1 + \mu(\partial_G \Delta H_{\text{circ}}) \circ \gamma_I^f(\sigma)} - \frac{1}{-1 + \mu(\partial_G \Delta H_{\text{circ}}) \circ \lambda_I^3(\sigma)} \right) d\sigma \\ \omega_-^f(I) &= \lim_{T \rightarrow -\infty} \int_0^T \left(\frac{1}{-1 + \mu(\partial_G \Delta H_{\text{circ}}) \circ \gamma_I^f(\sigma)} - \frac{1}{-1 + \mu(\partial_G \Delta H_{\text{circ}}) \circ \lambda_I^4(\sigma)} \right) d\sigma. \end{aligned} \quad (39)$$

Since the system is 14π -periodic in the time s due to the identification of s with g , it is more convenient to write these in integrals as

$$\begin{aligned} \omega_+^f(I) &= \lim_{N \rightarrow +\infty} \int_0^{14N\pi} \left(\frac{1}{-1 + \mu(\partial_G \Delta H_{\text{circ}}) \circ \gamma_I^f(\sigma)} - \frac{1}{-1 + \mu(\partial_G \Delta H_{\text{circ}}) \circ \lambda_I^3(\sigma)} \right) d\sigma. \\ \omega_-^f(I) &= \lim_{N \rightarrow -\infty} \int_0^{14N\pi} \left(\frac{1}{-1 + \mu(\partial_G \Delta H_{\text{circ}}) \circ \gamma_I^f(\sigma)} - \frac{1}{-1 + \mu(\partial_G \Delta H_{\text{circ}}) \circ \lambda_I^4(\sigma)} \right) d\sigma. \end{aligned}$$

Then, taking (37) into account, we obtain

$$\omega_{\pm}^f(I) = \lim_{N \rightarrow \pm\infty} \left(\int_0^{14N\pi} \frac{1}{-1 + \mu(\partial_G \Delta H_{\text{circ}}) \circ \gamma_I^f(\sigma)} d\sigma + N(14\pi + \mathcal{T}_0(I)) \right),$$

from which the formulas for ω_{\pm}^f in (34) follow.

Finally we compute $\omega_{\text{in}}^f(I)$. This term corresponds to the contribution of \mathcal{P}_0^6 to the outer map in formula (28). Then, taking into account that t is defined modulo 2π , it is straightforward to obtain $\omega_{\text{in}}^f(I)$ in (34). \square

3 The elliptic problem

Everything is now set up to study the elliptic problem. We obtain perturbative expansions of the inner and outer maps. To this end, we apply Poincaré-Melnikov techniques to the reduced elliptic problem, which is given by

$$\begin{aligned} \frac{d}{ds}\ell &= \frac{\partial_L H}{-1 + \mu\partial_G \Delta H_{\text{circ}} + \mu e_0 \partial_G \Delta H_{\text{ell}}} & \frac{d}{ds}L &= -\frac{\partial_\ell H}{-1 + \mu\partial_G \Delta H_{\text{circ}} + \mu e_0 \partial_G \Delta H_{\text{ell}}} \\ \frac{d}{ds}g &= 1 & \frac{d}{ds}G &= -\frac{\frac{\partial_g H}{\partial_g H}}{-1 + \mu\partial_G \Delta H_{\text{circ}} + \mu e_0 \partial_G \Delta H_{\text{ell}}} \\ \frac{d}{ds}t &= \frac{1}{-1 + \mu\partial_G \Delta H_{\text{circ}} + \mu e_0 \partial_G \Delta H_{\text{ell}}} & \frac{d}{ds}I &= -\frac{\mu e_0 \partial_t \Delta H_{\text{ell}}}{-1 + \mu\partial_G \Delta H_{\text{circ}} + \mu e_0 \partial_G \Delta H_{\text{ell}}}. \end{aligned} \quad (40)$$

This system is a perturbation of (30). One can study the inner map either with this system or with the system associated to the Hamiltonian (15). Nevertheless, to simplify the exposition we use only (40) for both the inner and outer maps. Again, we consider the Poincaré map associated with this system and the section $\{g = 0\}$,

$$\mathcal{P}_{e_0} : \{g = 0\} \longrightarrow \{g = 0\}, \quad (41)$$

which is a perturbation of (21).

Two main results are introduced in this section:

- Existence of a normally hyperbolic invariant manifold with transversal intersections of its stable and unstable invariant manifolds for the elliptic problem (Theorem 2).
- Computation of the e_0 -expansions of the inner and outer maps associated to it (Theorem 3).

Theorem 2 is a direct consequence of Corollary 2.2, because we study the elliptic problem as a perturbation of the circular one.

The proof of Theorem 3 consists of several steps. In Section 3.2 we obtain the e_0 -expansion of the elliptic Hamiltonian, and from it, in Section 3.3, we deduce some properties of the e_0 -expansion of the flow associated to the system (40). In Section 3.4 we analyze the normally hyperbolic invariant cylinders $\tilde{\Lambda}_{e_0}^j$, which are the perturbation of the cylinders $\tilde{\Lambda}_0^j$ obtained in Corollary 2.2. This allows us to derive formulas for the inner map, perturbative in e_0 . Finally, in Section 3.5 we use the expansions to compute the outer maps using Poincaré-Melnikov techniques. The inner and outer maps are defined over the cylinder $\tilde{\Lambda}_{e_0}^3$, which is e_0 -close to the cylinder $\tilde{\Lambda}_0^3$ of Corollary 2.2.

3.1 The specific form of the inner and outer maps

For e_0 small enough the flow associated to the Hamiltonian (16) has a normally hyperbolic invariant cylinder Λ_{e_0} , which is e_0 -close to Λ_0 given in Corollary 2.1. Analogously, the Poincaré map \mathcal{P}_{e_0} associated to this system has a normally hyperbolic invariant cylinder $\tilde{\Lambda}_{e_0} = \Lambda_{e_0} \cap \{g = 0\}$. Moreover, $\tilde{\Lambda}_{e_0}$ is formed by seven connected components $\tilde{\Lambda}_{e_0}^j$, $j = 0, \dots, 6$, which are e_0 -close to the cylinders $\tilde{\Lambda}_0^j$ obtained in Corollary 2.2.

Recall that, by Corollary 2.2, in the invariant planes $I = \text{constant}$ there are forward and backward transversal heteroclinic connections between $\tilde{\Lambda}_0^3$ and $\tilde{\Lambda}_0^4$ provided $I \in \mathcal{D}^f$ and $I \in \mathcal{D}^b$ respectively. For the elliptic problem and e_0 small enough we have transversal heteroclinic connections in slightly smaller domains. We define

$$\mathcal{D}_\delta^* = \{I \in \mathcal{D}^* : \text{dist}(I, \partial \mathcal{D}^*) > \delta\}, \quad * = f, b. \quad (42)$$

Theorem 2. *Let \mathcal{P}_{e_0} be the Poincaré map associated to the Hamiltonian (16) and the section $\{g = 0\}$. Assume Ansatz 1. For any $\delta > 0$, there exists $e_0^* > 0$ such that for $0 < e_0 < e_0^*$ the map $\mathcal{P}_{e_0}^7$ has seven normally hyperbolic locally⁸ invariant manifolds $\tilde{\Lambda}_{e_0}^j$, which are e_0 -close in the \mathcal{C}^1 -topology to $\tilde{\Lambda}_0^j$. There exist functions $\mathcal{G}_{e_0}^j : [I_- + \delta, I_+ - \delta] \times \mathbb{T} \rightarrow (\mathbb{R} \times \mathbb{T})^3$, $j = 0, \dots, 6$, which can be expressed in coordinates as*

$$\mathcal{G}_{e_0}^j(I, t) = (\mathcal{G}_{e_0}^{j,L}(I, t), \mathcal{G}_{e_0}^{j,\ell}(I, t), \mathcal{G}_{e_0}^{j,G}(I, t), 0, I, t), \quad (43)$$

that parameterize $\tilde{\Lambda}_{e_0}^j$. In other words $\tilde{\Lambda}_{e_0}^j$ is a graph over (I, t) defined as

$$\tilde{\Lambda}_{e_0}^j = \{\mathcal{G}_{e_0}(I, t) : (I, t) \in [I_- + \delta, I_+ - \delta] \times \mathbb{T}\}.$$

Moreover, the invariant manifolds $W^u(\tilde{\Lambda}_{e_0}^3)$ and $W^s(\tilde{\Lambda}_{e_0}^4)$ intersect transversally provided $I \in \mathcal{D}_\delta^f$ and the invariant manifolds $W^u(\tilde{\Lambda}_{e_0}^4)$ and $W^s(\tilde{\Lambda}_{e_0}^3)$ intersect transversally provided $I \in \mathcal{D}_\delta^b$. One of these intersections is e_0 -close in the \mathcal{C}^1 -topology to the manifolds $\Gamma_0^{f,b}$ defined in Corollary 2.2.

Let $\Gamma_{e_0}^{f,b}$ denote these intersections. There exist functions

$$\mathcal{C}_{e_0}^*(I, t) = (\mathcal{C}_{e_0}^{*,L}(I, t), \mathcal{C}_{e_0}^{*,\ell}(I, t), \mathcal{C}_{e_0}^{*,G}(I, t), 0, I, t), \quad * = f, b$$

that parameterize them; namely,

$$\Gamma_{e_0}^* = \{\mathcal{C}_{e_0}^*(I, t) : (I, t) \in [I_- + \delta, I_+ - \delta] \times \mathbb{T}\}, \quad * = f, b.$$

For the elliptic problem, the coordinates (I, t) are symplectic not with respect to the canonical symplectic form $dI \wedge dt$. Indeed, if we pull back the canonical form $dL \wedge d\ell + dG \wedge dg + dI \wedge dt$ to the cylinders $\Lambda_{e_0}^j$, we obtain the symplectic form

$$\Omega_{e_0}^j = \left(1 + e_0 a_1^j(I, t) + e_0^2 a_2^j(I, t) + e_0^3 a_{\geq}^j(I, t)\right) dI \wedge dt, \quad (44)$$

for certain functions $a_k^j : [I_-, I_+] \times \mathbb{T} \rightarrow \mathbb{R}$. The functions a_{\geq}^j are the e_0^3 Taylor remainders, and thus depend on e_0 even if we do not write explicitly this dependence to simplify notation.

Remark 3.1. The objects and maps of Theorem 2 have increasing regularity when e_0 tends to 0. Indeed, by Gronwall's inequality the Lyapunov exponents of Λ_{e_0} tend to zero with e_0 . So for every $k \geq 1$, if e_0 is small enough, the invariant manifold Λ_{e_0} and subsequent objects are of class C^k (see Remark 2.5). For the sake of simplicity, we do not henceforth emphasize regularity issues. The main point is that for e_0 small enough all objects of our construction are smooth enough, and in particular it is possible to apply the KAM theorem to the invariant manifolds $\tilde{\Lambda}_0^j$.

Remark 3.2. Theorem 2 only guarantees local invariance for $\tilde{\Lambda}_{e_0}^j$. Namely, the boundary might not be invariant. Nevertheless, in Section 4 we show the existence of invariant tori in $\tilde{\Lambda}_{e_0}^j$ that act as boundaries of $\tilde{\Lambda}_{e_0}^j$. Thanks to these tori, one can choose $\tilde{\Lambda}_{e_0}^j$ to be invariant. For this reason, we refer to $\tilde{\Lambda}_{e_0}^j$ as a normally hyperbolic invariant manifold.

Our analysis depends heavily on the harmonic structure of the various maps involved. Thus we need the following definition.

Notation 3.3. *For every function f that is 2π -periodic in t , let $\mathcal{N}(f)$ denote the set of integers $k \in \mathbb{Z}$ such that the k -th harmonic of f (possibly depending on other variables) is non-zero.*

⁸See remark right below.

One can define inner and outer maps in the invariant cylinder $\tilde{\Lambda}_{e_0}^3$ given in Theorem 2 as we have done in $\tilde{\Lambda}_0^3$ for the circular problem. The next sections are devoted to the perturbative analysis of these maps. We state here the main outcome.

Theorem 3. *Let \mathcal{P}_{e_0} be the Poincaré map associated to the Hamiltonian (16) and the section $\{g = 0\}$. Assume Ansatz 1. The normally hyperbolic invariant manifold $\tilde{\Lambda}_{e_0}^3$ given in Theorem 2 of the map $\mathcal{P}_{e_0}^7$ has associated inner and outer maps.*

- The inner map is of the form

$$\mathcal{F}_{e_0}^{\text{in}} : \begin{pmatrix} I \\ t \end{pmatrix} \mapsto \begin{pmatrix} I + e_0 A_1(I, t) + e_0^2 A_2(I, t) + \mathcal{O}(e_0^3) \\ t + \mu \mathcal{T}_0(I) + e_0 \mathcal{T}_1(I, t) + e_0^2 \mathcal{T}_2(I, t) + \mathcal{O}(e_0^3) \end{pmatrix}, \quad (45)$$

where the functions A_1 , A_2 , \mathcal{T}_1 , and \mathcal{T}_2 satisfy

$$\mathcal{N}(A_1) = \{\pm 1\}, \quad \mathcal{N}(A_2) = \{0, \pm 1, \pm 2\} \quad (46)$$

$$\mathcal{N}(\mathcal{T}_1) = \{\pm 1\}, \quad \mathcal{N}(\mathcal{T}_2) = \{0, \pm 1, \pm 2\}. \quad (47)$$

- The outer maps are of the form

$$\mathcal{F}_{e_0}^{\text{out},*} : \begin{pmatrix} I \\ t \end{pmatrix} \mapsto \begin{pmatrix} I + e_0 B^*(I, t) + \mathcal{O}(e_0^2) \\ t + \mu \omega^*(I) + \mathcal{O}(e_0) \end{pmatrix}, \quad * = \text{f, b}, \quad (48)$$

where the functions B^* satisfy

$$\mathcal{N}(B^*) = \{\pm 1\}. \quad (49)$$

3.2 The e_0 -expansion of the elliptic Hamiltonian

Now we expand ΔH_{ell} in (16) with respect to e_0 . These expansions are used in Sections 3.3, 3.4 and 3.5. The most important goal is to see which harmonics in t have e_0 and e_0^2 terms. Note that the circular problem is independent of t .

Define the function

$$\mathcal{B}(r, v, g, t) = \frac{1}{|r e^{i(v+g-t)} - r_0(t) e^{i v_0(t)}|}. \quad (50)$$

This function is the potential $|q - q_0(t)|^{-1}$ expressed in terms of $g = \hat{g} - t$, where \hat{g} is the argument of the perihelion, the true anomaly v of the asteroid defined in (12) and the radius r . The functions $r_0(t)$ and $v_0(t)$ are the radius and the true anomaly of Jupiter. The functions $r_0(t)$ and $v_0(t)$ are the only ones in the definition of \mathcal{B} that depend on e_0 .

Then, the perturbation in (15) is expressed as

$$\begin{aligned} \mu \Delta H_{\text{circ}}(L, \ell, G, g) + \mu e_0 \Delta H_{\text{ell}}(L, \ell, G, g, t) = & -\frac{1-\mu}{\mu} \mathcal{B}\left(-\frac{r}{\mu}, v, g, t\right) \\ & -\frac{\mu}{1-\mu} \mathcal{B}\left(\frac{r}{1-\mu}, v, g-t, t\right) + \frac{1}{r} \Big|_{(r,v)=(r(L,\ell,G),v(L,\ell,G))}. \end{aligned}$$

First we deduce some properties of the expansion of the function \mathcal{B} :

$$\mathcal{B}(r, v, g, t) = \mathcal{B}_0(r, v, g) + e_0 \mathcal{B}_1(r, v, g, t) + e_0^2 \mathcal{B}_2(r, v, g, t) + \mathcal{O}(e_0^3). \quad (51)$$

From these properties, we deduce the expansion of ΔH_{ell} .

Lemma 3.4. *The functions in the e_0 -expansion of \mathcal{B} have the following properties.*

- \mathcal{B}_0 satisfies $\mathcal{N}(\mathcal{B}_0) = \{0\}$.

- \mathcal{B}_1 satisfies $\mathcal{N}(\mathcal{B}_1) = \{\pm 1\}$ and is given by

$$\mathcal{B}_1(r, v, g, t) = -\frac{1}{2\Delta^3(r, v, g)} (2 \cos t - 3r \cos(v + g + t) + r \cos(v + g - t)), \quad (52)$$

where

$$\Delta(r, v, g) = (r^2 + 1 - 2r \cos(v + g))^{1/2}.$$

- \mathcal{B}_2 satisfies $\mathcal{N}(\mathcal{B}_2) = \{0, \pm 1, \pm 2\}$.

Note that the elliptic problem is a peculiar perturbation of the circular problem in the sense that the k -th e_0 -order has non-trivial t -harmonics at most up to order k . This fact is crucial when we compare the inner and outer dynamics in Section 4.

Proof of Lemma 3.4. We look for the e_0 -expansions of the functions $r_0(t)$ and $v_0(t)$ involved in the definition of \mathcal{B} . We obtain them using the eccentric, true and mean anomalies of Jupiter.

From the relation $t = u_0 - e_0 \sin u_0$ (see (14)), we obtain that

$$u_0(t) = t + e_0 \sin t + \frac{e_0^2}{2} \sin 2t + \mathcal{O}(e_0^3).$$

Then, using $r_0 = 1 - e_0 \cos u_0$,

$$r_0(t) = 1 - e_0 \cos t + e_0^2 \sin^2 t + \mathcal{O}(e_0^3).$$

For the eccentric anomaly we use

$$\tan \frac{v_0}{2} = \sqrt{\frac{1+e_0}{1-e_0}} \tan \frac{u_0}{2}$$

(see (94)), to obtain

$$v_0 = u_0 + e_0 \sin u_0 + e_0^2 \left(\frac{9}{2} \sin u_0 - 2 \sin 2u_0 \right) + \mathcal{O}(e_0^3)$$

and then

$$v_0(t) = t + 2e_0 \sin t + e_0^2 \left(\frac{9}{2} \sin t - \sin 2t \right) + \mathcal{O}(e_0^3).$$

Plugging $r_0(t)$ and $v_0(t)$ into (50), it can be easily seen that the expansion (51) satisfies all the properties of \mathcal{B}_0 , \mathcal{B}_1 and \mathcal{B}_2 stated in the lemma. \square

One can now easily study the first order expansion of ΔH_{ell} :

$$\Delta H_{\text{ell}} = \Delta H_{\text{ell}}^1 + e_0 \Delta H_{\text{ell}}^2 + \mathcal{O}(e_0^2).$$

(recall from formula (16) that one power of e_0 has already been factored out of the definition of ΔH_{ell}). In particular,

$$\begin{aligned} \Delta H_{\text{ell}}^1(L, \ell, G, g, t) = & -\frac{1-\mu}{\mu} \mathcal{B}_1 \left(-\frac{r(L, \ell, G)}{\mu}, v(L, \ell, G), g, t \right) \\ & - \frac{\mu}{1-\mu} \mathcal{B}_1 \left(\frac{r(L, \ell, G)}{1-\mu}, v(L, \ell, G), g, t \right), \end{aligned} \quad (53)$$

where \mathcal{B}_1 is the function defined in Lemma 3.4.

Corollary 3.5. *The functions in the e_0 -expansion of ΔH_{ell} satisfy*

$$\mathcal{N}(\Delta H_{\text{ell}}^1) = \{\pm 1\} \quad \text{and} \quad \mathcal{N}(\Delta H_{\text{ell}}^2) = \{0, \pm 1, \pm 2\}.$$

3.3 Perturbative analysis of the flow

Before studying the inner and outer maps perturbatively, we need to study the first orders with respect to e_0 of the flow $\Phi_{e_0}\{s, (L, \ell, G, g, I, t)\}$ associated to the vector field (40), particularly their dependence on the variable t . Recall that we already know the dependence on t of the 0-order thanks to formulas (31) and (36).

Lemma 3.6. *The flow $\Phi_{e_0}\{s, (L, \ell, G, g, I, t)\}$ has a perturbative expansion*

$$\begin{aligned} \Phi_{e_0}\{s, (L, \ell, G, g, I, t)\} = & \Phi_0\{s, (L, \ell, G, g, I, t)\} + e_0\Phi_1\{s, (L, \ell, G, g, I, t)\} \\ & + e_0^2\Phi_2\{s, (L, \ell, G, g, I, t)\} + \mathcal{O}(e_0^3) \end{aligned}$$

that satisfies

$$\mathcal{N}(\Phi_1\{s, (L, \ell, G, g, I, t)\}) = \{\pm 1\} \quad (54)$$

$$\mathcal{N}(\Phi_2\{s, (L, \ell, G, g, I, t)\}) = \{0, \pm 1, \pm 2\}. \quad (55)$$

Proof. Let $z = (L, \ell, G, g, I)$ and let \mathcal{X}_{e_0} denote the vector field (40), which has expansion

$$\mathcal{X}_{e_0} = \mathcal{X}_0 + e_0\mathcal{X}_1 + e_0^2\mathcal{X}_2 + \mathcal{O}(e_0^3).$$

First we prove (54). The e_0 -order Φ_1 is a solution of the ordinary differential equation

$$\frac{d}{ds}\xi = D\mathcal{X}_0(\Phi_0\{s, (z, t)\})\xi + \mathcal{X}_1(\Phi_0\{s, (z, t)\})$$

with initial condition $\xi(0) = (0, 0)$. By (30), \mathcal{X}_0 is independent of t and thus,

$$D\mathcal{X}_0(\Phi_0\{s, (z, t)\}) = D\mathcal{X}_0(\Phi_0^{\text{circ}}(s, z)),$$

where Φ_0^{circ} is defined in (31). Then, this term is also independent of t . From Corollary 3.5, we deduce that $\mathcal{N}(\mathcal{X}_1) = \{\pm 1\}$ and thus \mathcal{X}_1 is written as

$$\mathcal{X}_1(z, t) = \mathcal{X}_1^+(z)e^{it} + \mathcal{X}_1^-(z)e^{-it},$$

Therefore, using formulas (31) and (36), we have

$$\mathcal{X}_1(\Phi_0\{s, (z, t)\}) = \left(\mathcal{X}_1^+(\Phi_0^{\text{circ}}\{s, z\})e^{i\tilde{\Phi}_0\{s, z\}}\right)e^{it} + \left(\mathcal{X}_1^-(\Phi_0^{\text{circ}}\{s, z\})e^{i\tilde{\Phi}_0\{s, z\}}\right)e^{-it}.$$

To prove (54), it is enough to use variation of constants formula. Consider $M_z(s)$, the fundamental matrix of the linear equation

$$\frac{d}{ds}\xi = D\mathcal{X}_0(\Phi_0^{\text{circ}}(s, z))\xi.$$

Then

$$\Phi_1\{s, (z, t)\} = \Phi_1^+\{s, z\}e^{it} + \Phi_1^-\{s, z\}e^{-it}$$

with

$$\Phi_1^\pm\{s, z\} = M_z(s) \int_0^s M_z^{-1}(\sigma) \left(\mathcal{X}_1^\pm(\Phi_0^{\text{circ}}\{s, z\})e^{\pm i\tilde{\Phi}_0\{s, z\}}\right) d\sigma.$$

The proof of (55) follows the same lines. Indeed, Φ_2 is a solution of an equation of the form

$$\frac{d}{ds}\xi = D\mathcal{X}_0(\Phi_0^{\text{circ}}\{s, z\})\xi + \Xi(s, g, I, t)$$

with initial condition $\xi(0) = (0, 0, 0)$. The function Ξ is given in terms of the previous orders of \mathcal{X}_{e_0} and Φ_{e_0} as

$$\Xi = \frac{1}{2}D^2\mathcal{X}_0(\Phi_0^{\text{circ}})(\Phi_1)^{\otimes 2} + D\mathcal{X}_1(\Phi_0^{\text{circ}})\Phi_1 + \mathcal{X}_2(\Phi_0^{\text{circ}}),$$

so it satisfies $\mathcal{N}(\Xi) = \{0, \pm 1, \pm 2\}$. Since the homogeneous linear equation is the same as the one for Φ_1 and does not depend on t , we easily obtain (55). \square

3.4 Perturbative analysis of the invariant cylinder and its inner map

This section is devoted to studying the normally hyperbolic invariant manifold of the elliptic problem $\tilde{\Lambda}_{e_0}^3$, whose existence was proved in Theorem 2, and the associated inner map. We study the inner map of the elliptic problem as a perturbation of (25), taking e_0 as the small parameter. The inner map is denoted by $\mathcal{F}_{e_0}^{\text{in}} : \tilde{\Lambda}_{e_0}^3 \rightarrow \tilde{\Lambda}_{e_0}^3$. It is defined as the (-14π) -Poincaré map of the flow Φ_{e_0} , given in Lemma 3.6, restricted to $\tilde{\Lambda}_{e_0}^3$.

We want to see which t -harmonics appear in the first orders of the inner map, and we also want to compute the first order of the I -component. To this end we use the classical theory of normally hyperbolic invariant manifolds [Fen74, Fen77]. This theory ensures the existence of the functions $\mathcal{G}_{e_0}^j$ parameterizing the normally hyperbolic manifolds $\tilde{\Lambda}_{e_0}^j$ of the map $\mathcal{P}_{e_0}^7$. Moreover, they can be made unique imposing

$$\pi_I \mathcal{G}_{e_0}^j(I, t) = I \quad \text{and} \quad \pi_t \mathcal{G}_{e_0}^j(I, t) = t, \quad (56)$$

where π_* is the projection with respect to the corresponding component of the function. Since we only need the cylinder $\tilde{\Lambda}_{e_0}^3$ and the dynamics on it, we consider the case $j = 3$. The map $\mathcal{G}_{e_0}^3$ satisfies the invariance equation

$$\tilde{\mathcal{P}}_{e_0} \circ \mathcal{G}_{e_0}^3 = \mathcal{G}_{e_0}^3 \circ \mathcal{F}_{e_0}^{\text{in}}, \quad (57)$$

where $\tilde{\mathcal{P}}_{e_0} = \mathcal{P}_{e_0}^7$ and $\mathcal{F}_{e_0}^{\text{in}}$ is the inner map of the elliptic problem, namely the Poincaré map $\mathcal{P}_{e_0}^7$ restricted to the cylinder $\tilde{\Lambda}_{e_0}^3$.

Since we have regularity with respect to parameters, the invariance equation allows us to obtain expansions of the parameterizations of both $\tilde{\Lambda}_{e_0}^3$ and the inner map $\mathcal{F}_{e_0}^{\text{in}}$ with respect to e_0 . Let us expand $\mathcal{G}_{e_0}^3$ and $\mathcal{F}_{e_0}^{\text{in}}$ as

$$\mathcal{G}_{e_0}^3 = \mathcal{G}_0^3 + e_0 \mathcal{G}_1^3 + e_0^2 \mathcal{G}_2^3 + \mathcal{O}(e_0^3) \quad (58)$$

$$\mathcal{F}_{e_0}^{\text{in}} = \mathcal{F}_0^{\text{in}} + e_0 \mathcal{F}_1^{\text{in}} + e_0^2 \mathcal{F}_2^{\text{in}} + \mathcal{O}(e_0^3). \quad (59)$$

Then, \mathcal{G}_0^3 is the function defined in (23) and $\mathcal{F}_0^{\text{in}}$ is the inner map of the circular problem obtained in (25), which is defined in $\tilde{\Lambda}_0^3$. Recall that

$$\tilde{\mathcal{P}}_{e_0}(L, \ell, G, 0, I, t) = \mathcal{P}_{e_0}^7(L, \ell, G, 0, I, t) = \Phi_{e_0}\{-14\pi, (L, \ell, G, 0, I, t)\}. \quad (60)$$

Then we have

$$\mathcal{N}(\tilde{\mathcal{P}}_1) = \{\pm 1\} \quad \text{and} \quad \mathcal{N}(\tilde{\mathcal{P}}_2) = \{0, \pm 1, \pm 2\}.$$

Expanding equation (57) with respect to e_0 , we deduce the properties of the inner map. They are summarized in the next lemma, which reproduces the part of Theorem 3 referring to the inner dynamics.

Recall that $\lambda_I^3(\sigma)$ has been defined in (32), $\tilde{\Phi}_0$ in (36) and \mathcal{G}_0^3 in Corollary 2.2.

Lemma 3.7. *Assume Ansatz 1. The expansions of the functions $\mathcal{G}_{e_0}^3$ and $\mathcal{F}_{e_0}^{\text{in}}$ in (58) and (59) satisfy that*

$$\mathcal{N}(\mathcal{G}_1^3) = \{\pm 1\} \quad \text{and} \quad \mathcal{N}(\mathcal{G}_2^3) = \{0, \pm 1, \pm 2\}$$

and

$$\mathcal{N}(\mathcal{F}_1^{\text{in}}) = \{\pm 1\} \quad \text{and} \quad \mathcal{N}(\mathcal{F}_2^{\text{in}}) = \{0, \pm 1, \pm 2\}.$$

Namely, the inner map is of the form

$$\mathcal{F}_{e_0}^{\text{in}} : \begin{pmatrix} I \\ t \end{pmatrix} \mapsto \begin{pmatrix} I + e_0 A_1(I, t) + e_0^2 A_2(I, t) + \mathcal{O}(\mu e_0^3) \\ t + \mu \mathcal{T}_0(I) + e_0 \mathcal{T}_1(I, t) + e_0^2 \mathcal{T}_2(I, t) + \mathcal{O}(\mu e_0^2) \end{pmatrix}, \quad (61)$$

where the functions A_1 , A_2 , \mathcal{T}_1 and \mathcal{T}_2 satisfy

$$\mathcal{N}(A_1) = \{\pm 1\}, \quad \mathcal{N}(A_2) = \{0, \pm 1, \pm 2\} \quad (62)$$

$$\mathcal{N}(\mathcal{T}_1) = \{\pm 1\}, \quad \mathcal{N}(\mathcal{T}_2) = \{0, \pm 1, \pm 2\}. \quad (63)$$

Moreover A_1 can be split as

$$A_1(I, t) = A_1^+(I)e^{it} + A_1^-(I)e^{-it},$$

with

$$A_1^\pm(I) = \mp i\mu \int_0^{-14\pi} \frac{\Delta H_{\text{ell}}^{1,\pm} \circ \lambda_I^3(\sigma)}{-1 + \mu \partial_G \Delta H_{\text{circ}} \circ \lambda_I^3(\sigma)} e^{\pm i\tilde{\lambda}_I^3(\sigma)} d\sigma, \quad (64)$$

where the functions $\Delta H_{\text{ell}}^{1,\pm}$ are defined as

$$\Delta H_{\text{ell}}^1(L, \ell, G, g, t) = \Delta H_{\text{ell}}^{1,+}(L, \ell, G, g)e^{it} + \Delta H_{\text{ell}}^{1,\pm}(L, \ell, G, g)e^{-it},$$

and

$$\tilde{\lambda}_I^3(\sigma) = \tilde{\Phi}_0\{\sigma, (\mathcal{G}_0^{3,L}(I), \mathcal{G}_0^{3,\ell}(I), \mathcal{G}_0^{3,G}(I), 0)\}. \quad (65)$$

From the properties of $\mathcal{G}_{e_0}^3$, we deduce the properties of the symplectic form $\Omega_{e_0}^3$ defined on the cylinder $\tilde{\Lambda}_{e_0}^3$. Recall that $\Omega_{e_0}^3$ is the pullback of the symplectic form $dL \wedge d\ell + dG \wedge dg + dI \wedge dt$ on the invariant cylinder $\tilde{\Lambda}_{e_0}^3$. In equation (44) we called a_j^3 the coefficients of its expansion:

$$\Omega_{e_0}^3 = (1 + e_0 a_1^3(I, t) + e_0^2 a_2^3(I, t) + e_0^3 a_{\geq}^3(I, t)) dI \wedge dt.$$

Corollary 3.8. *Assuming Ansatz 1, the functions a_1^3 and a_2^3 satisfy*

$$\mathcal{N}(a_1^3) = \{\pm 1\} \quad \text{and} \quad \mathcal{N}(a_2^3) = \{0, \pm 1, \pm 2\}.$$

Proof of Lemma 3.7. In the proof we omit the superscript 3 of the terms in the expansion of $\mathcal{G}_{e_0}^3$. Expanding equation (57) with respect to e_0 , we have that the first terms satisfy

$$\tilde{\mathcal{P}}_0 \circ \mathcal{G}_0 = \mathcal{G}_0 \circ \mathcal{F}_0^{\text{in}} \quad (66)$$

$$\tilde{\mathcal{P}}_1 \circ \mathcal{G}_0 + (D\tilde{\mathcal{P}}_0 \circ \mathcal{G}_0) \mathcal{G}_1 = \mathcal{G}_1 \circ \mathcal{F}_0^{\text{in}} + (D\mathcal{G}_0 \circ \mathcal{F}_0^{\text{in}}) \mathcal{F}_1^{\text{in}} \quad (67)$$

$$\begin{aligned} \tilde{\mathcal{P}}_2 \circ \mathcal{G}_0 + (D\tilde{\mathcal{P}}_1 \circ \mathcal{G}_0) \mathcal{G}_1 + \frac{1}{2} (D^2 \tilde{\mathcal{P}}_0 \circ \mathcal{G}_0) \mathcal{G}_1^{\otimes 2} + \\ + (D\tilde{\mathcal{P}}_0 \circ \mathcal{G}_0) \mathcal{G}_2 = \mathcal{G}_2 \circ \mathcal{F}_0^{\text{in}} + (D\mathcal{G}_1 \circ \mathcal{F}_0^{\text{in}}) \mathcal{F}_1^{\text{in}} \\ + \frac{1}{2} (D^2 \mathcal{G}_0 \circ \mathcal{F}_0^{\text{in}}) (\mathcal{F}_1^{\text{in}})^{\otimes 2} + (D\mathcal{G}_0 \circ \mathcal{F}_0^{\text{in}}) \mathcal{F}_2^{\text{in}}. \end{aligned} \quad (68)$$

By the uniqueness condition (56), \mathcal{G}_1 is of the form

$$\mathcal{G}_1(g, I, t) = (\tilde{\mathcal{G}}_1(g, I, t), 0, 0, 0)$$

with $\tilde{\mathcal{G}}_1(g, I, t) = (\mathcal{G}_1^L(g, I, t), \mathcal{G}_1^\ell(g, I, t), \mathcal{G}_1^G(g, I, t))$.

Equation (66) corresponds to the inner dynamics of the circular problem. We use equations (67) and (68) to deduce the properties of $\mathcal{F}_1^{\text{in}}$ and $\mathcal{F}_2^{\text{in}}$ respectively. These equations can be solved iteratively starting with (67). Since

$$D\mathcal{G}_0 = \begin{pmatrix} D\tilde{\mathcal{G}}_0 \\ \text{Id} \end{pmatrix} \quad \text{and} \quad D\mathcal{G}_i = \begin{pmatrix} D\tilde{\mathcal{G}}_i \\ 0 \end{pmatrix} \quad \text{for } i \geq 1, \quad (69)$$

we have

$$\mathcal{F}_1^{\text{in},*} = \pi_* \left(\tilde{\mathcal{P}}_1 \circ \mathcal{G}_0 + (D\tilde{\mathcal{P}}_0 \circ \mathcal{G}_0) \tilde{\mathcal{G}}_1 \right), \quad * = I, t.$$

Replacing this into (67) we obtain an equation for \mathcal{G}_1 . The equation for every Fourier t -coefficient is uncoupled. Hence, using the definition (60), the t -independence of $\tilde{\mathcal{P}}_0$, and the uniqueness of \mathcal{G}_1 , we deduce that $\mathcal{N}(\mathcal{G}_1) = \{\pm 1\}$. As a consequence we have $\mathcal{N}(\mathcal{F}_1^{\text{in}}) = \{\pm 1\}$.

Reasoning analogously and using (60) again, we see that $\mathcal{N}(\mathcal{G}_2) = \{0, \pm 1, \pm 2\}$ and $\mathcal{N}(\mathcal{F}_2^{\text{in}}) = \{0, \pm 1, \pm 2\}$.

Now it only remains to prove formula (64). Recall that the I -component of the inner map can be written as

$$\mathcal{F}_{e_0}^{\text{in}, I}(I, t) = \Phi_{e_0}^I \{-14\pi, \mathcal{G}_{e_0}(I, t)\}$$

since it is defined as the (-14π) -Poincaré map associated to the flow of system (40) restricted to the cylinder $\tilde{\Lambda}_{e_0}^3$. Recall that the minus sign in the time appears because the system (40) has the time reversed with respect to the original one. Then, we apply the Fundamental Theorem of Calculus and use (40) to obtain

$$\begin{aligned} \mathcal{F}_{e_0}^{\text{in}, I}(I, t) &= \int_0^{-14\pi} \frac{d}{ds} \Phi_{e_0}^I \{s, \mathcal{G}_{e_0}(I, t)\} ds \\ &= - \int_0^{-14\pi} \frac{\mu e_0 \partial_t \Delta H_{\text{ell}} \circ \Phi_{e_0} \{s, \mathcal{G}_{e_0}(I, t)\}}{-1 + \mu \partial_G \Delta H_{\text{circ}} \circ \Phi_{e_0} \{s, \mathcal{G}_{e_0}(I, t)\} + \mu e_0 \partial_g \Delta H_{\text{ell}} \circ \Phi_{e_0} \{s, \mathcal{G}_{e_0}(I, t)\}} ds. \end{aligned}$$

From the expansions of the Hamiltonian ΔH_{ell} (Corollary 3.5), of the flow Φ_{e_0} (Lemma 3.6) and of the function \mathcal{G}_{e_0} just obtained, we deduce

$$\mathcal{F}_{e_0}^{\text{in}, I}(I, t) = -e_0 \int_0^{-14\pi} \frac{\mu \partial_t \Delta H_{\text{ell}}^1 \circ \Phi_0 \{s, \mathcal{G}_0(I, t)\}}{-1 + \mu \partial_G \Delta H_{\text{circ}} \circ \Phi_0 \{s, \mathcal{G}_0(I, t)\}} ds + \mathcal{O}(e_0^2).$$

That is,

$$A_1(I, t) = - \int_0^{-14\pi} \frac{\mu \partial_t \Delta H_{\text{ell}}^1 \circ \Phi_0 \{s, \mathcal{G}_0(I, t)\}}{-1 + \mu \partial_G \Delta H_{\text{circ}} \circ \Phi_0 \{s, \mathcal{G}_0(I, t)\}} ds.$$

To deduce the formulas for A_1^\pm it is enough to split ΔH_{ell}^1 as

$$\Delta H_{\text{ell}}^1(L, \ell, G, g, t) = \Delta H_{\text{ell}}^{1,+}(L, \ell, G, g) e^{it} + \Delta H_{\text{ell}}^{1,\pm}(L, \ell, G, g) e^{-it},$$

and recall that, by formulas (31) and (36), Φ_0 can be written as

$$\Phi_0 \{s, (L, \ell, G, g, I, t)\} = \left(\Phi_{\text{circ}} \{s, (L, \ell, G, g, I)\}, t + \tilde{\Phi}_0 \{s, (L, \ell, G, g, I)\} \right).$$

□

3.5 The outer map

This section is devoted to studying the outer maps

$$\mathcal{F}_{e_0}^{\text{out},*} : \tilde{\Lambda}_{e_0}^3 \longrightarrow \tilde{\Lambda}_{e_0}^3, \quad * = \text{f, b} \quad (70)$$

for $e_0 > 0$.

Theorem 2 in Section 3.1 proves the existence of $\Gamma_{e_0}^*$ for $* = \text{f, b}$, transversal intersections between the invariant manifolds of $\tilde{\Lambda}_{e_0}^3$ and $\tilde{\Lambda}_{e_0}^4$. We proceed as in Section 2.3 to define the outer map $\mathcal{F}_{e_0}^{\text{out}}$. We study it as a perturbation of the outer map of the circular problem given in (29), using Poincaré-Melnikov techniques. As explained in Section 2.3, the original flow associated to the Hamiltonian (15) does not allow us to study perturbatively $\mathcal{F}_{e_0}^{\text{out}}$. Instead, we use the reduced elliptic problem defined in (40).

The results stated in Theorem 3 about the outer map follow from the next lemma. The lemma also shows how to compute the first order term of the outer map. We use the same notation as in Section 2.3. In particular, we use the trajectories of the circular problem $\gamma_I^{\text{f}, \text{b}}(\sigma)$ and $\lambda_I^{3,4}(\sigma)$ defined in (32), and we define their corresponding t -component of the flow as

$$\begin{aligned} \tilde{\gamma}_I^*(\sigma) &= \tilde{\Phi}_0 \{\sigma, (\mathcal{C}_0^{*,L}(I), \mathcal{C}_0^{*,\ell}(I), \mathcal{C}_0^{*,G}(I), 0)\}, \quad * = \text{f, b} \\ \tilde{\lambda}_I^j(\sigma) &= \tilde{\Phi}_0 \{\sigma, (\mathcal{G}_0^{j,L}(I), \mathcal{G}_0^{j,\ell}(I), \mathcal{G}_0^{j,G}(I), 0)\}, \quad j = 3, 4 \end{aligned} \quad (71)$$

where $\tilde{\Phi}_0$ is defined in (36) and \mathcal{C}_0^* and \mathcal{G}_0^j are given in Corollary 2.2.

Recall that

$$\Delta H_{\text{ell}}^{1,\pm}(\ell, L, g, G, t) = \Delta H_{\text{ell}}^{1,\pm}(\ell, L, g, G) e^{it} + \Delta H_{\text{ell}}^{1,\pm}(\ell, L, g, G) e^{-it},$$

as defined in Corollary 3.5, and that the functions ω_{\pm}^* are defined in (34).

Lemma 3.9. *Assume Ansatz 1. The outer maps $\mathcal{F}_{e_0}^{\text{out},*}$ have the following expansion with respect to e_0 :*

$$\mathcal{F}_{e_0}^{\text{out},*} : \begin{pmatrix} I \\ t \end{pmatrix} \mapsto \begin{pmatrix} I + e_0 (B^{*,+}(I) e^{it} + B^{*,-}(I) e^{-it}) + \mathcal{O}(e_0^2) \\ t + \mu \omega^*(I) + \mathcal{O}(e_0) \end{pmatrix}, \quad * = \text{f, b.} \quad (72)$$

The functions $B^{*,\pm}(I)$ are defined as

$$\begin{aligned} B^{\text{f},\pm}(I) &= B_{\text{out}}^{\text{f},\pm}(I) + B_{\text{in}}^{\text{f},\pm}(I) e^{\pm i \mu \omega_{\text{out}}^{\text{f}}(I)} \\ B^{\text{b},\pm}(I) &= B_{\text{in}}^{\text{b},\pm}(I) + B_{\text{out}}^{\text{b},\pm}(I) e^{\pm i \mu \omega_{\text{in}}^{\text{b}}(I)}, \end{aligned} \quad (73)$$

where $\omega_{\text{out}}^{\text{f}}(I)$ and $\omega_{\text{in}}^{\text{b}}(I)$ are the functions defined in (33) and (35) respectively and

$$\begin{aligned} B_{\text{out}}^{\text{f},\pm}(I) &= \pm i \mu \lim_{T \rightarrow +\infty} \int_0^T \left(\frac{\Delta H_{\text{ell}}^{1,\pm} \circ \gamma_I^{\text{f}}(\sigma)}{-1 + \mu \partial_G \Delta H_{\text{circ}} \circ \gamma_I^{\text{f}}(\sigma)} e^{\pm i \tilde{\gamma}_I^{\text{f}}(\sigma)} \right. \\ &\quad \left. - \frac{\Delta H_{\text{ell}}^{1,\pm} \circ \lambda_I^3(\sigma)}{-1 + \mu \partial_G \Delta H_{\text{circ}} \circ \lambda_I^3(\sigma)} e^{\pm i (\tilde{\lambda}_I^3(\sigma) + \mu \omega_+^{\text{f}}(I))} \right) d\sigma \\ &\quad \mp i \mu \lim_{T \rightarrow -\infty} \int_0^T \left(\frac{\Delta H_{\text{ell}}^{1,\pm} \circ \gamma_I^{\text{f}}(\sigma)}{-1 + \mu \partial_G \Delta H_{\text{circ}} \circ \gamma_I^{\text{f}}(\sigma)} e^{\pm i \tilde{\gamma}_I^{\text{f}}(\sigma)} \right. \\ &\quad \left. - \frac{\Delta H_{\text{ell}}^{1,\pm} \circ \lambda_I^4(\sigma)}{-1 + \mu \partial_G \Delta H_{\text{circ}} \circ \lambda_I^4(\sigma)} e^{\pm i (\tilde{\lambda}_I^4(\sigma) + \mu \omega_-^{\text{f}}(I))} \right) d\sigma, \end{aligned} \quad (74)$$

$$\begin{aligned} B_{\text{out}}^{\text{b},\pm}(I) &= \pm i \mu \lim_{T \rightarrow +\infty} \int_0^T \left(\frac{\Delta H_{\text{ell}}^{1,\pm} \circ \gamma_I^{\text{b}}(\sigma)}{-1 + \mu \partial_G \Delta H_{\text{circ}} \circ \gamma_I^{\text{b}}(\sigma)} e^{\pm i \tilde{\gamma}_I^{\text{b}}(\sigma)} \right. \\ &\quad \left. - \frac{\Delta H_{\text{ell}}^{1,\pm} \circ \lambda_I^4(\sigma)}{-1 + \mu \partial_G \Delta H_{\text{circ}} \circ \lambda_I^4(\sigma)} e^{\pm i (\tilde{\lambda}_I^4(\sigma) + \mu \omega_+^{\text{b}}(I))} \right) d\sigma \\ &\quad \mp i \mu \lim_{T \rightarrow -\infty} \int_0^T \left(\frac{\Delta H_{\text{ell}}^{1,\pm} \circ \gamma_I^{\text{b}}(\sigma)}{-1 + \mu \partial_G \Delta H_{\text{circ}} \circ \gamma_I^{\text{b}}(\sigma)} e^{\pm i \tilde{\gamma}_I^{\text{b}}(\sigma)} \right. \\ &\quad \left. - \frac{\Delta H_{\text{ell}}^{1,\pm} \circ \lambda_I^3(\sigma)}{-1 + \mu \partial_G \Delta H_{\text{circ}} \circ \lambda_I^3(\sigma)} e^{\pm i (\tilde{\lambda}_I^3(\sigma) + \mu \omega_-^{\text{b}}(I))} \right) d\sigma, \end{aligned} \quad (75)$$

$$\begin{aligned} B_{\text{in}}^{\text{f},\pm}(I) &= \mp i \mu \int_0^{-12\pi} \frac{\Delta H_{\text{ell}}^{1,\pm} \circ \lambda_I^4(\sigma)}{-1 + \mu \partial_G \Delta H_{\text{circ}} \circ \lambda_I^4(\sigma)} e^{\pm i \tilde{\lambda}_I^4(\sigma)} d\sigma \\ B_{\text{in}}^{\text{b},\pm}(I) &= \mp i \mu \int_0^{-2\pi} \frac{\Delta H_{\text{ell}}^{1,\pm} \circ \lambda_I^3(\sigma)}{-1 + \mu \partial_G \Delta H_{\text{circ}} \circ \lambda_I^3(\sigma)} e^{\pm i \tilde{\lambda}_I^3(\sigma)} d\sigma. \end{aligned} \quad (76)$$

Proof. Recall that the outer maps are the composition of two maps. Indeed, as explained in Section 2.3, they are defined as

$$\begin{aligned} \mathcal{F}_{e_0}^{\text{out},\text{f}} &= \mathcal{P}_{e_0}^6 \circ \mathcal{S}_{e_0}^{\text{f}} : \tilde{\Lambda}_0^3 \longrightarrow \tilde{\Lambda}_0^3 \\ \mathcal{F}_{e_0}^{\text{out},\text{b}} &= \mathcal{S}_{e_0}^{\text{b}} \circ \mathcal{P}_{e_0} : \tilde{\Lambda}_0^3 \longrightarrow \tilde{\Lambda}_0^3. \end{aligned}$$

Thus, we study both maps perturbatively and then their composition leads to the proof of the lemma. We only deal with $\mathcal{F}_{e_0}^{\text{out},f}$ since the proof for $\mathcal{F}_{e_0}^{\text{out},b}$ is analogous.

To study $\mathcal{S}_{e_0}^f : \tilde{\Lambda}_0^3 \rightarrow \tilde{\Lambda}_0^4$ we use the Definition 2.3 of the (heteroclinic) outer map. Let us consider points $z \in \Gamma_{e_0}^*$, $x_+ \in \tilde{\Lambda}_{e_0}^4$ and $x_- \in \tilde{\Lambda}_{e_0}^3$ such that

$$\text{dist}(\mathcal{P}_{e_0}^n(z), \mathcal{P}_{e_0}^n(x_{\pm})) < C\lambda^{-|n|} \quad \text{for } n \in \mathbb{Z}^{\pm}$$

for certain constants $C > 0$ and $\lambda > 1$. Using the parameterizations of $\Gamma_{e_0}^f$ and $\tilde{\Lambda}_{e_0}^j$, $j = 3, 4$, given in Theorem 2, we write the points z and x_{\pm} in coordinates as $z = \mathcal{C}_{e_0}(I_0, t_0)$, $x_+ = \mathcal{G}_{e_0}^4(I_+, t_+)$ and $x_- = \mathcal{G}_{e_0}^3(I_-, t_-)$. Then, the I -component of the outer map is just given by

$$\mathcal{F}_{e_0}^{\text{out},I}(I_-, t_-) = I_+ = I_- + (I_+ - I_-).$$

To measure $I_+ - I_-$ we first deal with $I_0 - I_{\pm}$. Consider the flow Φ_{e_0} associated to the reduced elliptic problem (40). Applying the Fundamental Theorem of Calculus,

$$\begin{aligned} I_0 - I_+ &= \lim_{T \rightarrow -\infty} \int_T^0 \left(\frac{d}{ds} \Phi_{e_0} \{s, \mathcal{C}_{e_0}^f(I_0, t_0)\} - \frac{d}{ds} \Phi_{e_0} \{s, \mathcal{G}_{e_0}^4(I_+, t_+)\} \right) ds \\ I_0 - I_- &= \lim_{T \rightarrow +\infty} \int_T^0 \left(\frac{d}{ds} \Phi_{e_0} \{s, \mathcal{C}_{e_0}^f(I_0, t_0)\} - \frac{d}{ds} \Phi_{e_0} \{s, \mathcal{G}_{e_0}^3(I_-, t_-)\} \right) ds. \end{aligned}$$

Note that the change of sign in the limit of integration comes from the fact that system (40) has the time reversed.

Using the perturbative expansions of $\mathcal{C}_{e_0}^f$ and $\Lambda_{e_0}^j$ given in Theorem 2, equation (40), the perturbative expansion of the Hamiltonian (15) given in Corollary 3.5 and the perturbation of the flow Φ_{e_0} given in Lemma 3.6, we see that

$$\begin{aligned} I_0 - I_+ &= -e_0 \lim_{T \rightarrow -\infty} \int_T^0 \left(\frac{\mu \partial_t \Delta H_{\text{ell}}^1(L, \ell, G, g, t)}{-1 + \mu \partial_G \Delta H_{\text{circ}}(L, \ell, G, g)} \Big|_{(L, \ell, G, g, t) = (\Phi_0^{\text{circ}}, \Phi_0^t) \{s, \mathcal{C}_0^f(I_0, t_0)\}} \right. \\ &\quad \left. - \frac{\mu \partial_t \Delta H_{\text{ell}}^1(L, \ell, G, g, t)}{-1 + \mu \partial_G \Delta H_{\text{circ}}(L, \ell, G, g)} \Big|_{(L, \ell, G, g, t) = (\Phi_0^{\text{circ}}, \Phi_0^t) \{s, \mathcal{G}_0^4(I_+, t_+)\}} \right) ds + \mathcal{O}(e_0^2) \\ I_0 - I_- &= -e_0 \lim_{T \rightarrow +\infty} \int_T^0 \left(\frac{\mu \partial_t \Delta H_{\text{ell}}^1(L, \ell, G, g, t)}{-1 + \mu \partial_G \Delta H_{\text{circ}}(L, \ell, G, g)} \Big|_{(L, \ell, G, g, t) = (\Phi_0^{\text{circ}}, \Phi_0^t) \{s, \mathcal{C}_0^f(I_0, t_0)\}} \right. \\ &\quad \left. - \frac{\mu \partial_t \Delta H_{\text{ell}}^1(L, \ell, G, g, t)}{-1 + \mu \partial_G \Delta H_{\text{circ}}(L, \ell, G, g)} \Big|_{(L, \ell, G, g, t) = (\Phi_0^{\text{circ}}, \Phi_0^t) \{s, \mathcal{G}_0^3(I_-, t_-)\}} \right) ds + \mathcal{O}(e_0^2), \end{aligned}$$

where Φ_0^{circ} and Φ_0^t are defined in (31) and (36) respectively.

Taking into account that ΔH_{ell}^1 satisfies that $\mathcal{N}(\Delta H_{\text{ell}}^1) = \{\pm 1\}$ (Corollary 3.5), one can easily obtain the formula for $B_{\text{out}}^{f, \pm}$ in (74).

To obtain the formula for $B_{\text{in}}^{f, \pm}$ we proceed as in the study of the inner map in Section 3.1. Finally, to obtain the formula for $B^{f, \pm}$ it is enough to compose both maps $\mathcal{P}_{e_0}^6$ and $\mathcal{S}_{e_0}^f$. \square

4 Existence of diffusing orbits

4.1 Existence of a transition chain of whiskered tori

The numerics of Appendix B.4 support the following ansatz, which is crucial to obtain the main theorem of this section, Theorem 4. The dynamical significance of this ansatz appears in the averaging lemma 4.2, which is one of the steps in the proof of the theorem.

Ansatz 3. *The functions of I*

$$\tilde{B}^{*,\pm}(I) = B^{*,\pm}(I) - \frac{e^{\pm i\mu\omega^*(I)} - 1}{e^{\pm i\mu\mathcal{T}_0(I)} - 1} A_1^\pm(I)$$

do not vanish over the domains \mathcal{D}^* , $*$ = f, b (defined in Corollary 2.2).

Next is the main result of this section.

Theorem 4. *Assume Ansätze 1, 2 and 3. For every $\delta > 0$ there exists $e_0^* > 0$ and $C > 0$ such that for every $0 < e_0 < e_0^*$ the map \mathcal{P}_{e_0} in (41) has a collection of invariant 1-dimensional tori $\{\mathbb{T}_i\}_{i=1}^N \subset \bar{\Lambda}_{e_0}$ such that*

- $\mathbb{T}_1 \cap \{I = I_- + \delta\} \neq \emptyset$ and $\mathbb{T}_N \cap \{I = I_+ - \delta\} \neq \emptyset$.
- Hausdorff $\text{dist}(\mathbb{T}_i, \mathbb{T}_{i+1}) < Ce_0^{3/2}$.
- These tori form a transition chain. Namely, $W_{\mathbb{T}_i}^u \cap W_{\mathbb{T}_{i+1}}^s \neq \emptyset$ for each $i = 1, \dots, N-1$.

Proof of Theorem 4. Once we have computed the first orders in e_0 of both the outer and the inner map, we want to understand their properties and compare their dynamics. To make this comparison we perform two steps of averaging [AKN88]. This change of coordinates straightens the I -component of the inner map at order $\mathcal{O}(e_0^3)$ in such a way that, in the new system of coordinates, the dynamics of both maps is easier to compare. Nevertheless, before averaging, we have to perform a preliminary change of coordinates to straighten the symplectic form $\Omega_{e_0}^3$ to deal with the canonical form $dI \wedge dt$.

Lemma 4.1. *Assume Ansatz 1. There exists an e_0 -close to the identity change of variables*

$$(I, t) = (I', t') + e_0 \varphi_1(I', t'), \quad (77)$$

defined on $\tilde{\Lambda}_{e_0}^3$, which transforms the symplectic form $\Omega_{e_0}^3$ defined in (44) into the canonical form

$$\Omega_0 = dI' \wedge dt'.$$

In the new coordinates,

- The inner map $\mathcal{F}_{e_0}^{\text{in}}$ in (45) reads

$$\mathcal{F}_{e_0}^{\text{in}'} : \begin{pmatrix} I' \\ t' \end{pmatrix} \mapsto \begin{pmatrix} I' + e_0 A_1(I', t') + e_0^2 A_2'(I', t') + \mathcal{O}(\mu e_0^3) \\ t' + \mu \mathcal{T}_0(I') + e_0 \mathcal{T}_1'(I', t') + e_0^2 \mathcal{T}_2'(I', t') + \mathcal{O}(\mu e_0^3) \end{pmatrix} \quad (78)$$

where A_1 is the function given in Lemma 3.7 and A_2' , \mathcal{T}_1' and \mathcal{T}_2' satisfy

$$\mathcal{N}(A_2') = \{0, \pm 1, \pm 2\}, \quad \mathcal{N}(\mathcal{T}_1') = \{\pm 1\} \quad \text{and} \quad \mathcal{N}(\mathcal{T}_2') = \{0, \pm 1, \pm 2\}.$$

- The outer maps $\mathcal{F}_{e_0}^{\text{out},f}$ and $\mathcal{F}_{e_0}^{\text{out},b}$ in (48) read

$$\mathcal{F}_{e_0}^{\text{out},*'} : \begin{pmatrix} I' \\ t' \end{pmatrix} \mapsto \begin{pmatrix} I' + e_0 B^*(I', t') + \mathcal{O}(\mu e_0^2) \\ t' + \mu \omega^*(I') + \mathcal{O}(\mu e_0) \end{pmatrix}, \quad * = f, b, \quad (79)$$

where B^* are the functions given in Lemma 3.9.

Proof. We show that there exists a change of coordinates of the form

$$\begin{cases} I = I' + e_0^2 f_2(I', t') + \mathcal{O}(e_0^3) \\ t = t' + e_0 g_1(I', t') + e_0^2 g_2(I', t') + \mathcal{O}(e_0^3) \end{cases} \quad (80)$$

with

$$\mathcal{N}(g_1) = \{\pm 1\}, \quad \mathcal{N}(g_2) = \{0, \pm 1, \pm 2\} \quad \text{and} \quad \mathcal{N}(f_2) = \{0, \pm 1, \pm 2\}, \quad (81)$$

which straightens the symplectic form $\Omega_{e_0}^3$. In fact, we look for the inverse change. Namely, we look for a change of coordinates of the form

$$\begin{cases} I' = I + e_0^2 \tilde{f}_2(I, t) + e_0^3 \tilde{f}_{\geq}(I, t) \\ t' = t + e_0 \tilde{g}_1(I, t) \end{cases} \quad (82)$$

such that the pullback of $\Omega_0 = dI' \wedge dt'$ with respect to this change is the symplectic form $\Omega_{e_0}^3$. Even though we do not write it explicitly, \tilde{f}_{\geq} depends on e_0 . To obtain this change, it is enough to solve the equations

$$\partial_t \tilde{g}_1 = a_1^3, \quad \partial_I \tilde{f}_2 = a_2^3, \quad \partial_I \tilde{f}_{\geq} = b,$$

where

$$b = a_{\geq}^3 - \partial_t \tilde{g}_1 \partial_I \tilde{f}_2 - e_0 \partial_t \tilde{g}_1 \partial_I \tilde{f}_{\geq} + \partial_I \tilde{g}_1 \partial_t \tilde{f}_2 + e_0 \partial_I \tilde{g}_1 \partial_t \tilde{f}_{\geq}$$

and a_1^3 , a_2^3 and a_{\geq}^3 are the functions introduced in (44). These equations can be solved iteratively.

Recall that by Corollary 3.8 we have $\mathcal{N}(a_1^3) = \{\pm 1\}$. Then, we take \tilde{g}_1 as the primitive of a_1^3 with zero average, which satisfies

$$\mathcal{N}(\tilde{g}_1) = \{\pm 1\}. \quad (83)$$

The other equations can be solved taking

$$\tilde{f}_2(I, t) = \int_0^I a_2^3(J, t) dJ \quad \tilde{f}_{\geq}(I, t) = \int_0^I b(J, t) dJ.$$

Note that b depends on \tilde{g}_1 and \tilde{f}_2 , which have been already obtained. Since by Corollary 3.8 we have $\mathcal{N}(a_2^3) = \{0, \pm 1, \pm 2\}$, one can deduce that

$$\mathcal{N}(\tilde{f}_2) = \{0, \pm 1, \pm 2\}. \quad (84)$$

To obtain the change (80) it is enough to invert the change (82). Then, formulas (83) and (84) imply (81).

To finish the proof of the lemma it remains to check the properties of the inner and outer maps in the new coordinates. They follow from (81). \square

Once we have straightened the symplectic form, we perform two steps of averaging of the inner map.

Lemma 4.2. *Assume Ansätze 1 and 2. There exists a symplectic change of variables e_0 -close to the identity,*

$$(I', t') = (\mathcal{I}, \tau) + e_0 \varphi_2(\mathcal{I}, \tau), \quad (85)$$

defined on $\tilde{\Lambda}_{e_0}^3$, that:

- Transforms the inner map $\mathcal{F}_{e_0}^{\text{in}'}$ in (78) into

$$\tilde{\mathcal{F}}_{e_0}^{\text{in}} : \begin{pmatrix} \mathcal{I} \\ \tau \end{pmatrix} \mapsto \begin{pmatrix} \mathcal{I} + \mathcal{O}(\mu e_0^3) \\ \tau + \mu \mathcal{T}_0(\mathcal{I}) + e_0^2 \tilde{\mathcal{T}}_2(\mathcal{I}) + \mathcal{O}(\mu e_0^3) \end{pmatrix}. \quad (86)$$

- Transforms the outer maps $\mathcal{F}_{e_0}^{\text{out}, \text{f}'}$ and $\mathcal{F}_{e_0}^{\text{out}, \text{b}'}$ in (79) into

$$\tilde{\mathcal{F}}_{e_0}^{\text{out}, *}: \begin{pmatrix} \mathcal{I} \\ \tau \end{pmatrix} \mapsto \begin{pmatrix} \mathcal{I} + e_0 \tilde{B}^*(\mathcal{I}, \tau) + \mathcal{O}(\mu e_0^2) \\ \tau + \mu \omega^*(\mathcal{I}) + \mathcal{O}(\mu e_0) \end{pmatrix}, \quad * = \text{f}, \text{b}, \quad (87)$$

where

$$\tilde{B}^*(\mathcal{I}, \tau) = \tilde{B}^{*,+}(\mathcal{I}) e^{i\tau} + \tilde{B}^{*, -}(\mathcal{I}) e^{-i\tau}$$

with

$$\tilde{B}^{*, \pm}(\mathcal{I}) = B^{*, \pm}(\mathcal{I}) - \frac{e^{\pm i \mu \omega^*(\mathcal{I})} - 1}{e^{\pm i \mu \mathcal{T}_0(\mathcal{I})} - 1} A_1^{\pm}(\mathcal{I}).$$

With the functions introduced in this lemma, Ansatz 3 can be restated as $\tilde{B}^{*,\pm}(\mathcal{I}) \neq 0$ over the domains \mathcal{D}^* .

Note that we can do two steps of averaging globally in the whole cylinder $\tilde{\Lambda}_{e_0}$ due to the absence of resonances in the first orders in e_0 . Namely, there are no *big gaps*. This contrasts with the typical situation in Arnol'd diffusion (see e.g. [DdlLS06]).

Proof. We perform two steps of (symplectic) averaging. To this end we consider a generating function of the form

$$\mathcal{S}(\mathcal{I}, t') = \mathcal{I}t' + e_0 \mathcal{S}_1(\mathcal{I}, t') + e_0^2 \mathcal{S}_2(\mathcal{I}, t'),$$

which defines the change (85) implicitly as

$$\begin{aligned} I &= \mathcal{I} + e_0 \partial_{t'} \mathcal{S}_1(\mathcal{I}, t') + e_0^2 \partial_{t'} \mathcal{S}_2(\mathcal{I}, t') \\ \tau &= t' + e_0 \partial_{\mathcal{I}} \mathcal{S}_1(\mathcal{I}, t') + e_0^2 \partial_{\mathcal{I}} \mathcal{S}_2(\mathcal{I}, t'). \end{aligned}$$

By Ansatz 2 we have (26) and by Theorem 3 we know the t' -harmonics of the functions A_i and \mathcal{T}_i . Then, it follows that the functions \mathcal{S}_i corresponding to two steps of averaging are globally defined in $\tilde{\Lambda}_{e_0}^3$. In these new variables, taking into account that the inner map is exact symplectic, one can see that the inner map is of the form (86).

To obtain a perturbative expression for the outer maps $\tilde{\mathcal{F}}_{e_0}^{\text{out},*}$, we need to compute \mathcal{S}_1 explicitly:

$$\mathcal{S}_1(\mathcal{I}, t) = -\frac{iA_1^+(\mathcal{I})}{e^{i\mu T_0(\mathcal{I})} - 1} e^{it} + \frac{iA_1^-(\mathcal{I})}{e^{-i\mu T_0(\mathcal{I})} - 1} e^{-it}.$$

Applying this change to the outer maps $\mathcal{F}_{e_0}^{\text{out},*}$ in (72), we obtain (87). \square

In the new coordinates (\mathcal{I}, τ) the inner map $\tilde{\mathcal{F}}_{e_0}^{\text{in}}$ in (86) is a e_0^3 -close to integrable map. Moreover, thanks to Ansatz 2 it is twist. Therefore we can apply KAM theory to prove the existence of invariant curves in $\tilde{\Lambda}_{e_0}^3$. We use a version of the KAM Theorem from [DdlLS00] (see also [Her83]).

KAM theorem. *Let $f : [0, 1] \times \mathbb{T} \rightarrow [0, 1] \times \mathbb{T}$ be an exact symplectic \mathcal{C}^l map with $l > 4$. Assume that $f = f_0 + \delta f_1$, where $f_0(I, \psi) = (I, \psi + A(I))$, A is \mathcal{C}^l , $|\partial_I A| > M$ and $\|f_1\|_{\mathcal{C}^l} \leq 1$. Then, if $\delta^{1/2} M^{-1} = \rho$ is sufficiently small, for a set of ω of Diophantine numbers of exponent $\theta = 5/4$, we can find invariant tori which are the graph of \mathcal{C}^{l-3} functions u_ω , the motion on them is \mathcal{C}^{l-3} conjugate to the rotation by ω , and $\|u_\omega\|_{\mathcal{C}^{l-3}} \leq C\delta^{1/2}$.*

Applying this theorem to the map $\tilde{\mathcal{F}}_{e_0}^{\text{in}}$ we obtain the KAM tori (see Remark 3.1 for the matter of their regularity). Moreover, this theorem ensures that the distance between these tori is no larger than $e_0^{3/2}$. The results of Lemma 4.2 and the KAM theorem lead to the existence of a transition chain of invariant tori, as explained next.

The transition chain is obtained comparing the outer and inner dynamics. We do this comparison in the coordinates (\mathcal{I}, τ) given by Lemma 4.2 and thus we deal with the maps $\tilde{\mathcal{F}}_{e_0}^{\text{in}}$ and $\tilde{\mathcal{F}}_{e_0}^{\text{out},*}$ in (86) and (87) respectively.

The KAM theorem ensures that there exists a torus \mathbb{T}_1 such that $\mathbb{T}_1 \cap \{I = I_- - \delta\} \neq \emptyset$. Either $\tilde{\mathcal{F}}_{e_0}^{\text{out},f}$ or $\tilde{\mathcal{F}}_{e_0}^{\text{out},b}$ are defined for points in \mathbb{T}_1 . Assume without loss of generality that $\tilde{\mathcal{F}}_{e_0}^{\text{out},f}$ is defined for points in \mathbb{T}_1 . Thanks to Ansatz 3, $\mathcal{F}_{e_0}^{\text{out},f}(\mathbb{T}_1)$ satisfies

$$\text{dist}(\mathbb{T}_1, \mathcal{F}_{e_0}^{\text{out},f}(\mathbb{T}_1)) \geq C e_0$$

for a constant $C > 0$ independent of e_0 . Then, the KAM theorem ensures that there exists a torus \mathbb{T}_2 such that $\mathbb{T}_2 \cap \mathcal{F}_{e_0}^{\text{out},f}(\mathbb{T}_1) \neq \emptyset$. Iterating this procedure, choosing at each step either $\tilde{\mathcal{F}}_{e_0}^{\text{out},f}$ or $\tilde{\mathcal{F}}_{e_0}^{\text{out},b}$, we obtain the transition chain. This completes the proof of Theorem 4. \square

4.2 Shadowing

To finish the proof of Theorem 1 it remains to prove the existence of a diffusing orbit using a Lambda Lemma. The study of the Lambda lemma, often also called Inclination Lemma, was initiated in the seminal work of Arnol'd [Arn64]. In the past decades there have been several works proving analogous results in more general settings [CG94, Mar96, Cre97, FM00, Sab13]. Here, we use a version of the Lambda Lemma proven in [FM00] (Theorem 7.1 of that paper).

Lemma 4.3. *Let f be a C^1 symplectic map in a $2(d+1)$ symplectic manifold. Assume that the map leaves invariant a C^1 d -dimensional torus \mathbb{T} and the motion on the torus is an irrational rotation. Let Γ be a $d+1$ manifold intersecting $W_{\mathbb{T}}^u$ transversally. Then,*

$$W_{\mathbb{T}}^s \subset \overline{\bigcup_{i>0} f^{-i}(\Gamma)}.$$

An immediate consequence of this lemma is that any finite transtion chain can be shadowed by a true orbit. The proof of Theorem 1 follows from the following lemma.

Lemma 4.4. *Assume Ansätze 1, 2 and 3. Consider the transition chain of invariant tori $\{\mathbb{T}_i\}_{i=1}^N$ obtained in Theorem 4 and a sequence of positive numbers $\{\varepsilon_i\}_{i=1}^N$. Then, we can find a point $P = (L_0, \ell_0, G_0, g_0, I_0)$ and a sequence of times T_i such that*

$$\Phi(T_i, P) \in B_{\varepsilon_i}(\mathbb{T}_i),$$

where Φ is the flow associated to Hamiltonian (16) and $B_{\varepsilon_i}(\mathbb{T}_i)$ is a neighborhood of size ε_i of the torus \mathbb{T}_i .

Proof. Consider $P' \in W_{\mathbb{T}_1}^s$. Then, there exists a ball B_1 centered on P' and a time $T_1 > 0$, such that

$$\Phi(T_1, B_1) \subset B_{\varepsilon_1}(\mathbb{T}_1). \quad (88)$$

Since $W_{\mathbb{T}_1}^u$ and $W_{\mathbb{T}_2}^s$ intersect transversally, by Lemma 4.3, we know that $W_{\mathbb{T}_2}^s \cap B_1 \neq \emptyset$. Thus, there exists a closed ball $B_2 \subset B_1$ centered at a point in $W_{\mathbb{T}_2}^s$ that satisfies

$$\Phi(T_2, B_2) \subset B_{\varepsilon_2}(\mathbb{T}_2)$$

for some time $T_2 > 0$. Hence, proceeding by induction, we obtain a sequence of nested closed balls

$$B_N \subset B_{N-1} \subset \dots \subset B_1$$

and a sequence of times $\{T_i\}_{i=1}^N$, such that

$$\Phi(T_j, B_i) \subset B_{\varepsilon_i}(\mathbb{T}_i) \quad \text{for } i \leq j.$$

Therefore, the intersection $\bigcap_{i=1}^N B_i$ is non-empty and any point belonging to it shadows the transition chain of tori. \square

In terms of the elliptical elements of the asteroid, such a diffusing orbit can be described as follows. The orbit starts near the resonant cylinder Λ_{e_0} . The eccentricity of the primaries is small: this is an essential feature of both the proof above and the qualitative behavior of the orbit. Over a time interval of length $\ll 1/e_0$, the orbit closely follows a hyperbolic periodic orbit of the circular problem. The semi major axis is roughly constant equal to $7^{2/3}$ and the Jacobi constant to -1.81 . The asteroid turns around the primaries, making one full turn over a time interval of 7 periods of Jupiter. In the frame rotating approximately with the primaries, the Keplerian ellipse of the asteroid precesses counterclockwise with fast frequency approximately equal to -1 ; in the inertial frame of reference, it rotates only μ -slowly (see e.g. [AKN88, Féj02a]), while the eccentricity e slowly oscillates around $e = 0.48$.

At some point (as soon as we can if we want to save time), the orbit undergoes a heteroclinic excursion, during which a heteroclinic orbit is shadowed over a time interval of size $\mathcal{O}(-\ln(\mu e_0)/\sqrt{\mu})$. During this excursion, the semi major axis itself undergoes an oscillation of magnitude $\mathcal{O}(\sqrt{\mu})$, eventually coming back to its initial approximate value $7^{2/3}$. On the other hand, the Jacobi constant and the eccentricity have increased by $\mathcal{O}(\mu e_0)$.

This process is repeated, and the increments in the eccentricity accumulate to reach the value $e = 0.67$ in finite time.

A Numerical study of the normally hyperbolic invariant cylinder of the circular problem.

We devote this appendix to the numerical study of the hyperbolic invariant manifold of the circular problem given in Corollary 2.1 and its invariant manifolds. In other words, we show numerical results which justify the properties of the circular problem stated in Ansatz 1.

Numerical analysis has several sources of error: mainly round-off errors in computer arithmetics, and approximations of ideal mathematical objects (e.g. linear approximation of local stable/unstable manifolds). In our analysis, we have tried to evaluate such errors, and check that they are appropriately small. We do *not* claim to give a fully rigorous proof of Ansatz 1, which would require Computer-Assisted techniques as in [WZ03]. Indeed, we have focused our efforts to keep the numerics relatively simple and, hopefully, convincing. One could think of several possible numerical computations to prove our result. The most numerically demanding one would be to check directly that some given orbit has an adequate drift of eccentricity. This computation would not bring much light to the mechanism of instability, and moreover it would involve formidable numerical analysis problems, due to the necessarily very long time of integration. On the contrary, our line of proof allows us to use numerical verifications involving only orbits of the circular problem –a dramatic simplification, as we will see below.

Let us make a few more specific comments on the strategy of our numerical analysis. As mentioned in Section 2, the circular problem has a conserved quantity, the Jacobi constant which we denote by J (see (5)), which corresponds to energy when the system is expressed in rotating coordinates. Thus it is natural to fix the Jacobi constant $J = J_0$ and perform our analysis for a given J_0 . This allows us to reduce the dimension of the computations by one. Finally, we let J vary and repeat the computations for all J in the range of interest $J \in [J_-, J_+]$.

Another important comment is on the choice of coordinates. For numerics we prefer Cartesian coordinates, since the equations of motion are explicit in these coordinates. Thus we carry out our computations of the hyperbolic structure of the circular problem in Cartesian (Appendix A).

On the other hand, for perturbative analysis we have used Delaunay coordinates throughout this paper. Thus, in Appendix B we explain how to change coordinates from Cartesian to Delaunay, and we carry out our computations of the inner and outer maps of the circular and elliptic problems in Delaunay.

Regarding the integration method, we use a variable-order Taylor method specially generated to integrate the equations of motion and variational equations of the circular problem. The Taylor method has been generated using the “taylor” package of Å. Jorba and M. Zou (see <http://www.maia.ub.es/~angel/taylor/>). The main advantage of using a Taylor method is that it is very fast for long-time integrations (without sacrificing accuracy).

A.1 Computation of the periodic orbits

Consider the circular problem in rotating Cartesian coordinates

$$J(x, y, p_x, p_y) = \frac{1}{2}(p_x^2 + p_y^2) + yp_x - xp_y - \frac{1-\mu}{r_1} - \frac{\mu}{r_2}, \quad (89)$$

where

$$\begin{aligned} r_1^2 &= (x - \mu_2)^2 + y^2, \\ r_2^2 &= (x + \mu_1)^2 + y^2. \end{aligned}$$

Recall that the energy of the circular problem in rotating coordinates coincides with the Jacobi constant J in (5). From now on in this appendix we will refer to J as the energy of the system.

We follow the convention to place the large mass (Sun) to the left of the origin, and the small mass (Jupiter) to the right. (This is opposite to the astrodynamics convention). Thus we choose $\mu_1 = \mu$ as the small mass, and $\mu_2 = 1 - \mu$ as the large mass. Notice that equation (89) is reversible with respect to the involution

$$R(x, p_x, y, p_y) = (x, -p_x, -y, p_y). \quad (90)$$

Thus, a solution of the system is symmetric if and only if it intersects the symmetry axis $\text{Fix}(R) = \{y = 0, p_x = 0\}$. This symmetry will facilitate our numerical computations. Note that the involution R is just the involution (19) expressed in rotating Cartesian coordinates.

Let the energy be fixed to $J = J_0$. We look for a resonant periodic orbit λ_{J_0} of (89) in the level of energy J_0 . As a first approximation to λ_{J_0} , we look for a resonant periodic orbit of the two-body problem, i.e. of the Hamiltonian (18) with $\mu = 0$. Let us denote the approximate periodic orbit by $\tilde{\lambda}_{J_0} = (L, \ell, G, g)$. The actions L and G are determined by the resonant condition $L^3 = 7$ and energy condition $-\frac{1}{2L^2} - G = J_0$. To determine $\tilde{\lambda}_{J_0}$ completely, we choose that the asteroid is initially at the perihelion, i.e. we impose an initial condition $\tilde{\lambda}_{J_0}(0) = (L^0, \ell^0, G^0, g^0)$ with $\ell^0 = 0$ and $g^0 = 0$. Switching to Cartesian coordinates, we obtain an initial condition (x^0, p_x^0, y^0, p_y^0) with $p_x^0 = 0$ and $y^0 = 0$.

Next we refine the trajectory $\tilde{\lambda}_{J_0}$ into a true periodic orbit λ_{J_0} for the system (89) with $\mu = 10^{-3}$. Consider the Poincaré section

$$\Sigma^+ = \{y = 0, p_y > 0\}$$

in the circular problem (89), and let $P: \Sigma^+ \rightarrow \Sigma^+$ be the associated Poincaré map. Since we are in rotating coordinates, this section corresponds to collinear configurations of the three bodies.

Remark A.1. In numerical integrations, we use a variable-order Taylor method with local error tolerance 10^{-16} . Moreover, a point is considered to be on the Poincaré section whenever $|y| < 10^{-16}$ and $p_y > 0$.

Furthermore, the momentum variable p_y can be eliminated. Indeed, since $\partial_{p_y} J \neq 0$, p_y in the region of the phase space we deal with, it can be recovered from the other variables using the energy condition $J(x, p_x, y, p_y) = J_0$. Hence, the Poincaré map is a two-dimensional symplectic map at each energy level, acting only on (x, p_x) .

Notice that, in the rotating frame, a 1:7 resonant periodic orbit makes 6 turns around the origin. See Figure 5. In principle, we could look for the periodic orbit as a periodic point $p = (x, p_x)$ of the Poincaré map: $p = P^6(p)$. This would imply solving a system of two equations. Thanks to the reversibility (90), in fact it is only necessary to solve one equation. Notice that our initial condition (x, p_x) is at the symmetry section $\{y = 0, p_x = 0\}$, so the periodic orbit must be symmetric. Thus it is enough to impose the condition that the trajectory $\lambda_{J_0}(t)$ after *half* the period is again at the symmetry section. Hence we set up the problem as simple one-dimensional root finding: we look for a point $p = (x, 0)$, such that its third iterate $P^3(p)$ has momentum $p_x = 0$:

$$\pi_{p_x}(P^3(p)) = 0.$$

(Here, $\pi_{p_x}: \mathbb{R}^2 \rightarrow \mathbb{R}$ is the projection onto the p_x component).

In order to solve this problem, we use a Newton-like method. Specifically, we use a modified version of Powell's Hybrid method (see the GSL manual [GG09] for details) without scaling. In our computations, the Newton method converges in less than 5 iterations. As a test of the software, we have checked that the rate of convergence of the Newton method is quadratic.

Remark A.2. We ask for an accuracy of 10^{-14} in the Newton method, i.e. a point $p = (x, 0)$ is accepted as a root if and only if its third iterate $P^3(p)$ has momentum $|p_x| < 10^{-14}$.

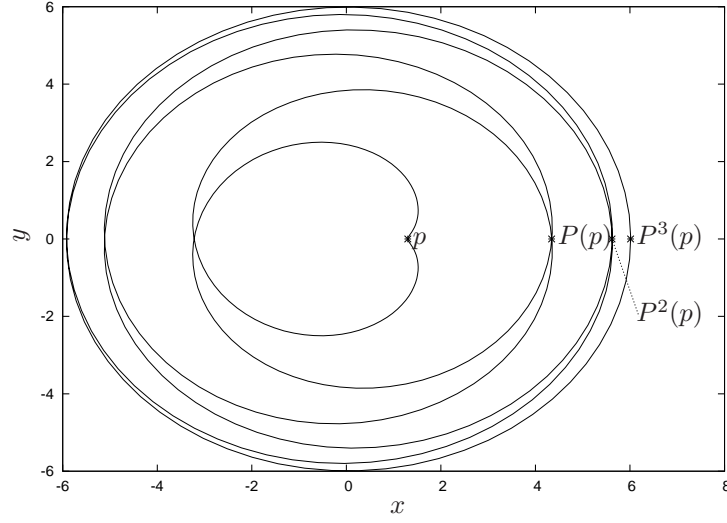


Figure 5: Resonant periodic orbit $\lambda_{-1.6}$ of the circular problem in rotating Cartesian coordinates.

For the Newton method, we need to compute the derivative of the Poincaré map. For each $\xi \in \mathbb{R}^4$, let $u(t, \xi)$ be the solution of the system with initial condition $u(0, \xi) = \xi$. Let $T : \Sigma^+ \rightarrow \mathbb{R}$ be the Poincaré return time. The derivative of the Poincaré map at a point $p \in \mathbb{R}^4$ is given by the partial derivative $DP(p) = u_\xi(T(p), p)$. It is well-known that $u_\xi(t, p)$ is the matrix solution of the variational equation

$$\dot{W} = Df(u(t, p))W,$$

where f is the vector field of the circular problem. We compute $DP(p)$ by numerically integrating the variational equation using the Taylor method mentioned above.

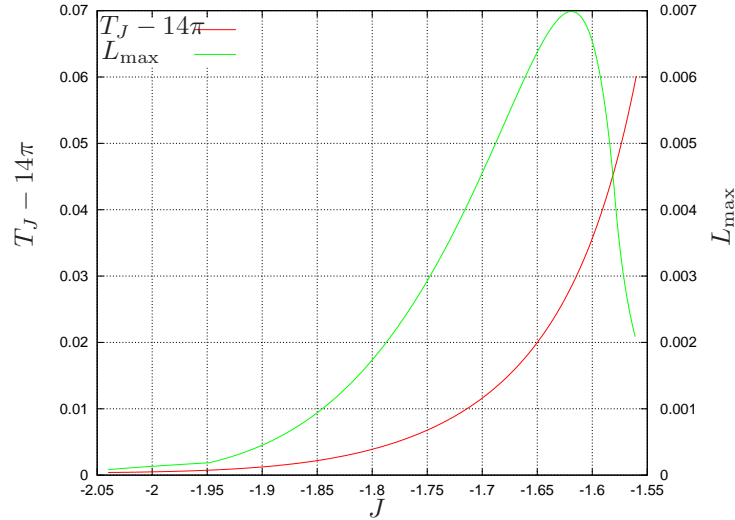


Figure 6: Resonant family of periodic orbits. We show normalized period $T_J - 14\pi$, and maximum deviation of L component with respect to the resonant value $7^{1/3}$ (see equation (92)).

For illustration, let us show some numerical results corresponding to the energy value $J = -1.6$. The first approximation $\tilde{\lambda}_{-1.6}$ from the two-body problem has initial condition $p^0 = (x^0, p_x^0) = (1.30253 \dots, 0)$.

After refining this initial condition via the Newton method, we obtain a resonant periodic orbit $\lambda_{-1.6}$ of the circular problem passing through the point $p = (x, p_x) = (1.29858 \dots, 0)$, with period $T_{-1.6} = 44.01796 \dots \sim 14\pi$. See Figure 5. The periodic orbit $\lambda_{-1.6}$ is symmetric, with the points p and $P^3(p)$ located at the symmetry section (they have $y = 0$ and $p_x = 0$). Notice that, in rotating coordinates, the trajectory of the asteroid makes 6 turns around the origin before closing up at the point p .

Finally, we let J change and, using this procedure, we are able to obtain the resonant periodic orbit for energy levels

$$J \in [\bar{J}_-, \bar{J}_+] = [-2.04, -1.56]. \quad (91)$$

See Figure 6. This family of resonant periodic orbits constitutes the normally hyperbolic invariant manifold Λ_0 given in Corollary 2.1. Notice that the period T_J stays close to the resonant period 14π of the unperturbed system. From Figure 6, we obtain the bound

$$|T_J - 14\pi| < 60\mu,$$

which is the first bound given in Ansatz 1.

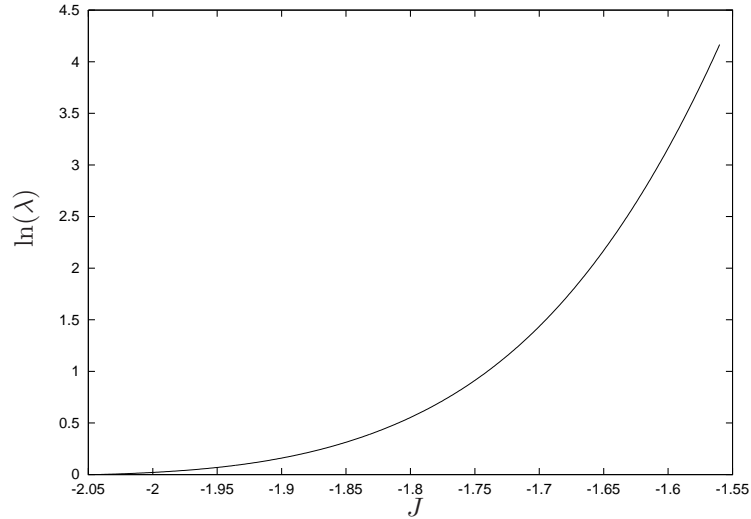


Figure 7: Characteristic exponent $\ln(\lambda)$ as a function of energy level J (the other exponent is $-\ln(\lambda)$).

To determine the stability of the periodic orbit λ_{J_0} , we compute the eigenvalues λ and λ^{-1} of the matrix $DP^6(p)$, where $DP^6(p)$ is the linearization of the iterated Poincaré map P^6 about the fixed point p .

Figure 7 shows the characteristic exponents $\ln(\lambda)$, $\ln(\lambda^{-1})$ as a function of energy. The family of periodic orbits is strongly hyperbolic as $J \rightarrow \bar{J}_+$, and weakly hyperbolic as $J \rightarrow \bar{J}_-$. Note that one would expect that we are in a nearly integrable regime since μ is small. Then one would expect the eigenvalues to be close to 1. Nevertheless, in this problem the non-integrability is very noticeable when one increases μ to $\mu = 10^{-3}$. This is due to the effect of the perturbing body (Jupiter) on the asteroid, as the asteroid passes close to it.

Furthermore, we verify that (the square of) the semi-major axis L stays close to the resonant value $7^{1/3}$. Integrating the periodic orbit in Delaunay coordinates $\lambda_J(t) = (L_J(t), \ell_J(t), G_J(t), g_J(t))$ over one period T_J , we compute the quantity

$$L_{\max}(J) = \max_{t \in [0, T_J]} |L_J(t) - 7^{1/3}|. \quad (92)$$

The function $L_{\max}(J)$ is plotted in Figure 6. Notice that we obtain the bound

$$|L_J(t) - 7^{1/3}| < 7\mu$$

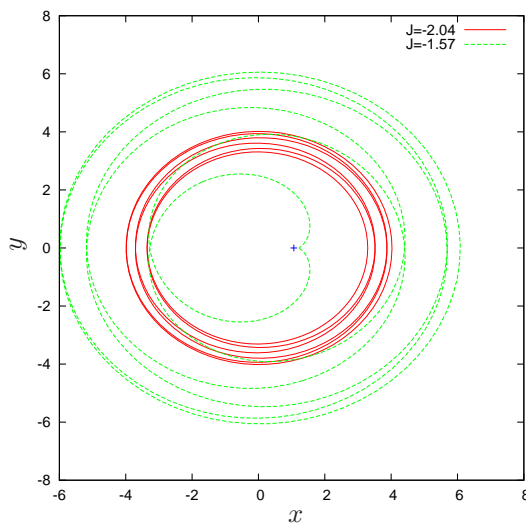


Figure 8: Extremal periodic orbits of the family: circular periodic orbit with $J = \bar{J}_-$ (in red), elliptical periodic orbit with $J = \bar{J}_+$ (in green). The Lagrange equilibrium point L_2 is marked with a '+' symbol.

for all $t \in \mathbb{R}$ and $J \in [\bar{J}_-, \bar{J}_+]$, which is the second bound given in Ansatz 1.

Let us briefly describe the family of periodic orbits λ_J . For illustration, see Figure 8. At one endpoint of the family, as $J \rightarrow \bar{J}_-$, the periodic orbit λ_J tends to a circular orbit of period 14π centered at the origin and passing far away from the primaries (Sun and Jupiter). Moreover, λ_J loses hyperbolicity when $J \rightarrow \bar{J}_-$. For instance, the periodic orbit $\lambda_{\bar{J}_-}$ of the two-body problem approximation has eccentricity $e(\bar{J}_-) = 0.09989 \dots$.

At the other endpoint of the family, as $J \rightarrow \bar{J}_+$, the periodic orbit λ_J tends to a homoclinic loop of the Lagrangian equilibrium point L_2 that makes 6 turns around the Sun-Jupiter system. (In rotating Cartesian coordinates, L_2 is located on the x axis at the point $x_2 \simeq 1.068$). This explains the fact that the period T_J “explodes” as $J \rightarrow \bar{J}_+$. Since we are interested in working close to the resonance, we avoid energies $J > \bar{J}_+$ where the period explodes.

A.2 Computation of invariant manifolds

In this appendix, we compute the stable and unstable invariant manifolds associated to the periodic orbits found in the previous section.

Consider first a fixed energy level $J = J_0$. Let λ_{J_0} be the resonant periodic orbit of the circular problem found in the previous section. To compute the invariant manifolds of the periodic orbit, we continue using the iterated Poincaré map. Thus we look for (one dimensional) invariant manifolds of a hyperbolic fixed point at each energy level. Let $p \in \lambda_{J_0}$ be a hyperbolic fixed point of the iterated Poincaré map $\tilde{P} = P^6$. Let λ, λ^{-1} be the eigenvalues of $D\tilde{P}(z)$ with $\lambda > 1$, and v_u, v_s be the associated eigenvectors.

Assume that we want to compute the unstable manifold $W^u(p)$. Let η be a small displacement in the unstable direction v_u . We approximate a piece of the local manifold by the linear segment between the points $p + \eta v_u$ and $\tilde{P}(p + \eta v_u)$. We call this segment a *fundamental domain*. We discretize the fundamental domain into an array of points, and iterate them by \tilde{P} to globalize the manifold. (The stable manifold is computed analogously using the inverse map \tilde{P}^{-1} .)

The error committed in the local approximation $\tilde{P}(p + \eta v_u) = p + \lambda \eta v_u + \mathcal{O}(\eta^2)$ of the manifold is given by

$$\text{err}(\eta) = \left\| \tilde{P}(p + \eta v_u) - p - \lambda \eta v_u \right\| \in \mathcal{O}(\eta^2).$$

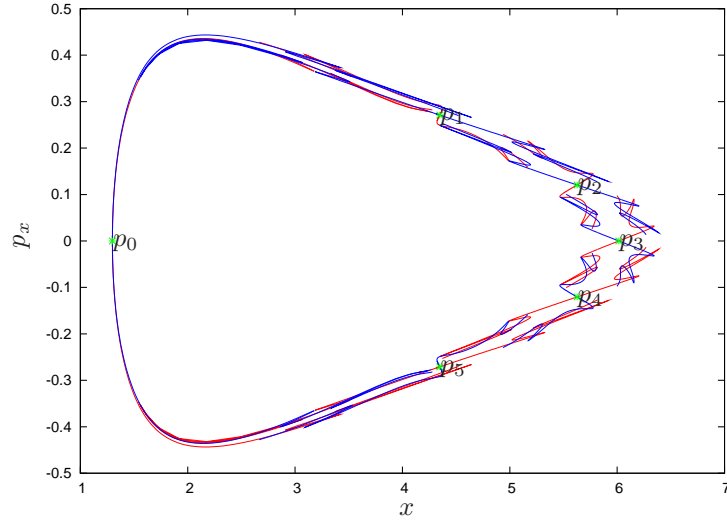


Figure 9: Invariant manifolds of the fixed points p_0, p_1, \dots, p_5 on the section Σ^+ . Unstable manifolds are plotted in red, stable in blue. The fixed points are marked in green.

Remark A.3. For each energy level J , we choose a displacement $\eta = \eta(J)$ such that the local error is $\text{err}(\eta) < 10^{-12}$.

One can think of p as a fixed point of the iterated Poincaré map $\tilde{P} = P^6$, or as a 6-periodic point of the Poincaré map P . If $p_i = P^i(p)$ are the iterates of p for $i = 0, \dots, 5$, then p_i are also fixed points of \tilde{P} . They have associated unstable and stable manifolds, which can be obtained from $W^{u,s}(p)$ by iteration.

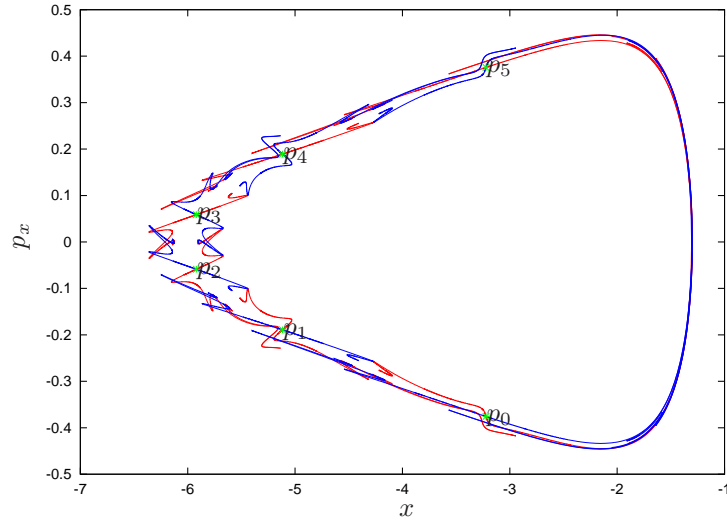


Figure 10: Invariant manifolds on the section Σ^- .

For illustration, let us show some numerical results corresponding to the energy value $J = -1.6$. Figure 9 shows the manifolds of all iterates $\{p_i\}_{i=0,\dots,5}$. Notice that the dynamics in Figure 9 is reversible with respect to the symmetry section $\{y = 0, p_x = 0\}$, as discussed in the previous section (see (90)). Figure 9 shows that the manifolds do intersect transversally at different homoclinic points. We are

interested in measuring the splitting angle between the manifolds. Unfortunately, the homoclinic points do not lie on the symmetry axis, which would be very useful in order to compute them.

In order to have the homoclinic points lie on the symmetry axis, we recompute the manifolds on the new Poincaré section

$$\Sigma^- = \{y = 0, p_y < 0\}.$$

Numerically, we just transport points on the unstable manifold from section Σ^+ to section Σ^- by the forward flow, and points in the stable manifold by the backward flow. See Figures 10 and 11. Now the points that lie on the symmetry line $p_x = 0$ are homoclinic points.

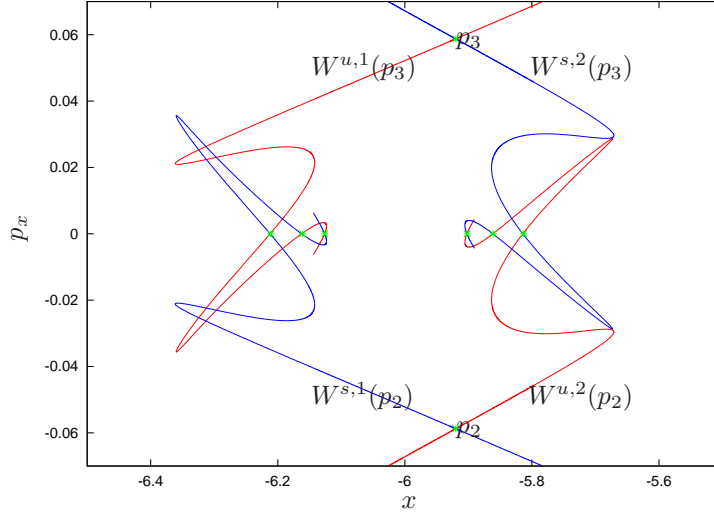


Figure 11: Invariant manifolds of the points p_2 and p_3 on the section Σ^- . Due to the symmetry, points that lie on the line $p_x = 0$ (marked in green) are intersection points.

A.3 Computation of transversal homoclinic points and splitting angle

In this appendix, we compute the angle between the invariant manifolds at one of the transversal intersections. We will restrict the range of energy values to

$$J \in [J_-, J_+] = [-1.81, -1.56], \quad (93)$$

or equivalently the range of eccentricities to $e \in [e_-, e_+] = [0.48, 0.67]$. This is the range where we can validate the accuracy of our computations (see Appendix A.4). Below $e_- = 0.48$, the splitting size becomes comparable to the numerical error that we commit in double precision arithmetic.

Remark A.4. In this paper we concentrate on proving the existence of global instabilities in the Restricted three-body problem; we are not so much concerned with finding the *maximal* range of eccentricities along which the asteroid drifts. Thus we do not investigate the transversality of the splitting below e_- . However, we are convinced that the maximal range of eccentricities is larger than $[e_-, e_+]$, in particular that the lower bound can be pushed well below e_- . We think that our mechanism of instability applies to this larger range of eccentricities. In fact, it is possible to study such exponentially small splitting using more sophisticated numerical methods, such as multiple-precision arithmetic, and high-order approximation of local invariant manifolds, see for instance [FS90, DRR99, GS08].

Consider first a fixed energy level $J = J_0$ that is close to the unperturbed situation, e.g. $J = -1.74$. The corresponding manifolds are given in Figure 12. In general, there are uncountably many intersection points. For instance, in Figure 11 we show six intersections on the symmetry line. However, when

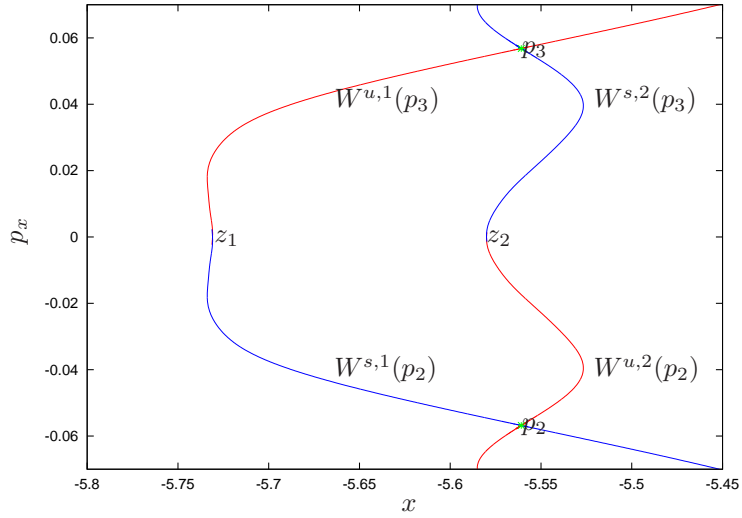


Figure 12: Invariant manifolds of the points p_2 and p_3 for the energy level $J = -1.74$.

the perturbation is small, there is one distinguished intersection point located “in the middle” of the homoclinic. We call it the *primary* intersection point.

Let us compute the primary intersection point z_1 corresponding to the “outer” splitting of the manifolds $W^{u,1}(p_3)$ and $W^{s,1}(p_2)$. For $J = -1.74$, the *primary* intersection z_1 corresponds to the *first* intersection of the manifolds with the $p_x = 0$ line, as we grow the manifolds from the fix points. Thanks to the symmetry, it is enough to look for the intersection of $W^{u,1}(p_3)$ with the $p_x = 0$ axis, because $W^{s,1}(p_2)$ must also intersect the axis at the same point.

To compute the intersection point z_1 , we continue using a linear approximation of the local manifold, and propagate a fundamental domain in the local manifold by iteration. Let v_u be the unstable eigenvector associated to the point p_3 . Consider the fundamental segment l_u between the points $p_3 + \eta v_u$ and $\tilde{P}(p_3 + \eta v_u)$, as in the previous section. First we look for the *smallest* natural n such that $\tilde{P}^n(l_u)$ intersects the $p_x = 0$ axis. Then we use a standard numerical method (bisection-like one-dimensional root finding) to find a point z_u in the fundamental segment l_u such that

$$\pi_{p_x}(\tilde{P}^n(z_u)) = 0.$$

Thus we obtain the homoclinic point $z_1 = \tilde{P}^n(z_u)$ in Figure 12. Numerically, we verify that z_1 is in the the $p_x = 0$ axis within 10^{-10} tolerance.

Finally, we vary energy J and use a continuation method to obtain the family of primary intersections $\{z_1\}_J$, using as seed the primary intersection $z_1|_{J=-1.74}$ found above. See Figure 13.

Remark A.5. For low energy levels (such as $J = -1.74$), corresponding to weak hyperbolicity, the invariant manifolds behave as if they were close to integrable, and the primary intersection corresponds to the *first* intersection of the manifolds with the $p_x = 0$ axis. For high energy levels (such as $J = -1.6$), corresponding to strong hyperbolicity, the manifolds develop some folds, and thus the primary intersection may not correspond to the *first* intersection of the manifolds with the $p_x = 0$ axis. See Figure 11.

In practice, we first identify the primary intersection at low energy levels, and then use a continuation method to obtain the primary family of intersections up to high energy levels.

Analogously, we compute the family of primary intersections $\{z_2\}_J$ corresponding to the inner splitting. See Figure 13.

Let us now compute the splitting angle between the manifolds $W^{u,1}(p_3)$ and $W^{s,1}(p_2)$ at the point z_1 . For illustration, we show some numerical results corresponding to the energy value $J = -1.74$. First we need the tangent vectors w_u and w_s to the manifolds at z_1 . See Figure 14. As found above, let z_u be

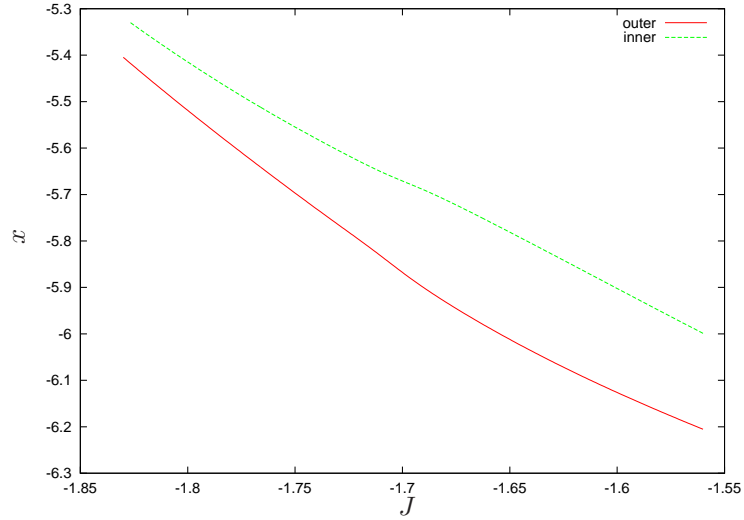


Figure 13: Family of primary intersection points corresponding to outer and inner splitting. For every energy level J , we plot the x coordinate of the intersection point z_1 and z_2 (the p_x coordinate is equal to zero). Notice that both families are continuous.

inner	outer
$(-1.695, -1.694)$	$(-1.701, -1.700)$
$(-1.726, -1.725)$	$(-1.731, -1.730)$
$(-1.756, -1.755)$	$(-1.760, -1.759)$
$(-1.781, -1.780)$	$(-1.784, -1.783)$
$(-1.802, -1.801)$	$(-1.805, -1.804)$

Table 1: Subintervals of $J \in [J_-, J_+]$ containing the zeros of inner splitting (left column) and outer splitting (right column).

the point in the unstable fundamental segment that maps to z_1 , i.e. $\tilde{P}^n(z_u) = z_1$. Consider the tangent vector v_u to the manifold $W^{u,1}(p_3)$ at the point z_u . (Recall that at this point the linear approximation is good enough, so we can use as v_u the unstable eigenvector.) Multiply v_u by the Jacobian of \tilde{P} at the successive iterates $\tilde{P}^i(p_u)$, for $i = 0, \dots, n-1$. This way, we obtain the tangent vector to the unstable manifold at z_1 . Let us denote this vector $w_u = (w_1, w_2)$. We normalize it to $\|w_u\| = 1$.

Due to reversibility, the vector w_s tangent to the stable manifold at z_1 is $w_s = (w_1, -w_2)$. See Figure 14. Notice that we choose the tangent vectors with the appropriate orientation, i.e. with the same orientation as the trajectories on the manifolds.

Thus the oriented splitting angle between w_u and w_s is

$$\sigma = 2 \arctan_2(-w_1, -w_2),$$

where \arctan_2 is the arctangent function of two variables, which uses the signs of the two arguments to determine the sign of the result.

Finally, we let J change and, using this procedure, we are able to obtain the splitting angle for energy levels $J \in [J_-, J_+]$. See Figure 15. The splitting angle is nonzero for all energy values except for a discrete set of them. The splitting angle oscillates around zero with decreasing amplitude as $J \rightarrow J_-$. Numerically, we find that the zeros of the splitting angle are contained in the intervals listed in Table 1.

Notice that the inner and outer splittings behave similarly. However, they become zero at different values of J , as seen in Table 1. Thus, when one of the intersections becomes tangent, the other one is

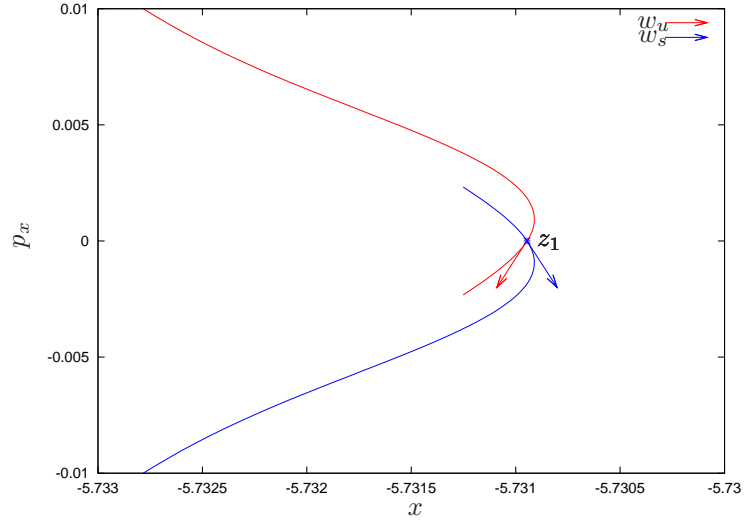


Figure 14: Outer splitting of the manifolds for energy level $J = -1.74$. This is a magnification of Figure 12 at the intersection point z_1 . We show the vectors w_u, w_s tangent to the unstable and stable manifolds at z_1 . The splitting angle σ is the angle between w_u and w_s .

p_x	x^u	x^s	$x^u - x^s$
-0.00002	-5.481541931871417	-5.481541932226887	0.000000000355470
-0.00001	-5.481541931790012	-5.481541931967703	0.000000000177691
0.00000	-5.481541931822124	-5.481541931822124	0.000000000000000
0.00001	-5.481541931967703	-5.481541931790012	-0.000000000177691
0.00002	-5.481541932226887	-5.481541931871417	-0.000000000355470

Table 2: Sampling of the manifolds $W^{u,1}(p_3)$ and $W^{s,1}(p_2)$ at different values of p_x , and their difference (last column).

still transversal, and we can always use one of them for diffusion.

A.4 Accuracy of computations

For small eccentricities, the splitting angle σ becomes very small. We need to check the validity of σ , making sure that the size of (accumulated) numerical errors in the computation is smaller than the size of σ .

The smallest splitting angle in Figure 15, corresponding to $J_- = -1.81$, is

$$\sigma(J_-) = -1.777970294158603 \times 10^{-5}.$$

We check the validity of $\sigma(J_-)$ by recomputing this angle using an alternative numerical method. First we compute the intersection of the manifolds $W^{u,1}(p_3)$ and $W^{s,1}(p_2)$ with the horizontal axis defined by

$$p_x = \frac{j}{10^5}$$

for $j \in (-2, -1, 1, 2)$.

In Table 2 we tabulate the x coordinate of $W^{u,1}(p_3)$ and $W^{s,1}(p_2)$ on these axes, and their difference $d = x^u - x^s$ gives the distance between the manifolds. We apply numerical differentiation to the last

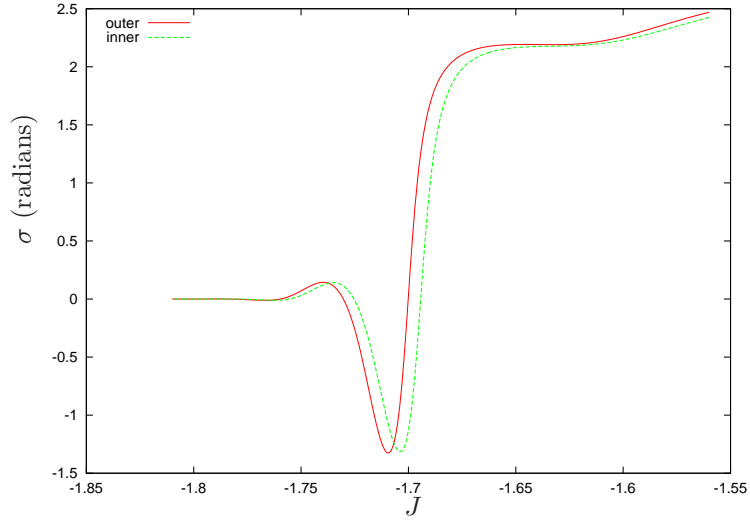


Figure 15: Splitting angle associated to inner and outer splitting.

column of this table, using central differences centered at z_1 with step sizes 0.00002 and 0.00004, and obtain the values:

$$d_1 = \frac{d(0.00001) - d(-0.00001)}{0.00002} = -0.0000177691.$$

$$d_2 = \frac{d(0.00002) - d(-0.00002)}{0.00004} = -0.0000177735.$$

Finally, we use Richardson extrapolation and obtain:

$$d = \frac{4d_1 - d_2}{3} = -0.0000177676333333333333.$$

Thus, using this alternative method, we obtain the splitting angle

$$\sigma(J_-) = \text{atan}(-0.0000177676333333333333) = -0.00001776763333146364.$$

Compare the splitting angle computed using the two methods. They differ by approximately 10^{-8} . This gives an estimate of the numerical error committed in our computation of the splitting angle.

We repeat this test for a range of energies $J \in [-1.81, -1.8]$. In Figure 16, we compare the splitting angle $\sigma(J)$ and the estimate of the numerical error $\text{err}(J)$. This error stays below 10^{-7} , and it is several orders of magnitude smaller than the splitting angle. For higher energy values $J \in [-1.8, -1.56]$, the splitting angle is large, so the numerical error is certainly smaller. Therefore we are confident that the splitting angle has been accurately computed in the range of eccentricities considered, $[J_-, J_+]$.

B Numerical study of the inner and outer dynamics

In Appendix A we have studied the periodic orbits and the invariant manifolds in rotating Cartesian coordinates (x, y, p_x, p_y) . Nevertheless, the study of the inner and outer maps are done in rotating Delaunay coordinates. Indeed since these coordinates are action-angle coordinates for the two body problem, it is much more convenient to use them to study the mean motion resonance.

The Poincaré section $\{y = 0\}$ is completely different from the section $\{g = 0\}$ which will be used from now on (see (21)). In particular, the periodic orbits $\{\lambda_J\}_{J \in [\bar{J}_-, \bar{J}_+]}$ obtained in Appendix A.1 intersect the section $\{y = 0\}$ six times whereas they intersect $\{g = 0\}$ seven times. However, we remark that the

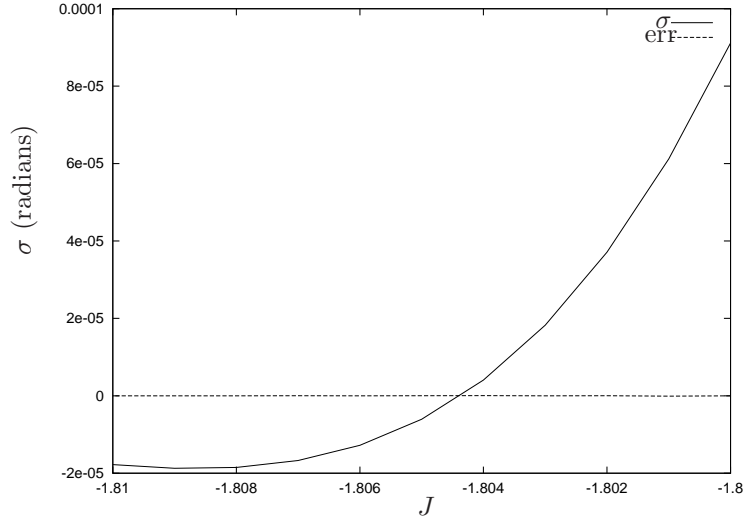


Figure 16: Splitting angle $\sigma(J)$ and estimate of the numerical error $\text{err}(J)$ as a function of energy level J .

homoclinic points z_1 and z_2 lie on the symmetry axis both in Cartesian and in Delaunay variables. See Figures 17 and 18.

To obtain the intersection of these periodic orbits with $\{g = 0\}$ we just need to express the 6-periodic points of the Poincaré map P obtained in Appendix A.1 in Delaunay coordinates and then iterate them by the flow of the circular problem expressed in Delaunay coordinates until they hit the section $\{g = 0\}$. We do the same with the homoclinic points. In Appendix B.1 we explain how to compute the change of coordinates and the vector field in Delaunay coordinates. Then, in Appendices B.2 and B.3 we study the inner and outer maps of the circular and elliptic problems respectively. Finally, in Appendix B.4 we compare the inner and outer maps of the elliptic problem, which leads to Ansatz 3.

B.1 From Cartesian to Delaunay and computation of $\partial_G \Delta H_{\text{circ}}$

We explain an easy way to obtain the rotating Delaunay coordinates from rotating Cartesian (or polar) coordinates in the circular problem. First recall that G can be computed as

$$G = r(-p_x \sin \phi + p_y \cos \phi).$$

The potential $\mu \Delta H_{\text{circ}}$ in Cartesian coordinates only depends on the position (x, y) of the asteroid, and can be easily computed. Then, one can use the equation

$$J = -\frac{1}{2L^2} - G + \mu \Delta H_{\text{circ}}$$

to obtain L . Knowing L and G we can obtain the eccentricity e by

$$e = \sqrt{1 - \frac{G^2}{L^2}}.$$

Using that $r = L^2(1 - e \cos u)$, one can obtain u and from here ℓ using Kepler's equation $u - e \sin u = \ell$. On the other hand, from u we can obtain v using

$$\tan \frac{v}{2} = \sqrt{\frac{1+e}{1-e}} \tan \frac{u}{2}.$$

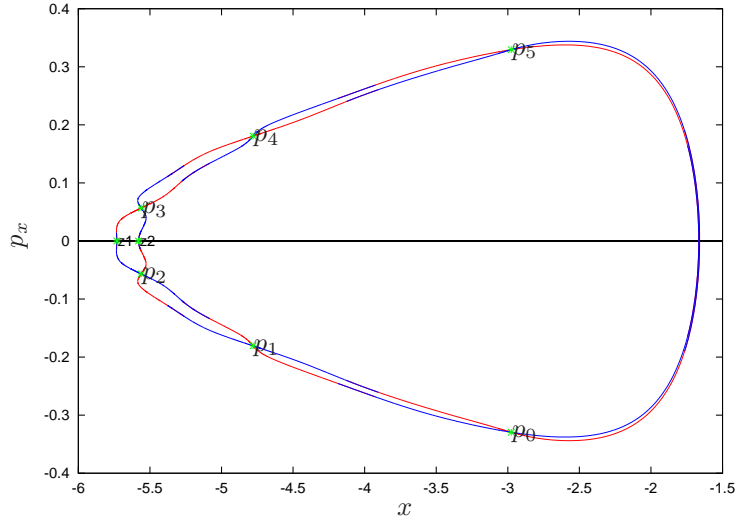


Figure 17: Energy $J = -1.74$. Resonance structure in Cartesian coordinates. The axis of symmetry is marked with a horizontal line.

Finally, we can deduce g using that $\phi = v + g$.

We devote the rest of this appendix to compute $\partial_G \Delta H_{\text{circ}}$. The other derivatives of ΔH_{circ} can be computed analogously. Let us define

$$D[r_0] = D[r_0](r, v, g) = (r^2 + r_0^2 - 2rr_0 \cos(v + g))^{-1/2}.$$

Then

$$\Delta H_{\text{circ}}(L, \ell, G, g) = -(1 - \mu)D[-\mu] - \mu D[1 - \mu] - D[0].$$

Thus by the chain rule there only remains to compute $\partial_G r$ and $\partial_G v$. First, let us point out that

$$\partial_G e = -\frac{G}{eL^2} = \frac{e^2 - 1}{eG}.$$

On the other hand, using that $\ell = u - e \sin u$, one has that

$$\partial_e u = \frac{\sin u}{1 - e \cos u}.$$

Then, since $r(L, e, \ell) = L^2(1 - e \cos u(e, \ell))$, using that

$$\cos v = \frac{\cos u - e}{1 - e \cos u}, \tag{94}$$

we have that

$$\partial_e r(L, e, \ell) = L^2 \cos v$$

and therefore,

$$\partial_G r(L, \ell, G) = -\frac{G \cos v}{e}.$$

To compute $\partial_G v$, let us point out that $\partial_G v = \partial_e v \partial_G e$. Therefore it only remains to compute $\partial_e v$, we obtain it using formula (94) and

$$\sin v = \frac{\sqrt{1 - e^2} \sin u}{1 - e \cos u}.$$

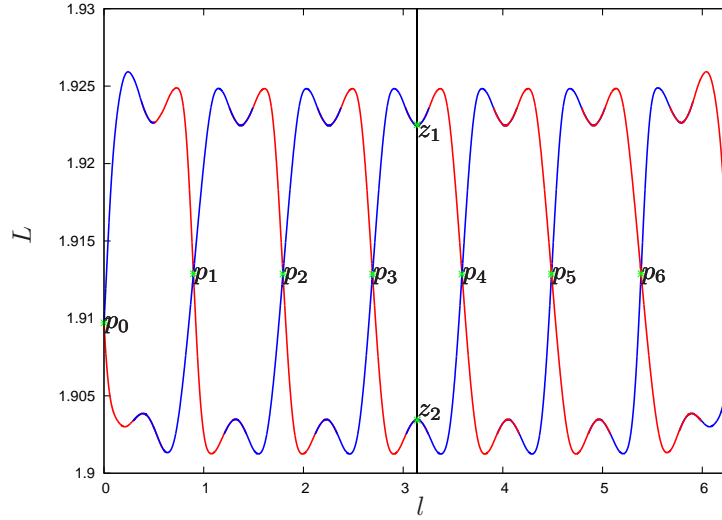


Figure 18: Energy $J = -1.74$. Resonance structure in Delaunay coordinates. The symmetry corresponds to $l = 0$ and $l = \pi$ and is marked with a vertical line.

Then,

$$\partial_e v = \frac{\sin v}{1 - e^2} (2 + e \cos v).$$

and therefore,

$$\partial_G v = -\frac{\sin v}{eG} (2 + e \cos v).$$

B.2 Inner and outer dynamics of the circular problem

In this appendix, we numerically compute the inner map $\mathcal{F}_0^{\text{in}}$ and the outer maps $\mathcal{F}_0^{\text{out},*}$ of the circular problem, given in Section 2. Recall that to compute these maps we deal with the extended system given by the Hamiltonian H in (16) with $e_0 = 0$ restricted to the energy level $H = 0$ and thus, we have that $I = -J$. Then, we consider $I \in [I_-, I_+] = [-J_+, -J_-]$, where the range $[-J_+, -J_-]$ is given in (93).

As seen in Section 2.2, the inner map has the form

$$\mathcal{F}_0^{\text{in}} : \begin{pmatrix} I \\ t \end{pmatrix} \mapsto \begin{pmatrix} I \\ t + \mu \mathcal{T}_0(I) \end{pmatrix}, \quad (95)$$

where $T_J = 14\pi + \mu \mathcal{T}_0(I)$ is the period of the periodic orbit obtained in Ansatz 1 on the corresponding level of energy J , which now corresponds to an invariant hyperplane $I = \text{constant}$.

Recall that we computed the periodic orbit λ_J as well as its period T_J in Appendix A.1. In particular, Figure 6 shows a plot of the function $T_J - 14\pi = \mu \mathcal{T}_0(I)$. Notice that the derivative of the function $\mathcal{T}_0(I)$ is nonzero for the whole range $[I_-, I_+]$. This shows that the inner map is twist. Moreover, Figure 6 shows that

$$0 < \mu \mathcal{T}_0(I) < 60\mu < \pi.$$

Therefore, the function $\mathcal{T}_0(I)$ satisfies the properties stated in Lemma 2.

As a test, we have computed the same function $\mathcal{T}_0(I)$ using two different methods. First by computing the period of the periodic orbit, as above. Then by computing the integral expression (38) using numerical integration. The difference in $\mathcal{T}_0(I)$ using both methods is of the order 10^{-12} .

As seen in Section 2.3, the outer maps have the form

$$\mathcal{F}_0^{\text{out},*} : \begin{pmatrix} I \\ t \end{pmatrix} \mapsto \begin{pmatrix} I \\ t + \mu \omega^*(I) \end{pmatrix}, \quad * = \text{f, b.} \quad (96)$$

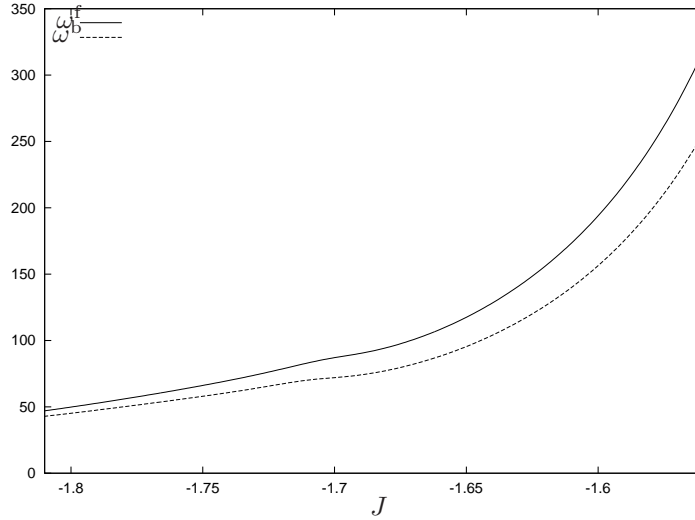


Figure 19: Functions $\omega^f(I)$ and $\omega^b(I)$ involved in the definition of the outer map (96) of the circular problem as a function of the Jacobi constant J (recall that in the circular problem $I = -J$).

For simplicity, let us only discuss the computation of $\omega^f(I)$ ($\omega^b(I)$ is computed analogously). Recall from Lemma 2.6 that the function $\omega^f(I)$ is defined as

$$\omega^f(I) = \omega_{\text{out}}^f(I) + \omega_{\text{in}}^f(I),$$

where, taking into account that the homoclinic orbit is symmetric with respect to the involution (19),

$$\omega_{\text{out}}^f(I) = \omega_+^f(I) - \omega_-^f(I) = 2\omega_+^f(I) \quad (97)$$

with

$$\omega_+^f(I) = \lim_{N \rightarrow +\infty} \left(\int_0^{14N\pi} \frac{(\partial_G \Delta H_{\text{circ}}) \circ \gamma_I^f(\sigma)}{-1 + \mu(\partial_G \Delta H_{\text{circ}}) \circ \gamma_I^f(\sigma)} d\sigma + N\mathcal{T}_0(I) \right), \quad (98)$$

$$\omega_{\text{in}}^f(I) = \int_0^{-12\pi} \frac{(\partial_G \Delta H_{\text{circ}}) \circ \lambda_I^4(\sigma)}{-1 + \mu(\partial_G \Delta H_{\text{circ}}) \circ \lambda_I^4(\sigma)} d\sigma. \quad (99)$$

To obtain $\omega^f(I)$, we compute the integrals (98) and (99) numerically, using a standard algorithm from the GSL library [GG09]. The integrals are computed within a relative error limit 10^{-9} .

The function $\partial_G \Delta H_{\text{circ}}$ involved in both integrals is given explicitly in Appendix B.1. The integral $\omega_{\text{in}}^f(I)$ is evaluated on a periodic trajectory $\lambda_I^4(\sigma)$ of the reduced circular problem (namely, with reparameterized time, see (30)) with initial condition p_4 , a fixed point of the Poincaré map \mathcal{P}_0^7 . The integral $\omega_+^f(I)$ is evaluated on a homoclinic trajectory $\gamma_I^f(\sigma)$ of the reduced circular problem with initial condition z_2 , the primary homoclinic point corresponding to the inner splitting found in Appendix A.3.

Next we make a couple of important remarks about the numerical computation of the integral $\omega_+^f(I)$. The key point is that the homoclinic orbit γ_I^f was already computed in Appendix A.3 with high accuracy, and we can exploit this information here. Recall that the primary homoclinic point z_2 was obtained as the n -th iterate of a point z_u in the local fundamental segment l_u under the Poincaré map:

$$z_2 = \{\mathcal{P}_0^7\}^n(z_u). \quad (100)$$

Moreover, recall that the point z_u was chosen to be suitably close to the fixed point p_3 for each energy level J . See Remark A.3.

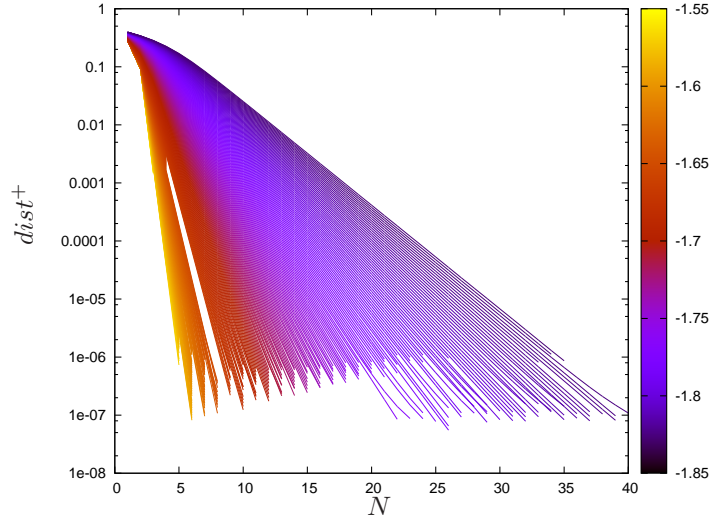


Figure 20: Exponential decay of the function dist^+ as a function of N (multiples of the period) for different energy levels. The energy levels $J \in [J_-, J_+]$ are color-coded.

Notice that the integral $\omega_+^f(I)$ is defined by a limit as $N \rightarrow \infty$, i.e. as the homoclinic orbit $\gamma_I^f(\sigma)$ asymptotically approaches the periodic orbit $\lambda_I^3(\sigma)$ in forward time (see equation (39)). Numerically, of course, we should stop integrating at an upper endpoint N large enough such that the integral converges. In practice, we choose the upper endpoint $N = N(I)$ to be the number of iterates $n = n(I)$ in (100). This means that we evaluate the integral along the homoclinic trajectory $\gamma_I^f(\sigma)$ until it reaches the point z_u , which is suitably close to the periodic orbit.

Notice also that integrating the homoclinic trajectory $\gamma_I^f(\sigma)$ forwards in the reduced system means integrating it backwards along the unstable manifold in the original system. This is numerically unstable, since numerical errors grow exponentially. In practice, we rewrite the integral (98) using the change of variables $\hat{\sigma} = \sigma - 14N\pi$ so that the homoclinic trajectory is integrated forwards along the unstable manifold, starting from the point z_u .

The computed values of the functions $\omega^f(I)$ and $\omega^b(I)$ are shown in Figure 19. Note that they are plotted as a function of the Jacobi constant J instead of as a function of I , so that they can be compared with Figure 6, where we have plotted $\mu\mathcal{T}_0(I) = T_J - 14\pi$ as a function of J .

To test the computation of the function ω_+^f , we directly verify the definition of the outer map in 2.3. Let $z_2 = (L_h, \ell_h, G_h, 0)$ be the primary homoclinic point, and let $p_3 = (L_p, \ell_p, G_p, 0)$ be the periodic point. Given a point $(L_h, \ell_h, G_h, 0, I, t)$ in the extended circular problem, we check that it is forward asymptotic (in the reparametrized time) to the point $(L_p, \ell_p, G_p, 0, I, t + \omega_+^f(I))$, where $t \in \mathbb{T}$ is arbitrary. Thus we check that the distance

$$\text{dist}^+(s) = |\Phi_0\{s, (L_h, \ell_h, G_h, 0, I, t)\} - \Phi_0\{s, (L_p, \ell_p, G_p, 0, I, t + \omega_+^f(I))\}| \xrightarrow{s \rightarrow \infty} 0$$

with exponential decay.

The result of the test is shown in Figure 20 for values of the energy $J \in [J_-, J_+]$ (recall that $J = -I$). Notice that the vertical axis is in logarithmic scale. Let $s = 14N\pi$. We plot the distance dist^+ as a function of N (multiples of the period). The test shows exponential decay of the distance function for all energy values, i.e. straight lines in the plot.

Recall that the periodic orbits $\lambda_I^{3,4}(s)$ become more hyperbolic as the energy I decreases. Thus, the rate of exponential convergence between the homoclinic and the periodic trajectory also increases, i.e. the straight lines have increasing slope in the plot. As explained above, the length of integration $N = N(I)$ along the homoclinic orbit is suitably chosen for each energy level. For $I \rightarrow I_-$, there is exponential decay up to time $s = 40 \cdot (14\pi) \approx 1760$.

B.3 Inner and outer dynamics of the elliptic problem

In this appendix, we numerically compute the first orders in e_0 of the inner map $\mathcal{F}_{e_0}^{\text{in}}$ and the outer maps $\mathcal{F}_{e_0}^{\text{out},*}$ of the elliptic problem, given in Section 3. In order to compare the inner and outer dynamics of the elliptic problem through Lemma 4.2, only some specific terms in the expansions of the inner and outer maps are necessary. Namely, we only need to compute the term A_1 in the expansion of the inner map (61), and the terms B^* in the expansion of the outer maps (72).

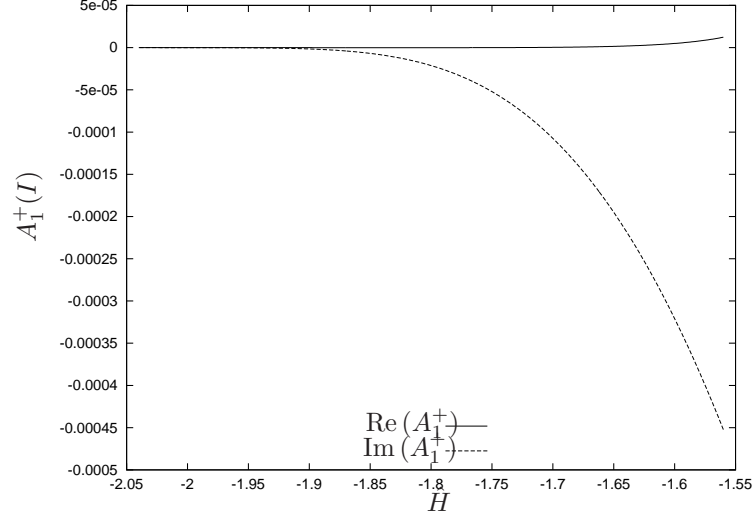


Figure 21: Function $A_1^+(I)$ (real and imaginary parts) involved in the definition of the inner map (61) of the elliptic problem as a function of the energy of the system in rotating coordinates \hat{H} . Recall that $\hat{H} = -I$.

Recall from Section 3.4 that A_1 can be split as

$$A_1(I, t) = A_1^+(I)e^{it} + A_1^-(I)e^{-it}.$$

Since A_1^+ and A_1^- are complex conjugate, it is only necessary to compute one of them. Let us compute the positive harmonic,

$$A_1^+(I) = -i\mu \int_0^{-14\pi} \frac{\Delta H_{\text{ell}}^{1,+} \circ \lambda_I^3(\sigma)}{-1 + \mu \partial_G \Delta H_{\text{circ}} \circ \lambda_I^3(\sigma)} e^{i\tilde{\lambda}_I^3(\sigma)} d\sigma. \quad (101)$$

Notice that the denominator is the same one used in the previous section for the inner and outer dynamics of the circular problem. Next we give the numerator $i\Delta H_{\text{ell}}^{1,+}$ explicitly. Let

$$\begin{aligned} \Delta H_{\text{ell}}^1(L, \ell, G, g, t) = & -\frac{1-\mu}{\mu} \mathcal{B}_1 \left(-\frac{r(L, \ell, G)}{\mu}, v(L, \ell, G), g, t \right) \\ & - \frac{\mu}{1-\mu} \mathcal{B}_1 \left(\frac{r(L, \ell, G)}{1-\mu}, v(L, \ell, G), g, t \right), \end{aligned}$$

where \mathcal{B}_1 is the function defined in Lemma 3.4. Then it is straightforward to see that

$$\begin{aligned} \Delta H_{\text{ell}}^{1,+}(l, L, g, G) = & -\frac{1-\mu}{\mu} \mathcal{B}_1^+ \left(-\frac{r(L, \ell, G)}{\mu}, v(L, \ell, G), g \right) \\ & - \frac{\mu}{1-\mu} \mathcal{B}_1^+ \left(\frac{r(L, \ell, G)}{1-\mu}, v(L, \ell, G), g \right), \end{aligned} \quad (102)$$

where

$$\mathcal{B}_1^+(r, v, g) = -\frac{1 - r \cos(v + g) - i2r \sin(v + g)}{2\Delta^3(r, v + g)}.$$

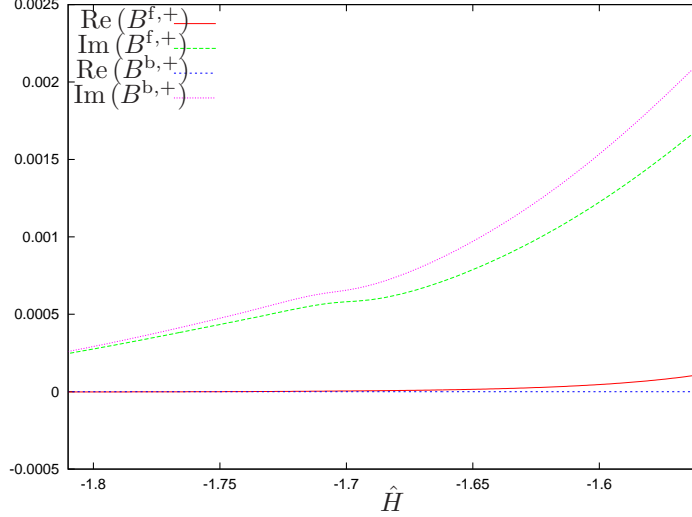


Figure 22: Functions $B^{f,+}$ and $B^{b,+}$ (real and imaginary parts) involved in the definition of the outer map (72) of the elliptic problem.

The computed value of the function A_1^+ is shown in Figure 21. We plot it as a function of the energy of the elliptic problem in rotating coordinates \hat{H} in (15). Recall that since we are working in the energy level $H = 0$ of the extended Hamiltonian H in (16), we have that $I = -\hat{H}$.

For the outer map, we compute the functions $B^*(I)$. Similarly to A_1 , it is only necessary to compute the positive harmonics $B^{*,+}$. Recall from Lemma 3.9 that the positive harmonics $B^{f,+}(I)$ and $B^{b,+}(I)$ are defined as

$$\begin{aligned} B^{f,+}(I) &= B_{\text{out}}^{f,+}(I) + B_{\text{in}}^{f,+}(I)e^{i\mu\omega_{\text{out}}^f(I)} \\ B^{b,+}(I) &= B_{\text{in}}^{b,+}(I) + B_{\text{out}}^{b,+}(I)e^{i\mu\omega_{\text{in}}^b(I)}, \end{aligned} \quad (103)$$

where ω_{out}^f and ω_{in}^b were obtained in Appendix B.2. To obtain $B_{\text{out}}^{*,+}$ and $B_{\text{in}}^{*,+}$, we compute the integrals (74)–(76) numerically, using the same techniques as in the previous Appendix B.2. In particular, the integrands of the Melnikov integrals (74) and (75), by construction, decay exponentially as $T \rightarrow \pm\infty$ and we take the same approximate limits of integration $\pm 14\pi N$ where $N = N(I)$ is the constant considered in Appendix B.2.

The computed values of the functions $B^{f,+}(I)$ and $B^{b,+}(I)$ are shown in Figure 22.

B.4 Comparison of the inner and outer dynamics of the elliptic problem

Finally, we verify the non-degeneracy condition

$$\tilde{B}^{*,\pm}(\mathcal{I}) \neq 0 \quad \text{for } \mathcal{I} \in \mathcal{D}^* \quad (104)$$

stated in Lemma 4.2, which implies the existence of a transition chain of tori. Since $B^{*,+}$ and $B^{*, -}$ are complex-conjugate, it is only necessary to compute one of them. Let us compute the positive harmonic,

$$\tilde{B}^{*,+}(\mathcal{I}) = B^{*,+}(\mathcal{I}) - \frac{e^{i\mu\omega^*(\mathcal{I})} - 1}{e^{i\mu\tau_0(\mathcal{I})} - 1} A_1^+(\mathcal{I}).$$

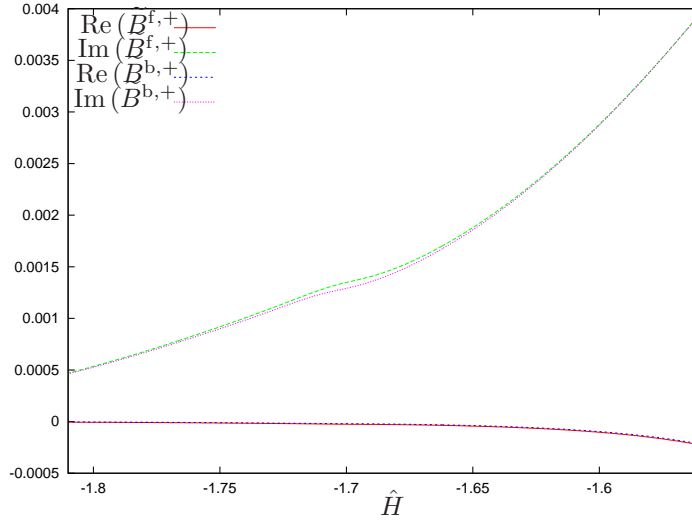


Figure 23: Functions $\tilde{B}^{f,+}$ and $\tilde{B}^{b,+}$ (real and imaginary parts).

All the functions involved in the expression above are known: \mathcal{T}_0 and ω^* are obtained in Appendix B.2 and A_1^+ and $B^{*,+}$ are obtained in Appendix B.3.

The computed values of the functions $\tilde{B}^{f,+}$ and $\tilde{B}^{b,+}$ are shown in Figure 23. Therefore, we see that the functions $\tilde{B}^{*,+}$ are not identically zero. This justifies Ansatz 3.

Remark B.1. Figure 23 also shows that $\tilde{B}^{f,+}$ and $\tilde{B}^{b,+}$ are almost identical, which is surprising for the authors. However, this fact is not relevant for the argument in Lemma 4.2; we only need that these functions do not vanish identically.

C The Main Result for the 3 : 1 resonance: instabilities in the Kirkwood gaps

We devote this appendix to show how the proof of Theorem 1 in Sections 2–4 can be adapted to deal with the 3 : 1 resonances. First, we state a more rigorous version of Main Result (3 : 1).

Theorem 5. *Assume Ansätze 4, 5 and 6. Then there exists $e_0^* > 0$ such that for $0 < e_0 < e_0^*$, there exist $T > 0$ and an orbit of the Hamiltonian (16) which satisfy*

$$G(0) > 0.56 \text{ and } G(T) < 0.32$$

whereas

$$\left| L(t) - 3^{-1/3} \right| \leq 100\mu.$$

Ansätze 4 and 5 are stated in Appendix C.1 and Ansatz 6 is stated in Appendix C.2. They are analogous to Ansätze 1, 2 and 3 but referred to the 3 : 1 resonance instead of the 1 : 7 one. To prove this theorem, we consider the Hamiltonian (16) and we study the resonance

$$\dot{\ell} \sim 3 \quad \text{and} \quad \dot{g} \sim -1. \quad (105)$$

As for the 1 : 7 resonance, without loss of generality, we take $H = 0$ and we look for a large drift in I , which being L almost constant, implies a big drift in G .

C.1 The circular problem

We first study the circular problem (18), close to the resonance $3^{-1}\dot{\ell} + \dot{g} \sim 0$. We assume the following ansatz. It has been verified numerically (see Appendix C.3). It replicates Ansatz 1.

Ansatz 4. *Consider the Hamiltonian (18) with $\mu = 10^{-3}$. Then, in each energy level $J \in [J_-, J_+] = [-1.6, -1.3594]$, there exists a hyperbolic periodic orbit $\lambda_J = (L_J(t), \ell_J(t), G_J(t), g_J(t))$ of period T_J which satisfies*

$$|T_J - 2\pi| < 15\mu,$$

and is smooth with respect to J , and

$$\left| L_J(t) - 3^{-1/3} \right| < 100\mu$$

for all $t \in \mathbb{R}$.

Each λ_J has two branches of stable and unstable invariant manifolds $W^{s,j}(\lambda_J)$ and $W^{u,j}(\lambda_J)$, $j = 1, 2$. Then, for each $J \in [J_-, J_+]$ either $W^{s,1}(\lambda_J)$ and $W^{u,1}(\lambda_J)$ or $W^{s,2}(\lambda_J)$ and $W^{u,2}(\lambda_J)$ intersect transversally.

Note that since now Jupiter is slower than the Asteriod, the period of these periodic orbits is approximately the period of Jupiter instead of the period of the asteroid. For the *Extended Circular Problem* given by the Hamiltonian (16) with $e_0 = 0$, the periodic orbits obtained in Ansatz 4 become invariant two-dimensional tori which belong to hyperplanes $I = \text{constant}$ for any

$$I \in [I_-, I_+] = [-J_+, -J_-] = [1.3594, 1.6].$$

Corollary C.1. *Assume Ansatz 4. Then, the Hamiltonian (16) with $\mu = 10^{-3}$ and $e_0 = 0$ has an analytic normally hyperbolic invariant 3-dimensional manifold Λ_0 , which is foliated by two-dimensional invariant tori.*

Moreover, Λ_0 has two branches of stable and unstable invariant manifolds, which we call $W^{s,j}(\Lambda_0)$ and $W^{u,j}(\Lambda_0)$, $j = 1, 2$. Then, in the invariant planes $I = \text{constant}$, for each $I \in [I_-, I_+]$ either $W^{s,1}(\Lambda_0)$ and $W^{u,1}(\Lambda_0)$ or $W^{s,2}(\Lambda_0)$ and $W^{u,2}(\Lambda_0)$ intersect transversally.

For the analysis of the 3 : 1 resonance is more convenient to consider the global Poincaré section $\{\ell = 0\}$ instead of the section $\{g = 0\}$ considered in Section 2, since now the asteroid moves faster than Jupiter. We consider the map

$$\mathcal{P}_0 : \{\ell = 0\} \longrightarrow \{\ell = 0\}, \quad (106)$$

induced by the flow associated to the Hamiltonian (16) with $e_0 = 0$. Now the intersection of the cylinder Λ_0 with the section $\{\ell = 0\}$ is formed by three cylinders $\tilde{\Lambda}_0^j$, $j = 0, 1, 2$. Namely,

$$\Lambda_0 \cap \{\ell = 0\} = \tilde{\Lambda}_0 = \bigcup_{j=0}^2 \tilde{\Lambda}_0^j. \quad (107)$$

As a whole $\cup_{j=0}^2 \tilde{\Lambda}_0^j$ is a normally hyperbolic invariant manifold for the Poincaré map \mathcal{P}_0 whereas each $\tilde{\Lambda}_0^j$ is a normally hyperbolic invariant manifold for \mathcal{P}_0^3 . These cylinders have a natural system of coordinates, which we use to study the inner and outer dynamics on them. We work with $\tilde{\Lambda}_0^1$ and $\tilde{\Lambda}_0^2$ since in each invariant plane $I = \text{constant}$ they are connected by at least one heteroclinic connection (of \mathcal{P}_0^3) which is symmetric with respect to the involution (19). As before, we call it a forward heteroclinic orbit if it is asymptotic to $\tilde{\Lambda}_0^1$ in the past and $\tilde{\Lambda}_0^2$ in the future and a backward heteroclinic orbit if it is asymptotic to $\tilde{\Lambda}_0^2$ in the past and to $\tilde{\Lambda}_0^1$ in the future. We denote by $\mathcal{D}^f \subset [I_-, I_+]$, where f stands for forward, the subset of $[I_-, I_+]$ where $W^u(\tilde{\Lambda}_0^1)$ and $W^s(\tilde{\Lambda}_0^2)$ intersect transversally and by $\mathcal{D}^b \subset [I_-, I_+]$, where b stands for backward, the subset of $[I_-, I_+]$ where $W^s(\tilde{\Lambda}_0^1)$ and $W^u(\tilde{\Lambda}_0^2)$ intersect transversally. By Corollary C.1 we have that $\mathcal{D}^f \cup \mathcal{D}^b = [I_-, I_+]$.

Corollary C.2. *Assume Ansatz 4. Then, the Poincaré map \mathcal{P}_0^3 defined in (106), which is induced by the Hamiltonian (16) with $\mu = 10^{-3}$ and $e_0 = 0$, has three analytic normally hyperbolic invariant manifolds $\tilde{\Lambda}_0^j$, $j = 0, 1, 2$. They are foliated by one-dimensional invariant curves. Moreover, there exist analytic functions $\mathcal{G}_0^j : [I_-, I_+] \times \mathbb{T} \rightarrow (\mathbb{R} \times \mathbb{T})^3$,*

$$\mathcal{G}_0^j(I, t) = \left(\mathcal{G}_0^{j,L}(I), 0, \mathcal{G}_0^{j,G}(I), \mathcal{G}_0^{j,g}(I), I, t \right),$$

that parameterize $\tilde{\Lambda}_0^j$, namely,

$$\tilde{\Lambda}_0^j = \left\{ \mathcal{G}_0^j(I, t) : (I, t) \in [I_-, I_+] \times \mathbb{T} \right\}.$$

The associated invariant manifolds $W^u(\tilde{\Lambda}_0^1)$ and $W^s(\tilde{\Lambda}_0^3)$ intersect transversally provided $I \in \mathcal{D}^f$; and $W^s(\tilde{\Lambda}_0^1)$ and $W^u(\tilde{\Lambda}_0^2)$ intersect transversally provided $I \in \mathcal{D}^b$. Moreover, one of the points of these intersections belongs to the symmetry axis of (19). Let us denote by Γ_0^* , $*$ = f, b, these intersections. Then, there exist analytic functions

$$\mathcal{C}_0^* : \mathcal{D}^j \times \mathbb{R} \rightarrow (\mathbb{R} \times \mathbb{T})^3, \quad (I, t) \mapsto \mathcal{C}_0^*(I, t), \quad * = f, b,$$

which parameterize them:

$$\Gamma_0^* = \left\{ \mathcal{C}_0^*(I, t) = (\mathcal{C}_0^{*,L}(I), 0, \mathcal{C}_0^{*,G}(I), \mathcal{C}_0^{*,g}(I), I, t) : (I, t) \in \mathcal{D}^* \times \mathbb{T} \right\}, \quad * = f, b.$$

Corollary C.1 gives global coordinates (I, t) for each cylinder $\tilde{\Lambda}_0^j$. These coordinates are symplectic with respect to the canonical symplectic form $\Omega_0 = dI \wedge dt$. We consider the inner and the two outer maps in the cylinder $\tilde{\Lambda}_0^1$.

The inner map The inner map $\mathcal{F}_0^{\text{in}} : \tilde{\Lambda}_0^1 \rightarrow \tilde{\Lambda}_0^1$ is defined as the Poincaré map \mathcal{P}_0^3 restricted to the symplectic invariant submanifold $\tilde{\Lambda}_0^1$. It is of the form

$$\mathcal{F}_0^{\text{in}} : \begin{pmatrix} I \\ t \end{pmatrix} \mapsto \begin{pmatrix} I \\ t + \mu \mathcal{T}_0(I) \end{pmatrix}, \quad (108)$$

where the function \mathcal{T}_0 is such that $2\pi + \mu \mathcal{T}_0(I)$ is the period of the periodic orbit obtained in Ansatz 4 on the corresponding energy surface. We assume the following ansatz, which asserts that this map is twist (see the corresponding Ansatz 2). It has been verified numerically (see Appendix C.3).

Ansatz 5. *The function $\mathcal{T}_0(I)$ satisfies*

$$\partial_I \mathcal{T}_0(I) \neq 0 \quad \text{for } I \in [I_-, I_+].$$

Therefore, the analytic symplectic inner map $\mathcal{F}_0^{\text{in}}$ is twist. Moreover, the function $\mathcal{T}_0(I)$ satisfies

$$0 < \mu \mathcal{T}_0(I) < \pi.$$

The outer map Proceeding as in Section 2.3, we define the outer map for the circular problem at the 3 : 1 resonance. Recall that it has been defined as a composition of the map given by Definition 2.3 and a suitable power of the Poincaré map \mathcal{P}_0 restricted to the cylinders $\tilde{\Lambda}_0^j$. For the 3 : 1 resonance, we consider outer maps $\mathcal{F}_0^{\text{out},*}$, $*$ = f, b, which connect $\tilde{\Lambda}_0^1$ to itself and are defined as

$$\begin{aligned} \mathcal{F}_0^{\text{out},f} &= \mathcal{P}_0^2 \circ \mathcal{S}^f : \tilde{\Lambda}_0^1 \longrightarrow \tilde{\Lambda}_0^1 \\ \mathcal{F}_0^{\text{out},b} &= \mathcal{S}^b \circ \mathcal{P}_0 : \tilde{\Lambda}_0^1 \longrightarrow \tilde{\Lambda}_0^1, \end{aligned}$$

where \mathcal{S}^f is the outer map which connects $\tilde{\Lambda}_0^1$ and $\tilde{\Lambda}_0^2$ through $W^u(\tilde{\Lambda}_0^1) \cap W^s(\tilde{\Lambda}_0^2)$ and \mathcal{S}^b is the outer map which connects $\tilde{\Lambda}_0^2$ and $\tilde{\Lambda}_0^1$ through $W^u(\tilde{\Lambda}_0^2) \cap W^s(\tilde{\Lambda}_0^1)$. Recall that we are abusing notation since

the forward and backwards outer maps are only defined provided $I \in \mathcal{D}^f$ and $I \in \mathcal{D}^b$ respectively and not in the whole cylinder $\tilde{\Lambda}_0^1$.

As for 1 : 7 case, these maps are of the form

$$\mathcal{F}_0^{\text{out},*} : \begin{pmatrix} I \\ t \end{pmatrix} \mapsto \begin{pmatrix} I \\ t + \mu\omega^*(I) \end{pmatrix}, \quad * = f, b. \quad (109)$$

Since we want to compute these outer maps using flows, we need to reparameterize time in the vector field associated to the Hamiltonian (16) with $e_0 = 0$, so that it preserves the section $\{\ell = 0\}$. We consider the following vector field, which corresponds to identifying the variable ℓ with time,

$$\begin{aligned} \frac{d}{ds}\ell &= 1 & \frac{d}{ds}L &= -\frac{\partial_\ell H}{L^{-3} + \mu\partial_L \Delta H_{\text{circ}}} \\ \frac{d}{ds}g &= \frac{-1 + \mu\partial_G \Delta H_{\text{circ}}}{L^{-3} + \mu\partial_L \Delta H_{\text{circ}}} & \frac{d}{ds}G &= -\frac{\partial_g H}{L^{-3} + \mu\partial_L \Delta H_{\text{circ}}} \\ \frac{d}{ds}t &= \frac{1}{L^{-3} + \mu\partial_L \Delta H_{\text{circ}}} & \frac{d}{ds}I &= 0 \end{aligned} \quad (110)$$

where H is Hamiltonian (16) with $e_0 = 0$. Notice that now we are not changing time direction, as happened in the 1 : 7 resonance. We refer to this system as a *reduced circular problem*. Recall that we denote by Φ_0^{circ} the flow associated to the (L, ℓ, G, g) components of equation (30) (which are independent of t and I). We use it to derive the formulas for the outer map. Let

$$\begin{aligned} \gamma_I^*(\sigma) &= \Phi_0^{\text{circ}}\{\sigma, (\mathcal{C}_0^{*,L}(I), 0, \mathcal{C}_0^{*,G}(I), \mathcal{C}_0^{*,g}(I))\}, \quad * = f, b \\ \lambda_I^j(\sigma) &= \Phi_0^{\text{circ}}\{\sigma, (\mathcal{G}_0^{j,L}(I), 0, \mathcal{G}_0^{j,G}(I), \mathcal{G}_0^{j,g}(I))\} \end{aligned} \quad (111)$$

be trajectories of the circular problem. Then, one can see that the functions $\omega^{f,b}(I)$ involved in the definition of the outer maps in (109) can be defined as

$$\omega^*(I) = \omega_{\text{out}}^*(I) + \omega_{\text{in}}^*(I),$$

where

$$\omega_{\text{out}}^*(I) = \omega_+^*(I) - \omega_-^*(I) \quad (112)$$

with

$$\begin{aligned} \omega_+^*(I) &= \lim_{N \rightarrow +\infty} \left(\int_0^{6N\pi} \frac{(\mu^{-1}(3 - L^{-3}) - \partial_L \Delta H_{\text{circ}}) \circ \gamma_I^*(\sigma)}{3(L^{-3} + \mu\partial_L \Delta H_{\text{circ}}) \circ \gamma_I^*(\sigma)} d\sigma + N\mathcal{T}_0(I) \right) \\ \omega_-^*(I) &= \lim_{N \rightarrow -\infty} \left(\int_0^{6N\pi} \frac{(\mu^{-1}(3 - L^{-3}) - \partial_L \Delta H_{\text{circ}}) \circ \gamma_I^*(\sigma)}{3(L^{-3} + \mu\partial_L \Delta H_{\text{circ}}) \circ \gamma_I^*(\sigma)} d\sigma + N\mathcal{T}_0(I) \right), \quad * = f, b \end{aligned} \quad (113)$$

and

$$\begin{aligned} \omega_{\text{in}}^f(I) &= \int_0^{4\pi} \frac{(\mu^{-1}(3 - L^{-3}) - \partial_L \Delta H_{\text{circ}}) \circ \lambda_I^2(\sigma)}{3(L^{-3} + \mu\partial_L \Delta H_{\text{circ}}) \circ \lambda_I^2(\sigma)} d\sigma \\ \omega_{\text{in}}^b(I) &= \int_0^{2\pi} \frac{(\mu^{-1}(3 - L^{-3}) - \partial_L \Delta H_{\text{circ}}) \circ \lambda_I^1(\sigma)}{3(L^{-3} + \mu\partial_L \Delta H_{\text{circ}}) \circ \lambda_I^1(\sigma)} d\sigma, \end{aligned} \quad (114)$$

where $\mathcal{T}_0(I)$ is the function in (108). Recall that along the periodic and homoclinic orbits $(3 - L^{-3}) \sim \mu$.

C.2 The elliptic problem

We study now the elliptic problem. Reasoning as for the 1 : 7 resonance, for e_0 small enough the system associated to the Hamiltonian (16) has a normally hyperbolic invariant cylinder Λ_{e_0} , which is e_0 -close to Λ_0 given in Corollary 2.1. Analogously, the Poincaré map

$$\mathcal{P}_{e_0} : \{\ell = 0\} \longrightarrow \{\ell = 0\}$$

associated to the flow of (16) and the section $\{\ell = 0\}$ has a normally hyperbolic invariant cylinder $\tilde{\Lambda}_{e_0} = \Lambda_{e_0} \cap \{\ell = 0\}$. Moreover, it is formed by three connected components $\tilde{\Lambda}_{e_0}^j$, $j = 0, 1, 2$, which are e_0 -close to the cylinders $\tilde{\Lambda}_{e_0}^j$ obtained in Corollary C.2 and have natural coordinates (I, t) as happened for the circular case.

We look for perturbative expansions of the inner and outer maps. For the 3 : 1 resonances they are computed using the new reduced elliptic problem

$$\begin{aligned} \frac{d}{ds}\ell &= 1 & \frac{d}{ds}L &= -\frac{\partial_\ell H}{L^{-3} + \mu\partial_L\Delta H_{\text{circ}} + \mu e_0\partial_L\Delta H_{\text{ell}}} \\ \frac{d}{ds}g &= \frac{\partial_G H}{L^{-3} + \mu\partial_L\Delta H_{\text{circ}} + \mu e_0\partial_L\Delta H_{\text{ell}}} & \frac{d}{ds}G &= -\frac{\frac{\partial_g H}{\partial_g H}}{L^{-3} + \mu\partial_L\Delta H_{\text{circ}} + \mu e_0\partial_L\Delta H_{\text{ell}}} \\ \frac{d}{ds}t &= \frac{1}{L^{-3} + \mu\partial_L\Delta H_{\text{circ}} + \mu e_0\partial_L\Delta H_{\text{ell}}} & \frac{d}{ds}I &= -\frac{\mu e_0\partial_t\Delta H_{\text{ell}}}{L^{-3} + \mu\partial_L\Delta H_{\text{circ}} + \mu e_0\partial_L\Delta H_{\text{ell}}}, \end{aligned} \quad (115)$$

which is a perturbation of (110).

For the elliptic problem, the coordinates (I, t) are symplectic not with respect to the canonical symplectic form $dI \wedge dt$ but with respect to a symplectic form

$$\Omega_{e_0}^j = \left(1 + e_0 a_1^j(I, t) + e_0^2 a_2^j(I, t) + e_0^3 a_{\geq}^j(I, t)\right) dI \wedge dt, \quad (116)$$

with certain functions $a_k^j : [I_-, I_+] \times \mathbb{T} \rightarrow \mathbb{R}$ which satisfy

$$\mathcal{N}(a_1^3) = \{\pm 1\} \quad \text{and} \quad \mathcal{N}(a_2^3) = \{0, \pm 1, \pm 2\},$$

(see (84) for the definition of \mathcal{N} and Corollary 3.8 for the corresponding result for the 1 : 7 resonance).

In the invariant cylinder $\tilde{\Lambda}_{e_0}^1$, one can define inner and outer maps as we have done in $\tilde{\Lambda}_0^1$ for the circular problem. We proceed as in Section 3 for the 1 : 7 resonance.

The inner map We study first the inner map. As for the circular problem, it is defined the map $\mathcal{P}_{e_0}^3$ in (41) restricted to the normally hyperbolic invariant manifold $\tilde{\Lambda}_{e_0}^1$. For e_0 small enough, proceeding as in the proof of Lemma 3.7, one can see that it is of the form

$$\mathcal{F}_{e_0}^{\text{in}} : \begin{pmatrix} I \\ t \end{pmatrix} \mapsto \begin{pmatrix} I + e_0 A_1(I, t) + e_0^2 A_2(I, t) + \mathcal{O}(e_0^3) \\ t + \mu \mathcal{T}_0(I) + e_0 \mathcal{T}_1(I, t) + e_0^2 \mathcal{T}_2(I, t) + \mathcal{O}(e_0^3) \end{pmatrix}, \quad (117)$$

with functions A_1 , A_2 , \mathcal{T}_1 , and \mathcal{T}_2 satisfying

$$\mathcal{N}(A_1) = \{\pm 1\}, \quad \mathcal{N}(A_2) = \{0, \pm 1, \pm 2\} \quad (118)$$

$$\mathcal{N}(\mathcal{T}_1) = \{\pm 1\}, \quad \mathcal{N}(\mathcal{T}_2) = \{0, \pm 1, \pm 2\}. \quad (119)$$

Thus, A_1 can be split as,

$$A_1(I, t) = A_1^+(I)e^{it} + A_1^-(I)e^{-it}.$$

Moreover, the Fourier coefficients are defined as

$$A_1^\pm(I) = \mp i\mu \int_0^{6\pi} \frac{\Delta H_{\text{ell}}^{1,\pm} \circ \lambda_I^1(\sigma)}{L^{-3} + \mu\partial_G\Delta H_{\text{circ}} \circ \lambda_I^1(\sigma)} e^{\pm i\tilde{\lambda}_I^1(\sigma)} d\sigma,$$

where the functions $\Delta H_{\text{ell}}^{1,\pm}$ are defined as

$$\Delta H_{\text{ell}}^1(L, \ell, G, g, t) = \Delta H_{\text{ell}}^{1,+}(L, \ell, G, g)e^{it} + \Delta H_{\text{ell}}^{1,\pm}(L, \ell, G, g)e^{-it},$$

and $\lambda_I^1(\sigma)$ has been defined in (111). Finally, $\tilde{\lambda}_I^1(\sigma)$ is defined as

$$\tilde{\lambda}_I^1(\sigma) = \tilde{\Phi}_0\{\sigma, (\mathcal{G}_0^{1,L}(I), \mathcal{G}_0^{1,\ell}(I), \mathcal{G}_0^{1,G}(I), 0)\}, \quad (120)$$

where \mathcal{G}_0^3 has been introduced in Corollary C.2 and

$$\tilde{\Phi}_0\{s, (L, \ell, G, g)\} = t + \int_0^s \frac{1}{L^{-3} + \mu\partial_L\Delta H_{\text{circ}}(\Phi_0^{\text{circ}}\{\sigma, (L, \ell, G, g)\})} d\sigma. \quad (121)$$

The function $\tilde{\Phi}_0$ is analogous to the corresponding function for the 1 : 7 resonance, defined in (36).

The outer map We study now the outer maps

$$\mathcal{F}_{e_0}^{\text{out},*} : \tilde{\Lambda}_{e_0}^1 \longrightarrow \tilde{\Lambda}_{e_0}^1, \quad * = \text{f, b} \quad (122)$$

for $e_0 > 0$. Thanks to Ansatz 4, we know that for e_0 small enough, there exist transversal intersections of the invariant manifolds of $\tilde{\Lambda}_{e_0}^1$ and $\tilde{\Lambda}_{e_0}^2$. Thus, we can proceed as in Section 2.3 to define the outer maps $\mathcal{F}_{e_0}^{\text{out}}$ for the 3 : 1 resonance and we study them as a perturbation of the outer maps of the circular problem given in (109). We use the reduced elliptic problem defined in (115) and we compute their first order. To this end, we use the notation $\gamma_I^{\text{f},\text{b}}(\sigma)$ and $\lambda_I^{1,2}(\sigma)$ defined in (111). Analogously we define their corresponding t -component of the flow as

$$\begin{aligned} \tilde{\gamma}_I^*(\sigma) &= \tilde{\Phi}_0\{\sigma, (\mathcal{C}_0^{*,L}(I), \mathcal{C}_0^{*,\ell}(I), \mathcal{C}_0^{*,G}(I), 0)\}, \quad * = \text{f, b} \\ \tilde{\lambda}_I^j(\sigma) &= \tilde{\Phi}_0\{\sigma, (\mathcal{G}_0^{j,L}(I), \mathcal{G}_0^{j,\ell}(I), \mathcal{G}_0^{j,G}(I), 0)\}, \quad j = 1, 2 \end{aligned} \quad (123)$$

where \mathcal{C}_0^* and \mathcal{G}_0^j have been given in Corollary C.2 and $\tilde{\Phi}_0$ in (121).

Lemma C.3. *The outer map defined in (122) has the following expansion with respect to e_0 ,*

$$\mathcal{F}_{e_0}^{\text{out},*} : \begin{pmatrix} I \\ t \end{pmatrix} \mapsto \begin{pmatrix} I + e_0 (B^{*,+}(I)e^{it} + B^{*, -}(I)e^{-it}) + \mathcal{O}(e_0^2) \\ t + \mu\omega^*(I) + \mathcal{O}(e_0) \end{pmatrix}, \quad * = \text{f, b}. \quad (124)$$

Moreover, the functions $B^{*,\pm}(I)$ can be defined as

$$\begin{aligned} B^{\text{f},\pm}(I) &= B_{\text{out}}^{\text{f},\pm}(I) + B_{\text{in}}^{\text{f},\pm}(I)e^{\pm i\mu\omega_{\text{out}}^{\text{f}}(I)} \\ B^{\text{b},\pm}(I) &= B_{\text{in}}^{\text{b},\pm}(I) + B_{\text{out}}^{\text{b},\pm}(I)e^{\pm i\mu\omega_{\text{in}}^{\text{b}}(I)}, \end{aligned} \quad (125)$$

where $\omega_{\text{out}}^{\text{f}}(I)$ and $\omega_{\text{in}}^{\text{b}}(I)$ are the functions defined in (33) and (35) respectively and

$$\begin{aligned} B_{\text{out}}^{\text{f},\pm}(I) &= \pm i\mu \lim_{T \rightarrow +\infty} \int_0^T \left(\frac{\Delta H_{\text{ell}}^{1,\pm} \circ \gamma_I^{\text{f}}(\sigma)}{L^{-3} + \mu\partial_L \Delta H_{\text{circ}} \circ \gamma_I^{\text{f}}(\sigma)} e^{\pm i\tilde{\gamma}_I^{\text{f}}(\sigma)} \right. \\ &\quad \left. - \frac{\Delta H_{\text{ell}}^{1,\pm} \circ \lambda_I^1(\sigma)}{L^{-3} + \mu\partial_L \Delta H_{\text{circ}} \circ \lambda_I^1(\sigma)} e^{\pm i(\tilde{\lambda}_I^1(\sigma) + \mu\omega_+^{\text{f}}(I))} \right) d\sigma \\ &\quad \mp i\mu \lim_{T \rightarrow -\infty} \int_0^T \left(\frac{\Delta H_{\text{ell}}^{1,\pm} \circ \gamma_I^{\text{f}}(\sigma)}{L^{-3} + \mu\partial_L \Delta H_{\text{circ}} \circ \gamma_I^{\text{f}}(\sigma)} e^{\pm i\tilde{\gamma}_I^{\text{f}}(\sigma)} \right. \\ &\quad \left. - \frac{\Delta H_{\text{ell}}^{1,\pm} \circ \lambda_I^2(\sigma)}{L^{-3} + \mu\partial_L \Delta H_{\text{circ}} \circ \lambda_I^2(\sigma)} e^{\pm i(\tilde{\lambda}_I^2(\sigma) + \mu\omega_-^{\text{f}}(I))} \right) d\sigma, \end{aligned} \quad (126)$$

$$\begin{aligned} B_{\text{out}}^{\text{b},\pm}(I) &= \pm i\mu \lim_{T \rightarrow +\infty} \int_0^T \left(\frac{\Delta H_{\text{ell}}^{1,\pm} \circ \gamma_I^{\text{b}}(\sigma)}{L^{-3} + \mu\partial_L \Delta H_{\text{circ}} \circ \gamma_I^{\text{b}}(\sigma)} e^{\pm i\tilde{\gamma}_I^{\text{b}}(\sigma)} \right. \\ &\quad \left. - \frac{\Delta H_{\text{ell}}^{1,\pm} \circ \lambda_I^2(\sigma)}{L^{-3} + \mu\partial_L \Delta H_{\text{circ}} \circ \lambda_I^2(\sigma)} e^{\pm i(\tilde{\lambda}_I^2(\sigma) + \mu\omega_+^{\text{b}}(I))} \right) d\sigma \\ &\quad \mp i\mu \lim_{T \rightarrow -\infty} \int_0^T \left(\frac{\Delta H_{\text{ell}}^{1,\pm} \circ \gamma_I^{\text{b}}(\sigma)}{L^{-3} + \mu\partial_L \Delta H_{\text{circ}} \circ \gamma_I^{\text{b}}(\sigma)} e^{\pm i\tilde{\gamma}_I^{\text{b}}(\sigma)} \right. \\ &\quad \left. - \frac{\Delta H_{\text{ell}}^{1,\pm} \circ \lambda_I^1(\sigma)}{L^{-3} + \mu\partial_L \Delta H_{\text{circ}} \circ \lambda_I^1(\sigma)} e^{\pm i(\tilde{\lambda}_I^1(\sigma) + \mu\omega_-^{\text{b}}(I))} \right) d\sigma, \end{aligned} \quad (127)$$

$$\begin{aligned}
B_{\text{in}}^{\text{f},\pm}(I) &= \mp i\mu \int_0^{4\pi} \frac{\Delta H_{\text{ell}}^{1,\pm} \circ \lambda_I^2(\sigma)}{L^{-3} + \mu \partial_L \Delta H_{\text{circ}} \circ \lambda_I^2(\sigma)} e^{\pm i \tilde{\lambda}_I^2(\sigma)} d\sigma \\
B_{\text{in}}^{\text{b},\pm}(I) &= \mp \int_0^{2\pi} \frac{\Delta H_{\text{ell}}^{1,\pm} \circ \lambda_I^1(\sigma)}{L^{-3} + \mu \partial_L \Delta H_{\text{circ}} \circ \lambda_I^1(\sigma)} e^{\pm i \tilde{\lambda}_I^1(\sigma)} d\sigma
\end{aligned} \tag{128}$$

where

$$\Delta H_{\text{ell}}^{1,\pm}(\ell, L, g, G, t) = \Delta H_{\text{ell}}^{1,\pm}(\ell, L, g, G) e^{it} + \Delta H_{\text{ell}}^{1,\pm}(\ell, L, g, G) e^{-it}$$

has been defined in Corollary 3.5 and ω_{\pm}^* have been defined in (113).

Existence of diffusing orbits The last step to prove the existence of diffusing orbits can be done analogously to what has been done in Section 4 for the 1 : 7 resonance. Namely, we just need to obtain a change of coordinates $(I, t) = (\mathcal{I}, \tau) + e_0 \varphi(\mathcal{I}, \tau)$ which

1. Straigtens the symplectic form $\Omega_{e_0}^1$ (see (116)) into $\Omega_0 = d\mathcal{I} \wedge d\tau$.
2. Flattens the inner map in the I -direction.

This is summarized in the next lemma, which merges the corresponding Lemmas 4.1 and 4.2 for the 1 : 7 resonance.

Lemma C.4. *There exists a e_0 -close to the identity change of variables*

$$(I, t) = (\mathcal{I}, \tau) + e_0 \varphi(\mathcal{I}, \tau)$$

defined on $\tilde{\Lambda}_{e_0}^1$, which:

- Transforms the symplectic form $\Omega_{e_0}^1$ into the canonical form $\Omega_0 = d\mathcal{I} \wedge d\tau$.
- Transforms the inner map $\mathcal{F}_{e_0}^{\text{in}}$ in (117) into

$$\tilde{\mathcal{F}}_{e_0}^{\text{in}} : \begin{pmatrix} \mathcal{I} \\ \tau \end{pmatrix} \mapsto \begin{pmatrix} \mathcal{I} + \mathcal{O}(\mu e_0^3) \\ \tau + \mu \mathcal{T}_0(\mathcal{I}) + e_0^2 \tilde{\mathcal{T}}_2(\mathcal{I}) + \mathcal{O}(\mu e_0^3) \end{pmatrix} \tag{129}$$

- Transforms the outer maps $\mathcal{F}_{e_0}^{\text{out},\text{f}}$ and $\mathcal{F}_{e_0}^{\text{out},\text{b}}$ in (124) into

$$\tilde{\mathcal{F}}_{e_0}^{\text{out},*} : \begin{pmatrix} \mathcal{I} \\ \tau \end{pmatrix} \mapsto \begin{pmatrix} \mathcal{I} + e_0 \tilde{B}^*(\mathcal{I}, \tau) + \mathcal{O}(\mu e_0^2) \\ \tau + \mu \omega^*(\mathcal{I}) + \mathcal{O}(\mu e_0) \end{pmatrix}, \quad * = \text{f, b}, \tag{130}$$

where

$$\tilde{B}^*(\mathcal{I}, \tau) = \tilde{B}^{*,+}(\mathcal{I}) e^{i\tau} + \tilde{B}^{*,-}(\mathcal{I}) e^{-i\tau}$$

with

$$\tilde{B}^{*,\pm}(\mathcal{I}) = B^{*,\pm}(\mathcal{I}) - \frac{e^{\pm i\mu\omega^*(\mathcal{I})} - 1}{e^{\pm i\mu\mathcal{T}_0(\mathcal{I})} - 1} A_1^{\pm}(\mathcal{I}).$$

To be able to ensure the existence of transition chains of tori, we need to assume the following ansatz.

Ansatz 6. *The functions $\tilde{B}^{*,\pm}$ defined in Lemma C.4 satisfy*

$$\tilde{B}^{*,\pm}(\mathcal{I}) \neq 0 \quad \text{for } \mathcal{I} \in \mathcal{D}^*,$$

where \mathcal{D}^* are the domains considered in Corollary C.2.

With this ansatz, and also Ansätze 4 and 5, we can proceed as in Section 4 to prove the existence of a transition chain of tori and of orbits shadowing such chain.

C.3 Numerical study of the 3 : 1 resonance

In this section, we briefly describe our numerical analysis of the 3 : 1 resonance. In particular, we verify Ansätze 4, 5 and 6 numerically.

The numerical methodology used for the 3 : 1 resonance is analogous to the 1 : 7 resonance. Cartesian rotating coordinates are used for the computation of the hyperbolic structure of the circular problem (normally hyperbolic invariant cylinder, stable and unstable manifolds, and their homoclinic intersection). We now consider the Poincaré section

$$\tilde{\Sigma}^+ = \{y = 0, \dot{y} > 0\},$$

and the associated 2-dimensional symplectic Poincaré map $P: \tilde{\Sigma}^+ \rightarrow \tilde{\Sigma}^+$ acting on (x, p_x) . We now look for 3 : 1 resonant periodic orbits as 2-periodic points of the Poincaré map, i.e. letting $p = (x, p_x)$, we need to solve the equation

$$P^2(p) = p.$$

In fact, exploiting the symmetry of the problem, it is enough to use 1-dimensional root finding:

$$\pi_{p_x}(P^2(p)) = 0,$$

since we impose that the point p lies on the symmetry section $\{y = 0, p_x = 0\}$.

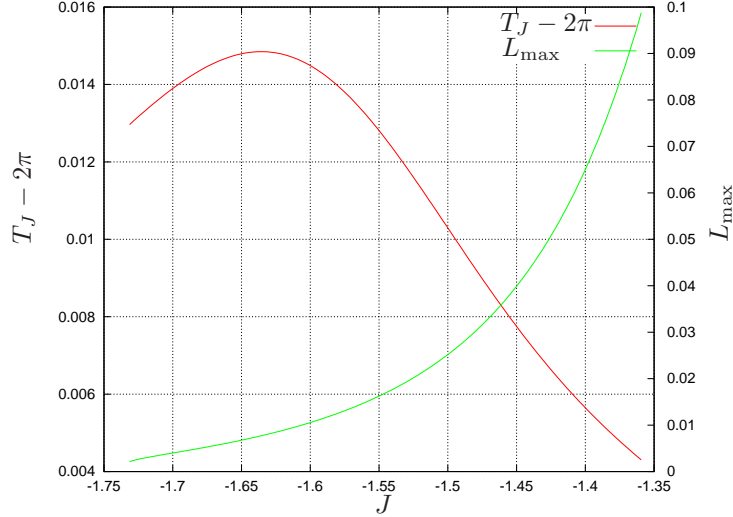


Figure 24: Resonant family of periodic orbits. We show normalized period $T_J - 2\pi$, and maximum deviation of L component with respect to the resonant value $3^{-1/3}$ (see equation (131)).

Thus we obtain the family of resonant periodic orbits for energy levels

$$J \in [\bar{J}_-, \bar{J}_+] = [-1.7314, -1.3594].$$

See Figure 24. Notice that the period T_J stays close to the resonant period 2π of the unperturbed system. From Figure 24, we obtain the bound

$$|T_J - 2\pi| < 15\mu,$$

which is the first bound given in Ansatz 4.

Furthermore, we verify that (the square of) the semi-major axis L stays close to the resonant value $3^{-1/3}$. Integrating the periodic orbit in Delaunay coordinates $\lambda_J(t) = (L_J(t), \ell_J(t), G_J(t), g_J(t))$ over one period T_J , we compute the quantity

$$L_{\max}(J) = \max_{t \in [0, T_J]} |L_J(t) - 3^{-1/3}|. \quad (131)$$

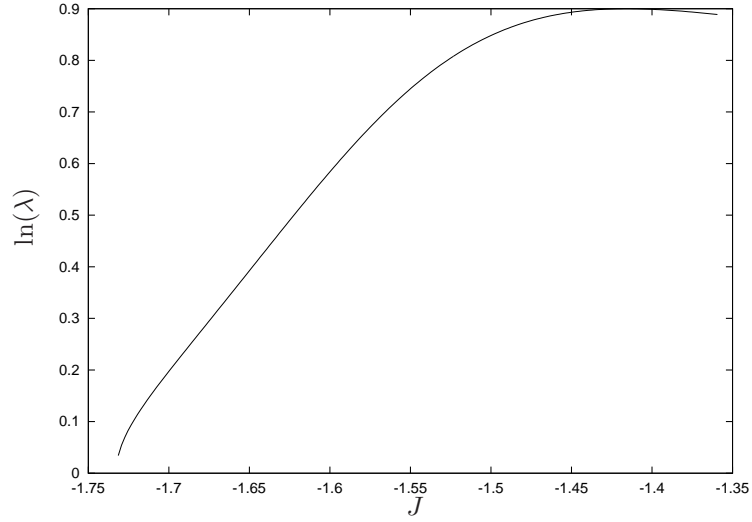


Figure 25: Characteristic exponent $\ln(\lambda)$ as a function of energy level J (the other exponent is $-\ln(\lambda)$).

The function $L_{\max}(J)$ is plotted in Figure 24. Notice that we obtain the bound

$$|L_J(t) - 3^{-1/3}| < 100\mu$$

for all $t \in \mathbb{R}$ and $J \in [\bar{J}_-, \bar{J}_+]$, which is the second bound given in Ansatz 4.

To determine the stability of the periodic orbits, we now compute the eigenvalues λ and λ^{-1} of $DP^2(p)$. Figure 25 shows the characteristic exponents $\ln(\lambda)$, $\ln(\lambda^{-1})$ as a function of energy. The family of periodic orbits is hyperbolic in the interval $[\bar{J}_-, \bar{J}_+]$, although the strength of hyperbolicity is weaker than in the 1 : 7 resonance. Compare with Figure 7.

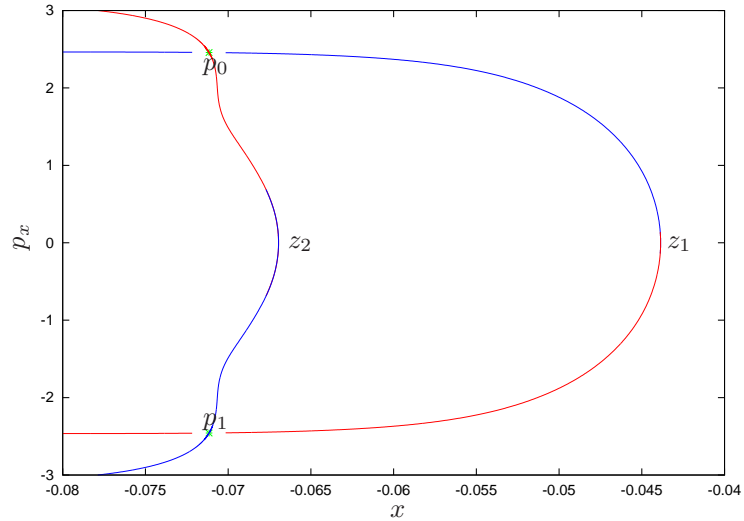


Figure 26: Invariant manifolds of the fixed points p_0 and p_1 for energy level $J = -1.3594$.

The stable and unstable invariant manifolds of the periodic orbits are computed using the same methodology explained for the 1 : 7 resonance. In particular, we switch to the new Poincaré section

$$\tilde{\Sigma}^- = \{y = 0, \dot{y} < 0\}$$

inner	outer
$(-1.453, -1.451)$	$(-1.477, -1.475)$
$(-1.537, -1.535)$	$(-1.553, -1.551)$
$(-1.593, -1.591)$	

Table 3: Subintervals of $J \in [J_-, J_+]$ containing the zeros of inner splitting (left column) and outer splitting (right column).

in order to have the homoclinic points lying on the symmetry axis. For illustration, we show the result corresponding to the energy value $J = -1.3594$ in Figure 26. The manifolds intersect transversally at the homoclinic points z_1 (outer splitting) and z_2 (inner splitting), as we will show below.

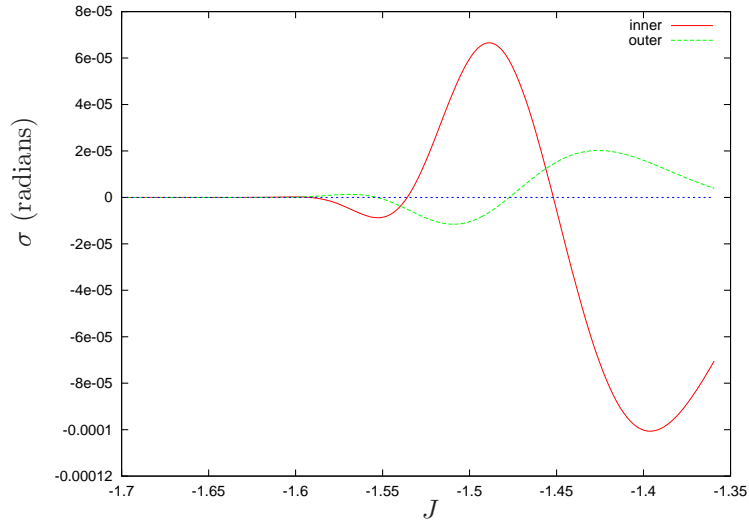


Figure 27: Splitting angle associated to inner and outer splitting.

Next we compute the splitting angle between the invariant manifolds at the homoclinic points. We will restrict the range of energy values to

$$J \in [J_-, J_+] = [-1.6, -1.3594], \quad (132)$$

or equivalently the range of eccentricities to $e \in [e_-, e_+] = [0.59, 0.91]$. This is the range where we can validate the accuracy of our computations (see Appendix A.4). Below $e_- = 0.59$, the splitting size becomes comparable to the numerical error that we commit in double precision arithmetic.

Remark C.5. In contrast with the 1 : 7 resonance, now the manifolds stay close to the integrable situation *for the whole range of energies*, i.e. they meet with small splitting angle as we will show below. Thus for the 3 : 1 resonance there is no difficulty in identifying the *primary* family of homoclinic points. Compare with Remark A.5.

Using the same methodology as for the 1 : 7 resonance, we are able to obtain the splitting angle for energy levels $J \in [J_-, J_+]$. See Figure 27. Numerically, we find that the zeros of the splitting angle are contained in the intervals listed in Table 3. As seen from the table, the inner and outer splittings become zero at different values of J . Thus, when one of the intersections becomes tangent, the other one is still transversal, and we can always use one of them for diffusion.

Again, we check the validity of $\sigma(J_-)$ by computing this splitting angle using two different numerical methods and comparing the results. They differ by less than 10^{-10} , which gives an estimate of the total numerical error.

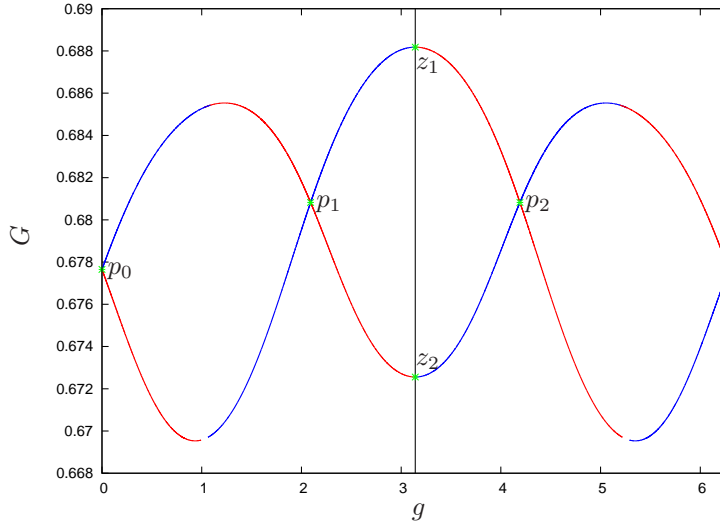


Figure 28: Energy $J = -1.7194$. Resonance structure in Delaunay coordinates. The symmetry corresponds to $g = 0$ and $g = \pi$ and is marked with a vertical line.

Recall that the study of the inner and outer maps is done in rotating Delaunay coordinates. As explained in Appendix C, for the analysis of the 3 : 1 resonance it is convenient to consider the Poincaré section $\{\ell = 0\}$. Thus, we transform the hyperbolic structure of the circular problem from Cartesian to Delaunay coordinates as explained in Appendix B.1. See Figure 28.

First we compute the inner map $\mathcal{F}_0^{\text{in}}$ and the outer maps $\mathcal{F}_0^{\text{out},*}$ of the circular problem, given in Appendix C.1. We consider $I \in [I_-, I_+] = [-J_+, -J_-]$, where the range $[-J_+, -J_-]$ is given in (132). For the inner map, Figure 24 shows a plot of the function $T_J - 2\pi = \mu\mathcal{T}_0(I)$. Notice that the derivative of the function $\mathcal{T}_0(I)$ is nonzero for the whole range $[I_-, I_+]$. This shows that the inner map is twist. Moreover, Figure 24 shows that

$$0 < \mu\mathcal{T}_0(I) < 15\mu < \pi.$$

Therefore, the function $\mathcal{T}_0(I)$ satisfies the properties stated in Ansatz 5.

Then we compute the first orders in e_0 of the inner map $\mathcal{F}_{e_0}^{\text{in}}$ and the outer maps $\mathcal{F}_{e_0}^{\text{out},*}$ of the elliptic problem, given in Appendix C.2. For brevity, we do not show the results here, since the plot of the functions A_1^+ , $B^{\text{f},+}$ and $B^{\text{b},+}$ does not convey much information.

Finally, we verify the non-degeneracy condition

$$\tilde{B}^{*,\pm}(\mathcal{I}) \neq 0 \quad \text{for } \mathcal{I} \in \mathcal{D}^*,$$

stated in Ansatz 6, which implies the existence of a transition chain of tori. The computed values of the functions $\tilde{B}^{\text{f},+}$ and $\tilde{B}^{\text{b},+}$ are shown in Figure 29. Therefore, we see that the functions $\tilde{B}^{*,+}$ are not identically zero. This justifies Ansatz 6.

D Conjectures on the speed of diffusion

Instabilities for nearly integrable systems are often called *Arnol'd diffusion*. As far as we know, this term was coined by Chirikov [Chi79]. In this section we state two conjectures about random behavior of orbits near resonances, where randomness is coming from initial condition.

A nearly integrable Hamiltonian systems of two degrees of freedom in the region of interest often can be reduced to a two-dimensional area-preserving twist map. To construct instability regions of these maps physicists often use a *resonance overlap criterion* (see e.g. [SUZ88], ch. 5, sect. 2). This criterion for nearby rational numbers p/q and p'/q' compares “sizes” of averaged potentials. If the sum of square

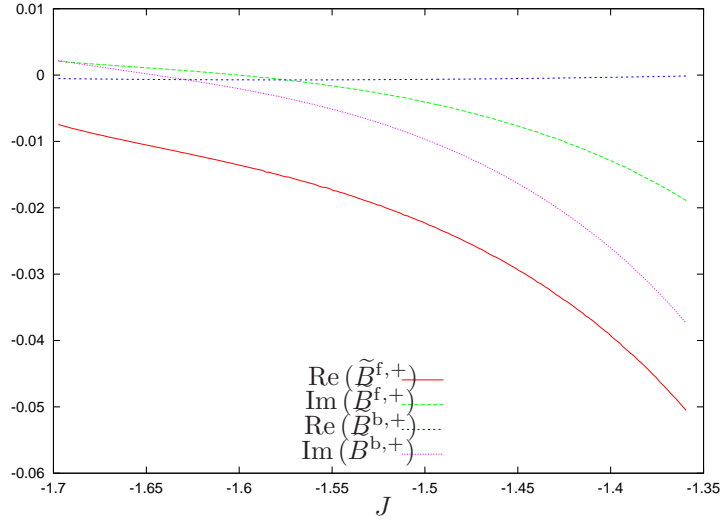


Figure 29: Functions $\tilde{B}^{f,+}$ and $\tilde{B}^{b,+}$ (real and imaginary parts).

roots of maxima of those potentials exceeds $|p/q - p'/q'|$, this is a strong indication that the corresponding periodic orbits can be connected. Doing this for an interval of rational numbers gives an approximation for a so-called Birkhoff Region of Instability (BRI).

If non-integrability is small, then most of the space is laminated by KAM invariant curves. In order to find channels outside of KAM curves, one considers a neighborhood of a resonance and computes size of a so-called *stochastic layer*. Heuristic formulas can be found e.g. in [Chi79], ch. 6.2 or in [SUZ88], ch. 5, sect. 3. Treschev [TZ10] estimated width of stochastic layer in a fairly general setting.

It turns out that Arnol'd's example and the elliptic problem near mean motion resonances can be viewed as a perturbation of a product of two area-preserving twist maps. In loose terms, for the first map we study orbits located near a resonance inside the corresponding stochastic layer. Width of a stochastic layer gives an approximation for time \mathcal{T} it takes for many orbits to go around the layer. Stochastic behavior for the other twist map occurs because it takes place “over” stochastic layer with random behavior. This randomness gives rise to “random compositions” of twist maps. Numerical experiments show behavior similar to a diffusion process (see e.g. [LL10, Figure 6.3] or [LFG07]). Its diffusion coefficient is proportional to square of the properly averaged perturbation divided by \mathcal{T} (see e.g. [Chi79], ch. 7.2, [SUZ88], ch.5, sect. 7).

However, mathematically such randomness is a dark realm since there are many phenomena competing with the diffusive behavior. For example, for twist maps here are a few serious obstacles:

- inside of a BRI there are elliptic islands, where orbits are confined and do not diffuse (see e.g. [Chi79], ch. 5.5 for a heuristic discussion of their size);
- even if elliptic islands occupy not a dominant part of the phase space, there exist the so-called, in mathematical literature, *Aubry-Mather sets*. In physics literature they are called *Cantor-Tori*. Orbits can stick to these sets for long periods of time (see e.g. [SUZ88], ch.5, sect. 7);
- similarly to sticking to Aubry-Mather sets orbits can stick to elliptic islands.

For systems of two and a half degrees of freedom near a resonance is also quite complicated. We turn to our attention to two basic examples: Arnol'd's example and the elliptic problem, both near a resonance.

In terms of a perturbation parameter ε of a nearly integrable system one would like to answer quantitatively the following natural questions. Fix a resonant segment Γ and consider Γ_ε a $\sqrt{\varepsilon}$ -neighborhood of this resonant segment.

- What is the natural time scale of diffusion? One would expect that there is an ε -dependent time scale T_ε in which one orbit diffuses by $\mathcal{O}(1)$ in action space and there is another time scale T_ε^* in which many orbits, in the measure sense, diffuse by $\mathcal{O}(1)$.
- Is there a natural time scale T_ε^* so that positive fraction of orbits in a ε -dependent region in Γ_ε diffuses by $\mathcal{O}(1)$?
- At junctions of two resonances which fraction of orbits chooses one resonance over the other?

Call T_ε^* *time scale of diffusion*. It seems a sophisticated question to distinguish orbits starting in Γ_ε and staying inside such a neighborhood in time scale of diffusion from those getting stuck near KAM tori located $C\sqrt{\varepsilon}$ -away⁹ from Γ with C large. In this paper we consider only the *a priori unstable case*, proposed by Arnol'd [Arn64]. In this case, away from small velocities, there is only one dominant resonance and making precise conjectures is simpler. This case will also motivate conjectures for certain a priori chaotic systems.

D.1 Speed of diffusion for a priori unstable systems and Positive measure

Consider the following nearly integrable Hamiltonian system proposed by Arnol'd [Arn64]:

$$H_\varepsilon(p, q, I, \phi, t) = \frac{1}{2}p^2 + \cos q - 1 + \frac{1}{2}I^2 + \varepsilon H_1(p, q, I, \phi, t), \quad \text{where } p, I \in \mathbb{R}, \quad \phi, q, t \in \mathbb{T}, \quad (133)$$

for an analytic perturbation εH_1 . This system is usually called *a priori unstable*. Proving *Arnol'd diffusion* for this system consists in showing that, for all small $\varepsilon > 0$ and a generic εH_1 , there exists orbits with

$$|I(t) - I(0)| > \mathcal{O}(1),$$

where $\mathcal{O}(1)$ is independent of ε . There has been a fascinating progress in this problem achieved by several groups (see [Ber08, CY04, DdLS06, DH09, Tre04]). Treschev [Tre04] not only proved existence of Arnol'd diffusion, but also gave an optimal estimate on speed, namely, he constructed orbits

$$|I(t) - I(0)| > c \frac{\varepsilon}{|\ln \varepsilon|} t$$

for some $c > 0$. One can see that this estimate is optimal, i.e. $|I(t) - I(0)| < C \frac{\varepsilon}{|\ln \varepsilon|} t$ for some $C > c$.

Heuristically the mechanism of diffusion is the following. For small $\varepsilon > 0$ the Hamiltonian H_ε has a 3-dimensional normally hyperbolic invariant cylinder Λ_ε close to $\Lambda_0 = \{p = q = 0\}$. A hypothetical diffusing orbit starts close to Λ_ε and makes a homoclinic excursion. Each homoclinic excursion takes approximately $\mathcal{O}(|\ln \varepsilon|)$ -time. Increment of $I(t)$ after such an excursion is $\mathcal{O}(\varepsilon)$.¹⁰ If one can arrange that all excursions lead to increments of $I(t)$ of the same sign, the result follows.

It seems natural that orbits will be trapped inside the resonance $p = 0$ for polynomially long time. Using this heuristic description one can conjecture that increments $I(t)$ can behave as a random walk for positive conditional measure for polynomially large time.

Positive measure conjecture *Consider the Hamiltonian H_ε with a generic perturbation εH_1 . Pick an ε -ball B_ε of initial conditions, whose center projects into $(p, q) = 0$, and denote the Lebesgue probability measure supported on it by Leb_ε . Then, for some constants $c, C > 0$ independent of ε , the set of initial conditions satisfying*

$$|I(T) - I(0)| > 1 \quad \text{for some} \quad 0 < T < C \frac{|\ln \varepsilon|}{\varepsilon^2}$$

is denoted Diff and has measure $\text{Leb}_{\sqrt{\varepsilon}}(\text{Diff}) > c$.

⁹This is so-called stickiness phenomenon (see e.g. [MG95, PW94])

¹⁰This is only an heuristic description as dynamics inside of the cylinder should come into play. Near so-called double resonance dynamics is different from the one near single resonances

Since a typical excursion takes $\mathcal{O}(|\ln \varepsilon|)$ -time and each increment is $\mathcal{O}(\varepsilon)$, we essentially conjecture that after $\mathcal{O}(\varepsilon^{-2})$ excursions with uniformly positive probability there will be drift of order $\mathcal{O}(\varepsilon)\mathcal{O}(\varepsilon^{-1}) = \mathcal{O}(1)$.

D.2 Structure of the restricted planar elliptic three-body problem

In this appendix we relate a priori unstable systems and the restricted planar elliptic three-body problem. Recall that we managed to write the Hamiltonian of the latter problem in the form

$$\begin{aligned} H_{\text{ell}}(L, \ell, G, g, t) &= H_{\text{circ}}(L, \ell, G, g, \mu) + \mu e_0 \Delta H_{\text{ell}}(L, \ell, G, g, t, \mu, e_0) \\ &= H_0^*(L, G) + \mu \Delta H_{\text{circ}}(L, \ell, G, g, \mu) + \mu e_0 \Delta H_{\text{ell}}(L, \ell, G, g, t, \mu, e_0) \\ &= -\frac{1}{2L^2} - G + \mu \Delta H_{\text{circ}}(L, \ell, G, g, \mu) + \mu e_0 \Delta H_{\text{ell}}(L, \ell, G, g, t, \mu, e_0). \end{aligned}$$

We have that

- H_0^* is an integrable Hamiltonian.
- H_{circ} is non-integrable and for H_{circ} in a certain interval of energy levels $[J_-, J_+]$ there is a family of hyperbolic periodic orbits $\{p_J\}$ whose invariant manifolds intersect transversally along at least one homoclinic.
- H_{ell} is a $\mathcal{O}(\mu e_0)$ -perturbation of H_{circ} such that certain Melnikov integral evaluated along a transverse homoclinic of H_{circ} is non-degenerate in two different ways: dependence on time is non-trivial and relation between inner and outer integrals is non-degenerate (see (9)).

Having all these non-degeneracy conditions we prove the existence of diffusing orbits. It is not difficult to prove, using averaging techniques, that for $\mu > 0$ small, there is a family of saddle periodic orbit $\{\gamma_J\}$ on some interval $[J_-, J_+]$, whose hyperbolicity is $\sim \sqrt{\mu}$. It seems, however, to be a non-trivial problem to establish the splitting of its separatrices. Due to reversibility (90) there are at least four homoclinic intersections (two for upper separatrices and two for lower ones). Having these two conditions it is natural to expect that at least one of the four associated Melnikov integrals is non-degenerate. Qualitative analysis shows that it should be possible to have a homoclinic excursion $\mathcal{O}(\mu e_0)$ -close to the invariant cylinder. Such an excursion takes $\mathcal{O}(|\ln(\mu e_0)|)/\sqrt{\mu}$ -time. If the excursion is selected properly, then the result of the excursion is that the increment of the eccentricity is $\mathcal{O}(\mu e_0)$. This makes us believe that the instability time obeys $T \sim -\frac{\ln(\mu e_0)}{\mu^{3/2} e_0}$ stated in (6).

Let us point out that we believe that our diffusion mechanism survives even for non-infinitesimal e_0 's, e.g. realistic $e_0 = 0.048$. To justify this, we review the above structure.

Notice that we use a 3-dimensional normally hyperbolic invariant cylinder and the intersection of its invariant manifolds to diffuse. The cylinder arises from the family of periodic orbits $\{\gamma_J\}_{J \in [J_-, J_+]}$ of the circular problem, which persist under the elliptic time-periodic perturbation $\mu e_0 \Delta H_{\text{ell}}(L, \ell, G, g, t, \mu, e_0)$ (see (15) and the derivation in the corresponding section). As the analysis carried out in Section 3.2 shows, in the neighborhood of this family $\{\gamma_J\}_{J \in [J_-, J_+]}$, the perturbation $\mu e_0 \Delta H_{\text{ell}}(L, \ell, G, \hat{g} - t, \mu, e_0)$ can be averaged out to $\mathcal{O}(\mu e_0^6)$. Thus, invariant cylinders could persist even for not very small e_0 's. However, estimating remainders analytically after several steps of averaging is nearly impossible. Numerically though it might be feasible.

Once the existence of an invariant cylinder is established, we need to justify the existence of transverse intersections of its manifolds. As before, analytically it is an insurmountable task, but numerically it seems to be an achievable goal.

If these two steps are done, then one could try to compute numerically inner and outer maps and show that they do not have common invariant curves. This is again a difficult, but numerically realistic task (see [DMR08] for the computation of the outer map in another problem in Celestial Mechanics).

On the other hand, the above asymptotics probably does not hold in the neighborhood of circular motions of the massless body, which might be much more stable than more eccentric motions. Yet many other factors might influence the local stability or instability of various objects (see section 1.2.3).

D.3 The Mather accelerating problem and its speed of diffusion

The structure we use to build diffusion is similar to the Mather acceleration problem. Let us recall this problem and state an interesting result of Piftankin [Pif06] on speed of diffusion.

Consider a Hamiltonian system

$$H(q, p, t) = K(q, p) + V(q, t), \quad q \in \mathbb{T}^2, \quad p \in \mathbb{R}^2, \quad t \in \mathbb{T},$$

where $K(q, p) = \frac{1}{2} \langle A^{-1}(q)p, p \rangle$ — kinetic energy corresponding to a riemannian metric $K(q, p) = \frac{1}{2} \langle A^{-1}(q)p, p \rangle$, $p = A(q) \dot{q}$, $\dot{q} \in T_q \mathbb{T}^2$ and $V(q, t)$ is a time-periodic potential energy. Since the system is not autonomous energy is not conserved.

H1 Suppose the geodesic flow associated to K has a hyperbolic periodic orbit Γ and transversal intersection of its invariant manifolds, which contains a homoclinic orbit $\gamma(t)$, $t \in \mathbb{R}$.

H2 The Melnikov integral is not constant. More exactly, define a function

$$\mathcal{L}(t) = \lim_{T \rightarrow +\infty} \int_{-T}^T V(\gamma(t), t) dt - \int_{-T+t^u}^{T+t^s} V(\gamma(t), t) dt.$$

The limit turns out to exist and is independent of a choice of t^s , t^u . This function is assumed to be non-constant.

Mather and his followers [Mat96, BT99, DdlLS00, GT08, Kal03, Pif06] proved existence of an orbit $(q_\tau(t), p_\tau(t))$, $t \in \mathbb{R}$ of unbounded energy. De la Llave [dlL04], Piftankin [Pif06], and Gelfreich-Turaev [GT08] proved that such an orbit can be chosen to have linear growth of energy

$$H(q_\tau(t), p_\tau(t)) \geq At + B \quad \text{for all } t \geq 0$$

for some $A > 0$ and $B \in \mathbb{R}$.

Notice that for large energies $H \sim \varepsilon^{-2}$ the conformal change of coordinates

$$\hat{p} = \frac{p}{\varepsilon}, \quad H = \varepsilon^{-2} \hat{H}, \quad t = \varepsilon \hat{t}$$

leads to the new Hamiltonian

$$\hat{H}(q, p, t) = K(q, p) + \varepsilon^2 V(q, \varepsilon \hat{t}).$$

It was shown in [dlL04, Pif06, GT08] that there are orbits diffusing linearly in the size of the perturbation. In order to see these orbits, notice that $K(q, p)$ has a horseshoe. Then, \hat{H} can be considered as a time-periodic perturbation over such a horseshoe. It is shown by different methods in [dlL04, Pif06, GT08] that for a generic time-periodic perturbation of a horseshoe there are linearly diffusing orbits.

D.4 Modified positive measure conjecture

For systems with the properties discussed above we can modify the positive measure conjecture as follows:

Positive measure conjecture for Mather type systems *Consider the Hamiltonian*

$$H_{\mu, \varepsilon}(L, \ell, G, g, t) = H_0^*(L, G) + \mu \Delta H_0(L, \ell, G, g, \mu) + \mu e_0 \Delta H_1(L, \ell, G, g, t, \mu, e_0)$$

such that

- for some interval $[J_-, J_+]$ the Hamiltonian $H_0^* + \mu \Delta H_0$ has a family of saddle periodic orbits $\{p_J\}_{J \in [J_-, J_+]}$,
- for each $J \in [J_-, J_+]$ there is at least one transverse intersection of its invariant manifolds,
- A Melnikov integral evaluated along a transverse homoclinic and inner dynamics are non-degenerate: the dependence of the Melnikov integral on time is non-trivial and the relation between inner and outer maps is non-degenerate (see (9)).

Pick a μe_0 -ball of initial conditions $B_{\mu e_0}$ whose action components are centered at a resonance between ℓ and g . Denote the Lebesgue probability measure supported on the ball $B_{\mu e_0}$ by Leb . Then for some constants $c, C > 0$ independent of μ and e_0 , the set of initial conditions satisfying

$$|G(T) - G(0)| > 1 \quad \text{for some} \quad 0 < T < C \frac{|\ln \mu e_0|}{\mu^{5/2} e_0^2}$$

is denoted Diff and has measure $\text{Leb}(\text{Diff}) > c$.

Here is an important difference between the system H_{μ, e_0} and an priori unstable one H_ε , given by (133): the Hamiltonian $H_0^* + \mu \Delta H_0$ already has “chaos” and a family of horseshoes on each energy surface with $J \in [J_-, J_+]$, while $H_0 = H_\varepsilon - \varepsilon H_1$ is integrable. As we pointed out above, for a generic time-periodic perturbation over a horseshoe there are orbits diffusing linearly fast [dL04, Pif06, GT08]. Yet we are interested in a set of conditional positive measure.

In order to see the time of diffusion on an heuristic level, notice that $H_0^* + \mu \Delta H_0$ has a family of saddle periodic orbits $\{p_J\}_{J \in [J_-, J_+]}$ whose exponents are $\sim \sqrt{\mu}$. Thus, one homoclinic excursion passing μe_0 -close to separatrices takes $|\ln \mu e_0|/\sqrt{\mu}$ -time. Each excursion might lead to increment of G of size $\sim \mu e_0$. Conjecturing that random walk approximation holds true to have $\mathcal{O}(1)$ -changes in G , we need $\mathcal{O}(\mu^{-2} e_0^{-2})$ excursions.

Acknowledgements

The authors acknowledge useful discussions with Abed Bounemoura, Marc Chaperon, Alain Chenciner, Anatole Katok, Àngel Jorba, Mark Levi, John Mather, Gennadi Piftankin, Philippe Robutel and Ke Zhang. P. R. acknowledges the assistance of À. Jorba with the “taylor” package (see <http://www.maia.ub.es/~angel/taylor>).

The authors warmly thank the Observatoire de Paris, the University of Maryland at College Park, the Pennsylvania State University, the Universitat Politècnica de Catalunya and the Fields Institute for their hospitality, stimulating atmosphere, and support.

J. F. has been partially supported by the French ANR (Projets ANR-12-BS01-0020 WKBHJ and ANR-10-BLAN 0102 DynPDE), M. G. and P. R. by the Spanish MCyT/FEDER grant MTM2009-06973 and the Catalan SGR grant 2009SGR859, and V. K. by NSF grant DMS-0701271.

References

- [AKN88] V.I. Arnold, V.V. Kozlov, and A.I. Neishtadt. *Dynamical Systems III*, volume 3 of *Encyclopaedia Math. Sci.* Springer, Berlin, 1988.
- [Arn63] V. I. Arnold. Small denominators and problems of stability of motion in classical and celestial mechanics. *Uspehi Mat. Nauk*, 18(6 (114)):91–192, 1963.
- [Arn64] V.I. Arnold. Instability of dynamical systems with several degrees of freedom. *Sov. Math. Doklady*, 5:581–585, 1964.
- [BB02] M. Berti and P. Bolle. A functional analysis approach to Arnold diffusion. *Ann. Inst. H. Poincaré Anal. Non Linéaire*, 19(4):395–450, 2002.
- [BBB03] M. Berti, L. Biasco, and P. Bolle. Drift in phase space: a new variational mechanism with optimal diffusion time. *J. Math. Pures Appl. (9)*, 82(6):613–664, 2003.
- [Ber08] P. Bernard. The dynamics of pseudographs in convex Hamiltonian systems. *J. Amer. Math. Soc.*, 21(3):615–669, 2008.
- [BKZ11] P. Bernard, V. Kaloshin, and K. Zhang. Arnold diffusion along normally hyperbolic cylinders. Preprint, 2011.

- [Bol06] S. Bolotin. Symbolic dynamics of almost collision orbits and skew products of symplectic maps. *Nonlinearity*, 19(9):2041–2063, 2006.
- [BT99] S. Bolotin and D. Treschev. Unbounded growth of energy in nonautonomous Hamiltonian systems. *Nonlinearity*, 12(2):365–388, 1999.
- [CC07] A. Celletti and L. Chierchia. KAM stability and celestial mechanics. *Mem. Amer. Math. Soc.*, 187(878):viii+134, 2007.
- [CG94] L. Chierchia and G. Gallavotti. Drift and diffusion in phase space. *Ann. Inst. H. Poincaré Phys. Théor.*, 60(1):144, 1994.
- [Cha04] M. Chaperon. Stable manifolds and the Perron-Irwin method. *Ergodic Theory Dynam. Systems*, 24(5):1359–1394, 2004.
- [Chi79] B. V. Chirikov. A universal instability of many-dimensional oscillator systems. *Phys. Rep.*, 52(5):264–379, 1979.
- [Cre97] J. Cresson. A λ -lemma for partially hyperbolic tori and the obstruction property. *Lett. Math. Phys.*, 42(4):363–377, 1997.
- [CY04] C.Q. Cheng and J. Yan. Existence of diffusion orbits in a priori unstable Hamiltonian systems. *J. Differential Geom.*, 67(3):457–517, 2004.
- [CZ11] M. Capiński and P. Zgliczyński. Transition tori in the planar restricted elliptic three-body problem. *Nonlinearity*, 24(5):1395–1432, 2011.
- [DdlLS00] A. Delshams, R. de la Llave, and T.M. Seara. A geometric approach to the existence of orbits with unbounded energy in generic periodic perturbations by a potential of generic geodesic flows of \mathbb{T}^2 . *Comm. Math. Phys.*, 209(2):353–392, 2000.
- [DdlLS06] A. Delshams, R. de la Llave, and T.M. Seara. A geometric mechanism for diffusion in hamiltonian systems overcoming the large gap problem: heuristics and rigorous verification on a model. *Mem. Amer. Math. Soc.*, 2006.
- [DdlLS08] A. Delshams, R. de la Llave, and T. M. Seara. Geometric properties of the scattering map of a normally hyperbolic invariant manifold. *Adv. Math.*, 217(3):1096–1153, 2008.
- [DGR11] A. Delshams, M. Gidea, and P. Roldán. Arnold’s mechanism of diffusion in the spatial circular restricted three-body problem: A semi-numerical argument. Preprint, 2011.
- [DH09] A. Delshams and G. Huguet. Geography of resonances and Arnold diffusion in a priori unstable Hamiltonian systems. *Nonlinearity*, 22(8):1997–2077, 2009.
- [dlL04] R. de la Llave. Orbits of unbounded energy in perturbations of geodesic flows by periodic potentials. A simple construction. Preprint, 2004.
- [DMR08] A. Delshams, J. Masdemont, and P. Roldán. Computing the scattering map in the spatial Hill’s problem. *Discrete Contin. Dyn. Syst. Ser. B*, 10(2-3):455–483, 2008.
- [DRR99] A. Delshams and R. Ramírez-Ros. Singular separatrix splitting and the Melnikov method: an experimental study. *Experiment. Math.*, 8(1):29–48, 1999.
- [Féj02a] J. Féjoz. Global secular dynamics in the planar three-body problem. *Celestial Mech. Dynam. Astronom.*, 84(2):159–195, 2002.
- [Féj02b] Jacques Féjoz. Quasiperiodic motions in the planar three-body problem. *J. Differential Equations*, 183(2):303–341, 2002.

- [Féj04] J. Féjoz. Démonstration du ‘théorème d’Arnold’ sur la stabilité du système planétaire (d’après Herman). *Ergodic Theory Dynam. Systems*, 24(5):1521–1582, 2004.
- [Féj13] J. Féjoz. On “Arnold’s theorem” in celestial mechanics -a summary with an appendix on the Poincaré coordinates. *Discrete and Continuous Dynamical Systems*, 33:3555–3565, 2013.
- [Fen72] N. Fenichel. Persistence and smoothness of invariant manifolds for flows. *Indiana Univ. Math. J.*, 21:193–226, 1971/1972.
- [Fen77] N. Fenichel. Asymptotic stability with rate conditions. II. *Indiana Univ. Math. J.*, 26(1):81–93, 1977.
- [Fen74] N. Fenichel. Asymptotic stability with rate conditions. *Indiana Univ. Math. J.*, 23:1109–1137, 1973/74.
- [FM00] E. Fontich and P. Martín. Differentiable invariant manifolds for partially hyperbolic tori and a lambda lemma. *Nonlinearity*, 13(5):1561–1593, 2000.
- [FS90] E. Fontich and C. Simó. The splitting of separatrices for analytic diffeomorphisms. *Ergodic Theory Dynam. Systems*, 10(2):295–318, 1990.
- [GDF⁺89] A. Giorgilli, A. Delshams, E. Fontich, L. Galgani, and C. Simó. Effective stability for a Hamiltonian system near an elliptic equilibrium point, with an application to the restricted three-body problem. *J. Differential Equations*, 77(1):167–198, 1989.
- [GdlL06] M. Gidea and R. de la Llave. Topological methods in the instability problem of Hamiltonian systems. *Discrete Contin. Dyn. Syst.*, 14(2):295–328, 2006.
- [GG85] A. Giorgilli and L. Galgani. Rigorous estimates for the series expansions of Hamiltonian perturbation theory. *Celestial Mech.*, 37(2):95–112, 1985.
- [GG09] M. Galassi and B. Gough. *GNU Scientific Library: Reference Manual*. A GNU manual. Network Theory Limited, 2009.
- [GK10a] J. Galante and V. Kaloshin. Destruction of invariant curves in the restricted planar circular three body problem using ordering condition. Preprint, 2010.
- [GK10b] J. Galante and V. Kaloshin. The method of spreading cumulative twist and application to the restricted planar circular three body problem. Preprint, 2010.
- [GK11] J. Galante and V. Kaloshin. Destruction of invariant curves in the restricted circular planar three-body problem by using comparison of action. *Duke Math. J.*, 159(2):275–327, 2011.
- [GS08] V. Gelfreich and C. Simó. High-precision computations of divergent asymptotic series and homoclinic phenomena. *Discrete Contin. Dyn. Syst. Ser. B*, 10(2-3):511–536, 2008.
- [GT08] V. Gelfreich and D. Turaev. Unbounded energy growth in Hamiltonian systems with a slowly varying parameter. *Comm. Math. Phys.*, 283(3):769–794, 2008.
- [Her83] M.R. Herman. *Sur les courbes invariantes par les difféomorphismes de l’anneau. Vol. 1*, volume 103 of *Astérisque*. Société Mathématique de France, Paris, 1983.
- [Her98] M. Herman. Some open problems in dynamical systems. In *Proceedings of the International Congress of Mathematicians (Berlin, 1998)*, volume Extra Vol. II, pages 797–808 (electronic), 1998.
- [Kal03] V. Kaloshin. Geometric proofs of Mather’s connecting and accelerating theorems. In *Topics in dynamics and ergodic theory*, volume 310 of *London Math. Soc. Lecture Note Ser.*, pages 81–106. Cambridge Univ. Press, Cambridge, 2003.

- [Kol57] A. N. Kolmogorov. Théorie générale des systèmes dynamiques et mécanique classique. In *Proceedings of the International Congress of Mathematicians, Amsterdam, 1954, Vol. 1*, pages 315–333. Erven P. Noordhoff N.V., Groningen, 1957.
- [Lap89] P.-S. Laplace. Variations séculaires des orbites des planètes. *Mém. Acad. royale des sciences de Paris, année 1787*, Œuvres complètes, Tome XI:295–301, 1789. <http://gallica.bnf.fr/ark:/12148/bpt6k77599c/f300>.
- [Las94] J. Laskar. Large scale chaos in the solar system. *Astron. Astrophys.*, 287, 1994.
- [Las06] J. Laskar. *Sfogliando La ‘Mécanique analytique’*, chapter Lagrange et la stabilité du système solaire. Edizioni Universitarie di Lettere Economia Diritto, 2006.
- [Las10] J. Laskar. Le système solaire est-il stable ? In *Le Chaos*, number XIV in Séminaire Poincaré, pages 221–246. Birkhäuser, 2010.
- [LFG07] E. Lega, C. Froeschlé, and M. Guzzo. Diffusion in Hamiltonian quasi-integrable systems. In *Topics in gravitational dynamics*, volume 729 of *Lecture Notes in Phys.*, pages 29–65. Springer, Berlin, 2007.
- [LL10] A.J. Lichtenberg and A. Lieberman. *Regular and Chaotic Dynamics*. Applied Mathematical Sciences. Springer, 2010.
- [Mar96] J. P. Marco. Transition le long des chaînes de tores invariants pour les systèmes hamiltoniens analytiques. *Ann. Inst. H. Poincaré Phys. Théor.*, 64(2):205–252, 1996.
- [Mat96] J. N. Mather. Manuscript. Unpublished, 1996.
- [Mey75] K. R. Meyer. The implicit function theorem and analytic differential equations. In *Dynamical systems—Warwick 1974 (Proc. Sympos. Appl. Topology and Dynamical Systems, Univ. Warwick, Coventry, 1973/1974; presented to E. C. Zeeman on his fiftieth birthday)*, pages 191–208. Lecture Notes in Math., Vol. 468. Springer, Berlin, 1975.
- [MG95] A. Morbidelli and A. Giorgilli. Superexponential stability of KAM tori. *J. Statist. Phys.*, 78(5-6):1607–1617, 1995.
- [Moe96] R. Moeckel. Transition tori in the five-body problem. *J. Differential Equations*, 129(2):290–314, 1996.
- [Moe02] R. Moeckel. Generic drift on Cantor sets of annuli. In *Celestial mechanics (Evanston, IL, 1999)*, volume 292 of *Contemp. Math.*, pages 163–171. Amer. Math. Soc., Providence, RI, 2002.
- [Mor02] A. Morbidelli. *Modern celestial mechanics: aspects of solar system dynamics*. Taylor and Francis, 2002.
- [Nie96] L. Niederman. Stability over exponentially long times in the planetary problem. *Nonlinearity*, 9(6):1703–1751, 1996.
- [NS04] A. I. Neishtadt and V. V. Sidorenko. Wisdom system: dynamics in the adiabatic approximation. *Celestial Mech. Dynam. Astronom.*, 90(3-4):307–330, 2004.
- [Pif06] G. N. Piftankin. Diffusion speed in the Mather problem. *Nonlinearity*, 19(11):2617–2644, 2006.
- [PT07] G. N. Piftankin and D. V. Treshchëv. Separatrix maps in Hamiltonian systems. *Uspekhi Mat. Nauk*, 62(2(374)):3–108, 2007.

- [PW94] A.D. Perry and S. Wiggins. KAM tori are very sticky: rigorous lower bounds on the time to move away from an invariant Lagrangian torus with linear flow. *Phys. D*, 71(1-2):102–121, 1994.
- [Rob05] P. Robutel. Frequency analysis and global dynamics of a planetary system. In D. Benest, editor, *Hamiltonian systems and Fourier analysis: new prospects for gravitational dynamics*, Advances in astronomy and astrophysics, pages 179–198. Cambridge Scientific Publishers, 2005.
- [Sab13] L. Sabbagh. An inclination lemma for normally hyperbolic manifolds with an application to diffusion. Preprint, 2013.
- [SM95] C. L. Siegel and J. K. Moser. *Lectures on celestial mechanics*. Classics in Mathematics. Springer-Verlag, Berlin, 1995.
- [SUZ88] R.Z. Sagdeev, D.A. Usikov, and G.M. Zaslavskij. *Nonlinear Physics: From the Pendulum to Turbulence and Chaos*. Contemporary Concepts in Physics Series. Harwood Academic Publishers, 1988.
- [SW92] G. J. Sussman and J. Wisdom. Chaotic evolution of the solar system. *Science*, 257:56–62, 1992.
- [Tre04] D. Treschev. Evolution of slow variables in a priori unstable hamiltonian systems. *Nonlinearity*, 17(5):1803–1841, 2004.
- [TZ10] D. Treschev and O. Zubelevich. *Introduction to the perturbation theory of Hamiltonian systems*. Springer Monographs in Mathematics. Springer-Verlag, Berlin, 2010.
- [Wis82] J. Wisdom. The origin of the Kirkwood gaps: a mapping for asteroidal motion near the 3/1 commensurability. *Astronom. J.*, 87(3):577–593, 1982.
- [WZ03] D. Wilczak and P. Zgliczynski. Heteroclinic connections between periodic orbits in planar restricted circular three-body problem—a computer assisted proof. *Comm. Math. Phys.*, 234(1):37–75, 2003.
- [Xue10] J. Xue. Continuous averaging proof of the nekhoroshev theorem with sharp stability constant c_2 . Preprint, Penn State University, 43 pp, 2010.
- [Zhe10] Y. Zheng. Arnold diffusion for a priori unstable systems and a five-body problem. Preprint, Penn State University, 51 pp, 2010.